Performance Optimization and Optimal Design of Six Wheeled Rover for Uneven Hard Terrain

A thesis submitted
in partial fulfillment for the degree of

Doctor of Philosophy

by

SAM NOBLE

Department of Aerospace Engineering
INDIAN INSTITUTE OF SPACE SCIENCE AND TECHNOLOGY
Thiruvananthapuram - 695547

August 2021

CERTIFICATE

This is to certify that the thesis titled **Performance Optimization and Optimal Design of Six Wheeled Rover for Uneven Hard Terrain**, submitted by **Sam Noble**, to the Indian Institute of Space Science and Technology, Thiruvananthapuram, for the award of the degree of **Doctor of Philosophy**, is a bonafide record of the research work done by him under my supervision. The contents of this thesis, in full or in parts, have not been submitted to any other Institute or University for the award of any degree or diploma.

Prof. K. Kurien Issac
Thesis Supervisor
Senior Professor
Department of Aerospace Engineering
IIST

Prof. Aravind Vaidyanathan
Professor & Head
Department of Aerospace Engineering
IIST

Place: Thiruvananthapuram
August 2021

DECLARATION

I declare that this thesis titled **Performance Optimization and Optimal Design of Six Wheeled Rover for Uneven Hard Terrain** submitted in fulfillment of the Degree of Doctor of Philosophy is a record of original work carried out by me under the supervision of **Prof. K. Kurien Issac**, and has not formed the basis for the award of any degree, diploma, associateship, fellowship or other titles in this or any other Institution or University of higher learning. In keeping with the ethical practice in reporting scientific information, due acknowledgements have been made wherever the findings of others have been cited.

Sam Noble
SC11D014

Place: Thiruvananthapuram
August 2021

ACKNOWLEDGEMENTS

First of all, I kneel before God Almighty who gave me the strength to thrive throughout the entire course of doctoral work.

I would like to express my sincere gratitude to my dear supervisor, Prof. K. Kurien Issac, for accepting me as a doctoral student, kind-hearted support, indispensable comments, and continuous encouragement provided during the past years. He has been a continuous source of support with immense knowledge, provided critical comments, and inspired me to think differently. This thesis would not have been possible without the help, and guidance from him.

I would like to thank Prof. Aravind V., Head, Department of Aerospace Engineering, Prof. C. Amarnath, Prof. Ashitava Ghosal, Dr. Raveendranath P., and Dr. Rajesh V. J. for serving as members of my doctoral committee and providing insightful comments and timely advice. I express my sincere gratitude to Dr. R. V. Ramanan, Prof. A. Salih, Prof. Manoj T. Nair, Prof. Deepu M. and Prof. Nirmala Rachel James, for the commendable support provided in many critical situations.

I would also like to thank Dr. Girish B. S. for the advice and technical discussions. I acknowledge my colleagues Dr. Praveen Krishna I. R., Dr. Arun C. O., Dr. Sam K. Zachariah, Dr. Bijudas C. R., Dr. Anup S. and Dr. P. Chakravarthy for the discussions and advices. I am grateful to Dr. Shine S. R. for helping me by generating the necessary thesis template in LaTeX.

I am much indebted to Dr. B. N. Suresh, the founder Director and Chancellor of IIST, former Directors Dr. K. S. Dasgupta, and Dr. V. K. Dadhwal, and Sri. S. Somanath current Director of IIST for their encouragement and advices during the research work. I would like to thank Dr. Raju K. George, Dean (R&D), Dr. A. Chandrasekar, Dean (Academic), Dr. Kuruvilla Joseph, Dean (SA, SW & Outreach) and Dr. Y. V. N. Krishna Murthy, Registrar for all the institutional support for the doctoral work.

Words are not enough to thank my room-mate and friend Dr. Sooraj V. S., for the countless discussions related to various matters over the years. A special thanks to all the faculty members of the Department of Aerospace Engineering, who has wholeheartedly helped me to manage dual responsibilities as a faculty member and as a part-time research scholar. Further it will be unfair if I do not thank Dr. Lekshmi V. Nair, Dr. Chris Prema S., Dr. Sreejalekshmi K. G., Dr. Sheeba Rani J., Dr. V. Sennaraj and Dr. Mary Gladis J. for the support at various stages. I express my sincere gratitude to the teaching community of IIST. I acknowledge all my friends, research scholars, and students of IIST who was with me, to strive towards this goal.

My sincere thanks also goes to all the staff members of Aerospace Engineering (technical and nontechnical), especially Mr. John Thomas, Ms. Ajitha and Ms. Gopika, as well as IIST academics, administration, library & information services, and other service divisions for their direct and indirect kind support during this period.

Last but not the least, my deepest gratitude to my family members for supporting me throughout the period of doctoral study. I am very grateful to my parents, who taught moral values, bringing me up and transforming me to a nice human being. I express my love and gratitude to my wife, Anisha, who helped and supported my research work in whatever way she can. A word of appreciation to my son Jeffrey, whose innocence brought smile into my face. I would not have made this, without the love, support, and their wholehearted prayers.

Sam Noble

ABSTRACT

Numerous scientific missions over the past few decades were sent to Moon, and planets for studying and understanding the unknown aspects of our solar system. Orbiting vehicles, landers, and exploration vehicles were used for those scientific missions. Wheeled mobile robots or rovers are a class of mobile robots, used as exploration vehicles for surface exploration. Rocker-bogie suspension system is so far the most used for these exploration missions. These robotic vehicles need to negotiate rough terrain through out their life spans. Their locomotion performance is one of the critical factors, which decides the success of the mission.

A detailed survey of literature indicated that significant progress has been made in performance optimization and optimal design of rocker-bogie suspension rovers. The most popular performance parameter is coefficient of friction needed for moving without slipping. We identified two aspects of the problem formulation which appeared possible to improve. One is the characterization of solution as one with equal contact force ratios for the three wheels, which we felt is not necessary for a minimax problem with non-linear functions. The other is the implied assumption in some of the formulations that the wheel torques have to be in the same direction. So we took up improved formulations for both optimal performance and optimal design as our major goal. We consider structured terrain like large steps, and stair cases.

For optimizing performance of a given rover, we were able to propose a smooth problem formulation which does not have the two lacunae mentioned above. As our formulation is smooth, we were able to use a state of the art gradient based non-linear programming numerical solver to obtain solutions. Some of these solutions clearly demonstrate that equal contact force ratio is not a necessary and in some cases, not even a sufficient condition for minimum. They also showed that all solutions need not have wheel torques in the same direction.

Our detailed understanding of the nature of solutions led to the proposal of two analytical, non-iterative algorithms, which we show to be as effective as the powerful numerical solver in finding global optima, and much faster, and is likely to be much easier to implement in an onboard controller.

We proposed the use of an onboard manipulator to shift centre of mass, to further improve performance. We formulated this also as a smooth optimization problem which can be easily solved using the NLP solver. We then briefly address the cases where the coefficient of friction between the wheels and ground are (a) known on one patch on the ground, and (b) fully known everywhere.

The next major problem addressed is that of optimizing the design of the rover itself, considering required friction coefficient as the objective function. We considered terrains of (a) single large step, (b) three large steps, (c) staircase, and (d) a combination of (b) and (c). We also considered rovers without and with manipulator for shifting centre of mass. We were able to formulate cases (a) and (b) as smooth optimization problems and obtain solutions which we show to be at least local minima using KKT conditions. For cases (c) and (d) we could not obtain smooth formulation. However, we were able to significantly reduce the problem size and obtain good solutions using genetic algorithm.

Our work has thrown up very effective mathematical formulations for performance optimization and optimal design of rocker-bogie suspension rovers. At the end, we suggest some important directions to pursue in future.

TABLE OF CONTENTS

LIST OF TABLES

LIST OF FIGURES

ABBREVIATIONS

ATHLETE	All Terrain Hex Limbed Extra Terrestrial Explorer
CNSA	China National Space Administration
CoM	Center of Mass
ccw	counter-clockwise
cw	clockwise
DoF	Degree of freedom
ESA	European Space Agency
ISRO	Indian Space Research Organization
JAXA	Japan Aerospace Exploration Agency
KKT	Karush Kuhn Tucker
LEMUR	Legged Excursion Mechanical Utility Rover
LPP	Linear Programming Problem
LRV	Lunar Roving Vehicle
MAMMOTH	Mars Analogue Multi MOde Traverse Hybrid
MBRSC	Mohammed Bin Rashid Space Centre
MER	Mars Exploration Rover
NASA	National Aeronautics and Space Administration
NLP	Nonlinear Programming
NPO	Lavochkin Scientific and Production Association
PEGASUS	Pentad Grade Assist SUSpension
SQP	Sequential Quadratic Programming
VIPER	Volatiles Investigating Polar Exploration Rover

NOTATION

F_1	Horizontal reaction force at rocker-bogie pivot, *N*
F_2	Vertical reaction force at rocker-bogie pivot, *N*
F_{N_i}	Normal force on i^{th} wheel, *N*
$F_{N_{min}}$	Minimum positive normal force, *N*
F_{T_i}	Traction force on i^{th} wheel, *N*
g	Acceleration due to gravity, *m/s*^{2}
H	Riser of staircase, *mm*
l_1	Distance between the first and middle wheel, *mm*
l_2	Distance between the first and rocker-bogie pivot, *mm*
l_4	Distance between the rocker-bogie pivot and last wheel, *mm*
l_5	Distance between the rocker-bogie pivot and center of mass of body, *mm*
l_{m_e}	Length of e^{th} segment of manipulator, *mm*
M_e	Mass of e^{th} segment of manipulator, *kg*
m_i	Mass of each wheel of i^{th} wheel, *kg*
r_i	Radius of the i^{th} wheel, *mm*
s	Step height, *mm*
T_r	Tread of staircase, *mm*
W_v	Weight of rover body, *N*
x_{De}	Centre of mass of e^{th} segment of manipulator
x_{manip}	x component of center of mass of manipulator
(x_{lo}, y_{lo})	Local coordinate attached to rover body
α	Angle between lines CH and center of mass of body, *rad*
β_i	Angle between the contact point of wheel with the vertical line, *rad*
θ_2	Angle between the lines AB and AC, *rad*
μ	Coefficient of friction between the wheel and ground

$\|\mu_i\|$	Absolute value of coefficient of friction on i^{th} wheel
μ_{avl}	Available coefficient of friction
μ_{avl_p}	Coefficient of friction available for a particular portion (patch) of terrain
μ^*_{uk}	Optimal solution of coefficient of friction for a fully unknown terrain
$\bigtriangledown\|\mu_i\|$	Gradient of absolute value of coefficient of friction on i^{th} wheel
τ_i	Torque on i^{th} wheel, *Nm*
ϕ_1	Angle between the first segment of manipulator with the body, *rad*
ϕ_2	Angle between the first and second segments of manipulator, *rad*

Subscripts

e	Segment number of manipulator
h	Pose number
i	Wheel number
p	Patch number

Note: The symbols/ notations that are not defined here are defined in the thesis wherever they appear first.

CHAPTER 1

Introduction

1.1 Background

For several decades now, in order to explore our planetary neighbours, scientists have been using Orbiting vehicles, Landers, and Exploration vehicles. Mobile robots or robotic vehicles are used for surface exploration on these planets, and are hence called exploration vehicles. As the name signifies, they explore the unexplored for our benefit and can be operated autonomously or semi-autonomously. These mobile robots need to move from one site to another carrying various scientific instruments. They play critical role in scientific experiments, helping in sample collection and analysis. Astronauts would also need the assistance of these vehicles, for operation and maintenance of future ground stations on planets. These vehicles would also help them to move from the landing location to their habitat and to visit target sites.

Based on the mode of surface locomotion, robotic vehicles can be classified as legged, tracked, wheeled and hybrid vehicles. Legged robots are walking robots, which walk like humans or animals. Ambler [1] and LEMUR [2] are examples of legged robots. Tracked vehicle uses continuous tracks, driven by wheels, and exemplified by Nanokhod [3] and maXXII [4]. Wheeled rover uses independently driven wheels as the basic element for locomotion, as demonstrated by Lunokhod rover missions [5] and Mars Exploration Rovers (MER) [6]. Hybrid rovers use actuated legs in addition to wheels attached to these legs. ATHLETE [7] and MAMMOTH [8] are examples of hybrid vehicles. Each locomotion mode has its own pros and cons. So far only wheeled locomotion has been used for planetary rover missions, due to its mechanical simplicity and higher reliability [5].

A wheeled rover suspension with only passive elements like unactuated kinematic pairs, springs, etc, is called a passive suspension. Active suspension rovers use actuators

to actuate the suspension joints. By actuating suspension joints, wheel ground interaction forces can be deliberately controlled to enhance mobility. Lunokhod [5], Shrimp [9], PEGASUS [10], and Sojourner [11] are a few examples of passive rovers. Gofor [12], ATHLETE [7], MAMMOTH [8], and VIPER [13], belong to the category of active suspension rovers. For driving the wheels and steering, both passive and active rovers require additional motors/actuators.

Various passive suspension mechanisms are used to connect the wheels of a rover to its vehicle body. Torison bar (Lunokhod [5]), double wishbone (LRV [14]), rocker-bogie (Sojourner [11], Spirit, Opportunity [6]), linkage mechanisms (Shrimp [9]), split and fit trailing arm suspension [15], and 3 bogie (Rosalind Franklin [16]) are some examples of passive suspension mechanisms.

A list of suspension systems of past, and proposed rover missions for planetary exploration is shown in Table 1.1. This table extends the list of Sanguino [27], so as to cover the newer developments. As can be seen from the table, predominantly passive articulated suspension rovers have been used or proposed for planetary exploration, and among them, rocker-bogie suspension is the most popular one. An extensive review of planetary rovers can be seen in [27].

1.2 Review of Literature

The broad aim of the thesis is to address the issue of improving mobility of six wheeled rocker-bogie suspension rovers.

Ability of the robotic vehicle to negotiate various terrains is defined as mobility. Various mobility metrics have been proposed. Required coefficient of friction between wheels and ground [12], energy [28, 29], traction force [30], maximum obstacle height, and stability [31] are some of them. Among these, coefficient of friction required between the wheels and the ground is the most popular, perhaps due to the fact that the available coefficient of friction in unexplored terrain, is unknown. We also consider the required coefficient of friction as the main objective function. Hence the review of literature here

Table 1.1: Suspension system of rovers for planetary exploration (Past / Proposed).

Name	Agency	Wheels	Suspension	Year
Lunokhod 1 [5]	NPO Lavochkin	8	Torsion bar	1970
Apollo 15 LRV [14]	NASA	4	DW	1971
Apollo 16 / 17 LRV [14]	NASA	4	DW	1972
Lunokhod 2 [5]	NPO Lavochkin	8	Torsion bar	1973
Sojourner [11]	NASA	6	Rocker-Bogie	1997
Spirit/ Opportunity [6]	NASA	6	Rocker-Bogie	2003
Curiosity [17]	NASA	6	Rocker-Bogie	2011
Yutu [18]	CNSA	6	Rocker-Bogie	2013
Pragyan [19]	ISRO	6	Rocker-Bogie	2017
Yutu-2 [20]	CNSA	6	Rocker-Bogie	2018
Tianwen-1 [21]	CNSA	6	Rocker-Bogie	2020
Perseverance [22]	NASA	6	Rocker-Bogie	2021
Chandrayaan-3 rover	ISRO	6	Rocker-Bogie	2021
MELOS [23]	JAXA	6	3 Bogie	2022
Rosalind Franklin [16]	ESA	6	3 Bogie	2022
VIPER [13]	NASA	4	Active	2022
Hakuto-R [24]	ispace & Draper lab	4	Bogie	2023
Chang'e 7 [25]	CNSA	*	*	2024
Rashid [26]	MBRSC	4	*	2024

* - Not announced.

DW : Double Wishbone.

is mainly confined to contributions considering this metric.

For mechanical systems, various dry friction models have been proposed (see Pennestri et al. [32] for a detailed discussion). Benson friction model, smooth Coulomb model, velocity based model, Karnopp model, etc are some of them. We use Coulomb's friction model.

Planetary rovers need to negotiate regolith as well as hard terrain. Interaction of wheels with sandy terrain have been studied, and models were proposed by Bekker [33], Wong and Reece [34], and others. Thrust, sinkage, drawbar pull, etc are some of the performance parameters considered. They are calculated based on certain empirical relations for the normal and shear stress distributions on the wheel, and certain soil parameters also feature in these relations. We do not describe these models here, as our study is confined to hard terrain.

The term "friction requirement" can be understood with reference to Figure 1.1. The available coefficient of friction μ should be greater than the ratio of traction force F_T and normal force F_N, to avoid slip. Hence the minimum required friction coefficient (μ) for the wheel at any instant, is $|F_T/F_N|$.

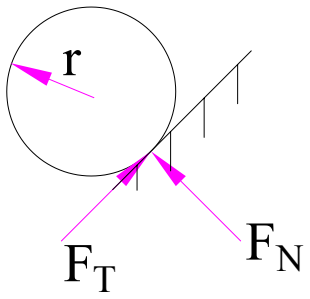

Figure 1.1: Traction and normal force acting on wheel.

Note that in 3D motion of wheels, the terms "longitudinal" and "lateral traction/force coefficients" are used for the force ratios. As our motions are purely longitudinal, "contact force ratio" which we use, stands for "longitudinal traction/force coefficient".

In the next subsection we consider contributions to minimizing friction requirement by providing optimal torques to rover wheels. In the subsequent subsection, we consider optimal design of rovers.

1.2.1 Minimizing Friction Requirement

We concentrate mainly on formulations and solution approaches. There are certain common equality and inequality constraints that a rover needs to satisfy. The forces have to satisfy the set of equilibrium conditions (usually static, but dynamic also), which can be mathematically written as $[A]\{x\} = \{B\}$, where x denotes the forces, including traction and normal force variables. The coefficient matrices $[A]$ and $\{B\}$ are related to the pose and contact points of the rover and gravitational forces (and inertia forces in the case of dynamic equilibrium). As the ground can only push on the wheel, and not pull it, the normal forces have to satisfy the non-adhesion condition, $F_N \geq 0$.

The problem of optimizing the mobility of a four wheeled actively articulated suspension rover, Gofor was addressed by Sreenivasan and Wilcox [12]. They considered Gofor rover negotiating a terrain with a desired velocity and acceleration. The decision variables used were wheel torques and rover pose. The objective function $\underset{i=1,2}{max}\left\{\left(F_{T_i}/F_{N_i}\right)^2\right\}$ (where i denotes the wheel number), is minimized for maximizing mobility. An analytical method was proposed for finding the optimal torques. A single variable quadratic equation was developed from the condition of equal force ratios. The other force variables were written in terms of this single variable. This equal friction angle approach was adopted from the characterisation used by Mukherjee and Waldron [35] for minimizing the maximum friction angle for a three finger grasp problem. The solution to this grasp problem was obtained by finding the roots of a higher degree polynomial. For Gofor, as the number of wheels is two, the equal force ratio condition reduces to that of finding roots of a quadratic equation. The coefficients of this quadratic are functions of pose, which is the additional decision variable.

A control strategy for six wheeled rocker-bogie suspension rover was proposed by Iagnemma et al. [28, 29]. They minimized power for flat terrain, and friction requirement for irregular terrain. For a given acceleration at a given pose and velocity, they defined friction requirement as $\underset{i=1,2,3}{max}\{F_{T_i}/F_{N_i}\}$. For minimization, they used an iterative method proposed by Chung and Waldron [36].

The same objective function and constraints used by Iagnemma et al. [28, 29] were

used by Lamon et al. [37, 38] for six wheeled rover. They neglected inertia forces, assuming slow motion, and proposed a rather elaborate algorithm for solving the problem, after studying the nature of the objective function in detail.

Mann and Shiller [31] addressed the six wheeled rocker-bogie rover control problem for the case where μ is known. They depicted the constraints corresponding to no slip and non-adhesion in the velocity-acceleration space. This helped them choose torques corresponding to feasible velocities and accelerations.

Krebs, Thueer and co-workers [39, 40, 41, 42, 43] proposed an alternative objective function $\sum_{i=1}^{3} \left((F_{T_i}/F_{N_i}) - \underset{j=1,2,3}{mean} \left\{ F_{T_j}/F_{N_j} \right\} \right)^2$. This formulation was extended for four wheeled and various types of six wheeled rovers. It has to be noted that, if the minimum is zero, minimizing this objective function becomes similar to solving the characterizing equation of equal contact force ratios posed by [12].

Three analytical approaches for the problem of minimizing friction requirement was proposed by Waldron and Abdallah [44]. Among them, the approach of minimizing friction angle is pertinent for our study. Rovers with four or more even number of wheels (contact points) was addressed, and 2D dynamic equations of motion were considered. Optimal friction angle approach assumed equal contact force ratio at the two points of contact, of a planar two wheeled rover. The optimal traction and normal forces were obtained by solving a quadratic equation in terms of contact force ratio. For problems with more contact points (2D), each pair of contact points were solved using optimal friction angle algorithm keeping a minimal normal force at other contact points. The pair of contacts with minimum friction angle was chosen as the optimal solution.

The problem of optimizing mobility of HyLoS2, a four wheeled actively articulated suspension rover, was addressed by Jarrault et al. [45]. They considered that the available friction coefficient is known. Maximizing the minimum margin of slip was considered as the objective function, subject to equilibrium equations, non-adhesion constraints, and torque limits. The margin of slip can be defined as the amount of tangential force that can be added to the tangential component of force at the contact point, without breaking the contact stability. An algorithm proposed by Dutta and Vidyasagar [46] was used for

optimization.

Reina and Fogila [47], optimized the performance of a four wheeled rover, by using the objective function $\sum_{i=1}^{2}\left((F_{T_i}) - \underset{j=1,2}{mean}\left\{F_{T_j}\right\}\right)^2$, which is essentially minimizing the differences between traction forces. The traction forces which need to be applied will be close to each other, and equal, when the objective function attains zero value.

Labenda [48] addressed the problem of optimizing mobility of a segmented rover, choosing as objective function the differences in normal forces between adjacent wheels to seek a more uniform normal force distribution.

The problem of controlling multisegmented rovers addressed by Siravuru et al. [49] considered three objective functions, subject to equilibrium equations, non-adhesion constraints, and limits on contact force ratios and torques. They concluded that the sum of contact force ratio, is the most appropriate objective function for their problem.

Numerical and analytical methods were proposed for finding the optimal performance of a four wheeled rover by Effati and Skonieczny [50, 51]. For solving the non-linear equations, they resorted to iterative numerical methods. Equations of motion, and equal contact force ratios condition, constituted the non-linear equations in their approach.

1.2.2 Optimal Design of Rovers

Meghdari et al. [52] appears to be the earliest contributor to optimal design of rovers. They optimized a Shrimp [53] like rover for climbing three types of staircases. The front four-bar, and the remaining suspension linkages of this rover were optimized. Primarily, a smooth climb was ensured for the front four-bar, by optimizing the parameters based on the kinematic considerations. Secondly, the remaining suspension linkage was optimized for making CoM path as close to a straight line as possible. They defined the sum of positive slopes of CoM path, evaluated at various points as rover climbs a staircase, as the objective function. In this case torques need not be considered explicitly. Tip over stability was addressed using appropriate constraints.

Optimal design and operation of a Shrimp like rover for climbing a staircase was

attempted by Nia et al. [54]. Accelerated motion on staircase was first obtained by simulating the rover climbing a staircase using nominal torques. They then optimized the linkage parameters and torques simultaneously, considering the poses and corresponding velocities and accelerations obtained in the above simulation. Contact force ratio was minimized subject to non-adhesion constraints, with an upper bound for contact force ratios. Solutions obtained appear to be very good. They are sensitive to terrain geometry. For climbing a 0.25 m $\times$ 0.25 m staircase using wheels of 0.14 m diameter, the coefficient of friction required was around 0.6.

A novel four-bar suspension mechanism for a six wheeled rover was proposed by Woo et al., and optimized [55]. To determine the optimal link lengths, first a nominal rover climbing the staircase was considered and four critical situations were identified. For each of the four critical situations, slightly different problem formulations were used, with the overall goal being equalization of contact force ratios.

Optimal design of Shrimp like rover, with feedback controller gains included as decision variables, was proposed by Sato and Ishii [56]. The rover was dynamically simulated for climbing a hump, and two types of stairs. Total traverse, time taken, average torque, slip, and body pitch were the five objective functions considered for the performance evaluation. The solution appears to have a disproportionately large front four-bar.

Optimal design of an ExoMars configuration rover moving on sandy terrain was addressed by Leite and Schafer [57]. Several objectives like rover mass, power consumption, wheel sinkage, and dynamic stability margin were considered. The ExoMars rover was simulated on sandy ground with a single stone and uneven hard ground.

Alamdari and Krovi [58] considered the design of the front four-bar of a Shrimp like six wheeled rover for climbing a single step of height equal to twice the wheel diameter. They consider combinations of variable length links (with a linear spring-damper replacing one rigid link) and linear and torsional springs. A desired path for the center of the wheel on the four bar is specified. The objective function minimized is a linear combination of maximum contact force ratio of the single wheel at various poses, and the sum of squares of error in position of its center. The kinematic parameters are par-

tially defined by precision points. The decision variables are the kinematic parameters of the linkage, and spring parameters, and applied forces at each pose. In addition to non-adhesion conditions, no slip conditions (assuming coefficient of friction is known) and limits on torques are included as inequalities.

A novel multi-constraint quadrilateral suspension mechanism based on parallel spring fork suspension was proposed by Yang et al. [59] for step climbing. The suspension linkage parameters were chosen as variables, and the values were decided based on various geometric constraints considered for each wheel climbing the step. The overall objective was to achieve better trafficability (ability to traverse without loss of traction [60]) for step climbing. The rover was experimentally demonstrated for climbing steps, and slopes.

Kim and Yu [61] attempted the design of a four wheeled rover using multi disciplinary design optimization. Wheel radius and wheel width were considered as the design parameters. Deformable terrain was considered, which is flat with inclinations in lateral and longitudinal directions. The objective functions were tractive coefficient and power margin, and the constraints imposed were the limits on wheel radius and wheel width. Tractive coefficient is affected by the drawbar pull, and power margin is defined as the difference between the power available and the power consumed.

Six wheeled rocker-bogie suspension rover was optimized by several teams [62, 63, 64, 65, 66, 67, 68]. The linkage parameters and CoM location were the decision variables for the optimal design attempted by Li et al. [62], for climbing a single step. Energy consumption, vertical displacement and body pitch were used as objective functions. Constraints for preventing rover body hitting the step corner, stability, and load equalization were used.

Ullrich et al. [63] optimized the rover for motion on uneven sandy terrain and a step. They used several objective functions, including the switchable one proposed by Iagnemma et al. [29], and also margin of static stability, margin of interference, wheel sinkage, and pitch variation.

Deviation of CoM path, from the straight line with slope related to staircase, was

considered as the objective function by Kim et al. [64] and Hong et al. [65]. In addition to this objective function, Hong et al. [65] considered maximum tilting angle of the cart, while climbing the stair. Three types of staircases were considered for the design. Constraints for preventing pivot interference with step, preventing interference between wheels, limits on wheel radii, and overall size limitation were used by Hong et al. [65], to ensure that the complex operation of climbing a staircase could be performed smoothly. In addition to rocker-bogie parameters, wheel radii were also used as decision variables. The rover wheels were actuated in the proposed rover by Kim et al. [64], while a manual pull up was used by Hong et al. [65].

Optimal design of a modified rocker-bogie suspension, which allows the movement of bogie pivot along a line, was attempted by Hong et al. [66]. Their objective was to minimize the deviation of CoM path from the straight line with slope related to staircase, and the backward movement of the rover (while climbing a staircase).

Power consumption and effective ground pressure were the objective functions used by Kshirsagar et al. [67] for climbing a single step. Constraints to prevent interference of bogie with step, and load equalization were also included.

An optimized rover for motion on an uneven terrain was attempted by Guodong et al. [68]. They tried to minimize the fluctuation of CoM. The decision variables were the rotation angle of the bogie with respect to the vehicle body, and the position of rocker-bogie pivot point. Limits on rotation angles and link lengths were imposed as constraints.

1.3 Observations

From the papers on optimizing performance of a given rover, we find that friction requirement is the most popular objective function.

Friction requirement is primarily defined as the maximum of the contact force ratios. This makes it a non-smooth function. It is important to note that powerful gradient based optimization solvers cannot be used to solve non-smooth optimization problems effectively.

Many authors [12, 39, 40, 41, 42, 43] use the condition that contact force ratios are equal at the minimum, in order to obtain solutions. We believe that this is not a sufficient condition. Also, as there are inequality constraints, and as the contact force ratios are non-linear functions, these conditions may not even be necessary conditions for solution.

Some authors [28, 29, 37, 38, 39, 40, 41, 42, 43] assume that the contact force ratios are positive. It is not clear to us that this needs to be the case in all situations.

Fairly elaborate formulations have been proposed for optimal design of rovers for climbing different types of terrains. Most papers consider structured terrains like steps and staircases. Several types of objective functions and constraints have been considered. Still the most popular objective function is friction requirement.

One thing we noticed regarding optimal design papers, is that the solutions are not checked to see whether the first order necessary conditions for constrained minima (KKT conditions) are satisfied.

The concept of shifting center of mass, has been used by some authors for improving performance and other aspects.

1.4 Research Objectives

Based on our survey of literature, and the observations we listed above, we can now state the objectives of our work. The broad aim of the thesis is to optimize mobility of six wheeled rocker-bogie suspension rovers. The specific objectives are:

- To develop smooth formulations for finding optimal torques of wheels which minimize friction requirement, at a given pose and contact pattern, and to solve the problem, without posing conditions like equality of contact force ratios, and allowing torques with different signs. We also propose to develop non-iterative methods for solving this problem.
- To explore the potential of shifting CoM with an onboard manipulator, to further reduce friction requirement.

- To develop smooth formulations for optimal design of the rover for climbing a single step, multiple steps, and staircases, minimizing the coefficient of friction required.

1.5 Organization of the Thesis

The contents of the thesis, as presented in the remaining six chapters, are briefly described below.

Chapters 2 and 3 deal with the problem of determining optimal torques (and also manipulator CoM locations) to minimize friction requirement at given poses. Chapter 2 focuses on formulating the problem as a smooth optimization problem, and solving it using a powerful gradient based iterative numerical optimization solver for such problems. Chapter 3 proposes analytical approaches for solving the problem.

In chapter 4 we generate minimal friction requirement and minimal torque requirement solutions for terrains whose coefficient of friction is partially or fully known.

In chapter 5 we formulate the problem of designing the rover optimally, as a smooth optimization problem, and discuss solutions for climbing a single large step, and several isolated large steps.

In chapter 6 we address the problem of optimally designing the rover for climbing a staircase of a specified geometry, and also several isolated large steps. This could not be posed as a smooth optimization problem, and hence solution was attempted using a technique which is suitable for non-smooth problems.

Chapter 7 concludes the thesis, summarizing the main contributions, and indicating directions for future work.

CHAPTER 2

Minimizing Friction Required for Climbing

Based on the literature survey, we identified two major problems to be addressed. Of these, the problem of optimizing the mobility of a given rover for negotiating uneven terrain, is addressed in this and the following two chapters.

Like many other authors, we regard friction requirement as the index of mobility, and try to minimize it. In this chapter, the emphasis is on formulating the problem as a smooth optimization problem, without a particular restriction and a particular characterization of solution, imposed by some of the earlier formulations. We obtain optimal solutions numerically, for various poses of two rovers, and explain different types of solutions in detail. We also investigate the effect of shifting the center of mass of the body-rocker subassembly using an onboard manipulator. Finally, using a dynamic simulation of the rover, we show that the optimal friction requirements obtained by us, are realizable by an idealized rover.

2.1 Mathematical Model

A six wheeled rover with the rocker-bogie suspension was considered for our study. Figure 2.1 shows the rover moving over an uneven prismatic terrain.

Geometry of rocker-bogie suspension rover considered for the study is shown in Figure 2.2, and its fixed parameters shown in 2.3. Two wheels (on one side) are connected to both ends of bogie. Their centers are ‘A’, and ‘B’. One end of rocker is connected to bogie with a revolute joint ‘C’, while the other end is connected to the wheel with center ‘H’. Rocker on one side is pivoted to body at ‘G’, and is connected to the rocker at the other side through a differential mechanism. The differential mechanism makes the two rockers move in opposite directions with respect to the body, leading to reduced pitching of

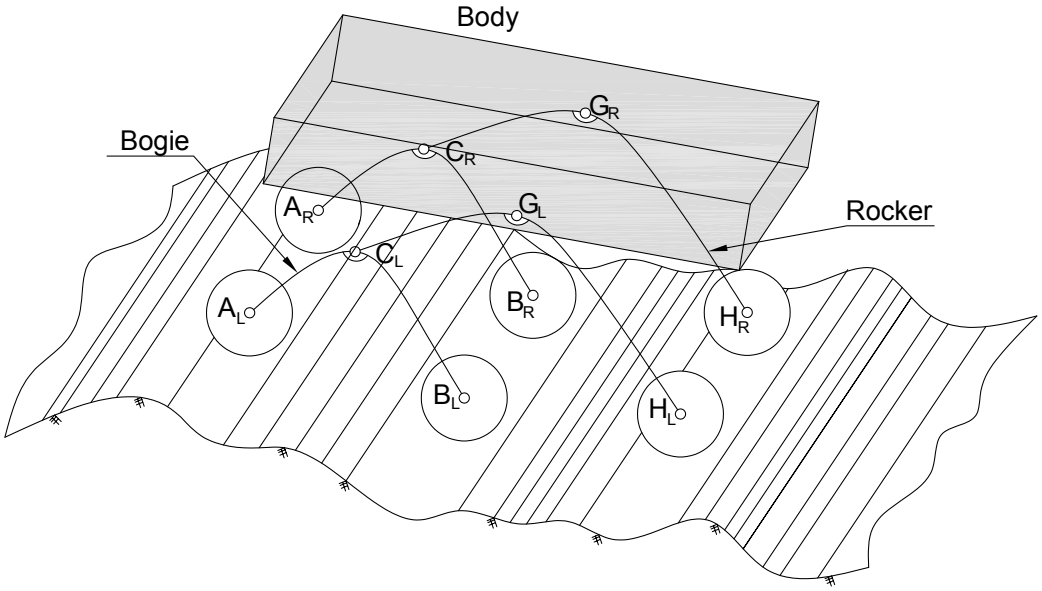

Figure 2.1: Rocker-bogie suspension moving on uneven terrain of 2D type.

the body as the wheels on the two sides encounter different terrains, and pitch differently. In the case of the motion we consider, as wheels on both sides move identically, the body maintains the same pitch angle as the two rockers, and so does not rotate with respect to the rockers. Thus a single CoM is sufficient for the body and the rocker together. The weight of the body is acting at point G_2. Wheels are assumed to be of the same radius,'r'. The weight of each wheel is $m_i g$, and its CoM is at the centre of the wheel, where i denotes the wheel number, 1, 2, 3, and g acceleration due to gravity. The contact point between ground and i^{th} wheel is defined using angle β_i measured in counter-clockwise direction, w.r.t. the vertical line passing through the center of the wheel. Due to both convex and concave nature, a single step is considered as a benchmark obstacle, like several earlier researchers. The single step of height 's' equal to wheel diameter is considered for this problem.

Assumptions

The following assumptions are made through out this work.

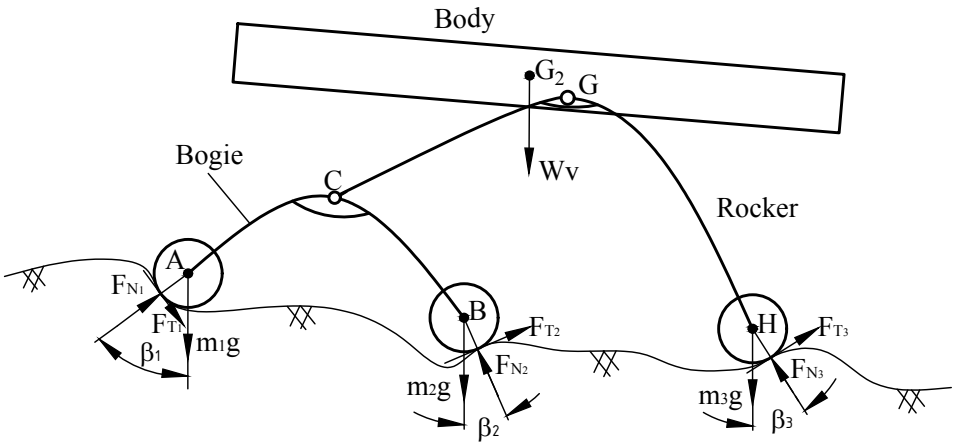

Figure 2.2: Rocker-bogie rover.

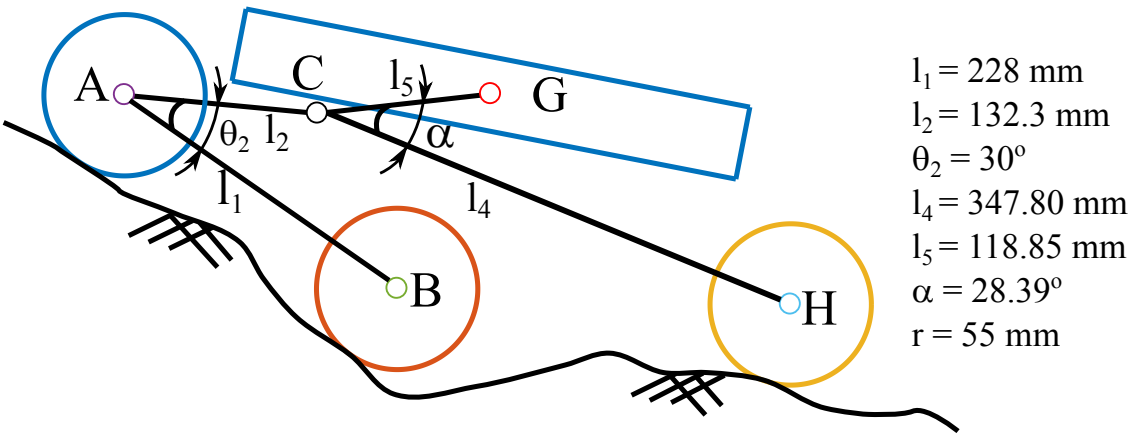

Figure 2.3: Rocker-bogie rover with dimension considered for the study.

(a) The terrain is such that when the rover moves without steering, the wheels on the left and right sides move identically.

(b) The rover velocity and acceleration are small enough for us to neglect inertia forces.

(c) Wheels and ground are rigid.

(d) There is only one active contact point for each wheel.

(e) Bogie mass is negligible.

(f) There are no limits on wheel motor torques.

Rocker-bogie suspension is specially designed to negotiate complex 3D terrains, and hence assuming 2D motions as we have done, is restrictive. 2D motions are valid only

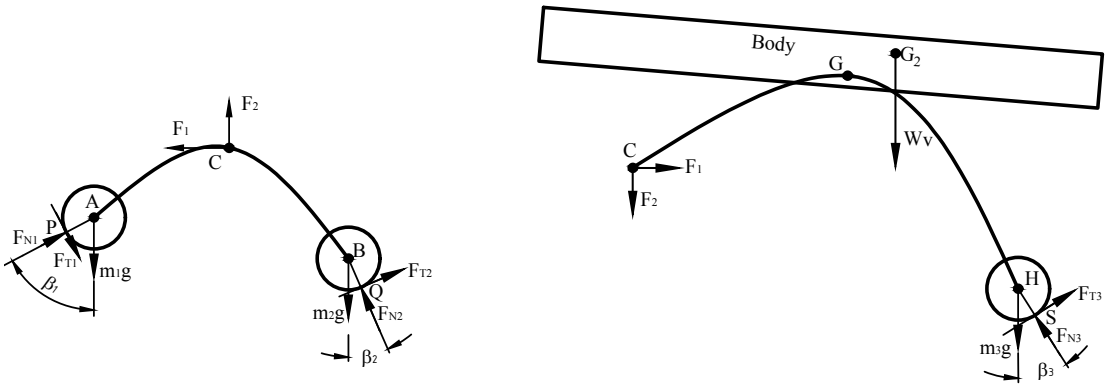

Figure 2.4: Free body diagrams of rocker and bogie. Body, rocker, and last wheel are regarded as a single rigid body. Bogie and its two wheels are also regarded as a single rigid body.

for structured features like ramps and staircases, and hence the scenarios we consider are mainly useful for motions inside buildings. In this work we address this set of restricted scenarios, as we see the possibility of improving upon the existing research on them.

Torque limits are not provided because, it was assumed that the maximum motor available is greater than the torques that need to be applied on wheels, which will keep it in equilibrium at all poses during the negotiation of the step. Torque limits can be incorporated in our formulation. But, we thought of going ahead with no limits on wheel torques. Later in Chapter 4, we address the problem of torque optimization, in the case where friction coefficient is known.

Equations of Equilibrium

Half the system - the three wheels, bogie, and rocker on one side, and half the body are considered for modeling. The bogie with two wheels is regarded as one body, and the rocker with one wheel and half the body, is regarded as the other body.

Thus the equilibrium equations consists of three equations for the bogie, and three for the body-rocker combination. This set of six equilibrium equations, relating eight forces, which are the six forces at the three contact points, and two reaction forces F_1 and F_2 at

joint C, can be written as

$$[A]\{x_F\} = \{F\}, \tag{2.1}$$

where $\{x_F\} = \{F_{N_1}, F_{T_1}, F_{N_2}, F_{T_2}, F_{N_3}, F_{T_3}, F_1, F_2\}^T$.

The free body diagrams are shown in Figure 2.4, and the six equilibrium equations are given below.

$$F_{T_{1x}} + F_{N_{1x}} - F_1 + F_{T_{2x}} + F_{N_{2x}} = 0 \tag{2.2}$$

$$F_{T_{1y}} + F_{N_{1y}} + F_2 + F_{T_{2y}} + F_{N_{2y}} = m_1 g + m_2 g \tag{2.3}$$

$$\begin{aligned} -(F_{N_{1x}} + F_{T_{1x}})Y_P + (F_{N_{1y}} + F_{T_{1y}})X_P + F_1 Y_C - F_2 X_C - \\ (F_{N_{2x}} + F_{T_{2x}})Y_Q + (F_{N_{2y}} + F_{T_{2y}})X_Q = m_1 g X_A + m_2 g X_B \end{aligned} \tag{2.4}$$

$$F_{T_{3x}} + F_{N_{3x}} + F_1 = 0 \tag{2.5}$$

$$F_{T_{3y}} + F_{N_{3y}} - F_2 = m_3 g + W_V \tag{2.6}$$

$$-(F_{N_{3x}} + F_{T_{3x}})Y_R + (F_{N_{3y}} + F_{T_{3y}})X_R = W_V X_G + m_3 g X_H \tag{2.7}$$

where $F_{N_{ix}}$ ($= F_{N_i} cos(\beta_i + \pi/2)$) and $F_{N_{iy}}$ ($= F_{N_i} sin(\beta_i + \pi/2)$) are the normal reaction forces of i^{th} wheel in X and Y directions respectively and $F_{T_{ix}}$ ($= F_{T_i} cos(\beta_i)$) and $F_{T_{iy}}$ ($= F_{T_i} sin(\beta_i)$) are the traction forces of i^{th} wheel in X and Y directions respectively. X_P, Y_P are the global coordinates of point P, etc.

Coefficients of $\{x_F\}$ in the six equilibrium equations (equations 2.2-2.7) constitute $[A]$ matrix and the right hand sides constitute $\{F\}$ matrix, in equation 2.1. For a given pose and wheel-ground contact points, these coefficients and right hand sides are known.

Non-adhesion Conditions

For every problem, in addition to equilibrium conditions, we introduce the *non-adhesion* conditions $F_{N_i} \geq 0,\ i = 1, 2, 3$, as the ground can only push the wheels, and not pull them.

2.2 Transforming a Non-smooth Formulation to a Smooth Formulation

The example below demonstrates how a max objective function is a non-smooth function, and how the non-smooth problem can be transformed to a smooth problem.

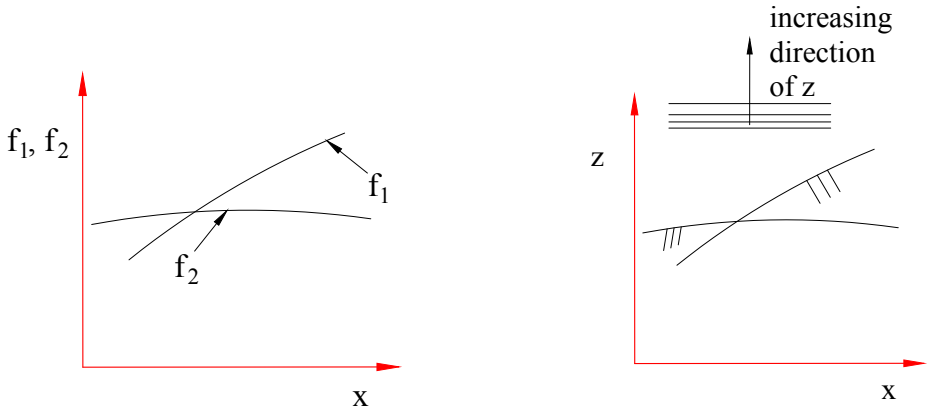

(a) Variation of $f_1(x)$, and $f_2(x)$.

(b) Smooth formulation.

Figure 2.5: Transformation from non-smooth to smooth formulation

Consider the objective function $max\ \{f_1(x), f_2(x)\}$, which is to be minimized (shown in Figure 2.5a). Due to the use of "max" operator in the objective function, the gradient is not defined everywhere. In Figure 2.5a, at the point where both the component functions are equal, the gradient is discontinuous, and hence the max function is non-smooth or non-differentiable. When the function has several independent variables, max functions have sharp valleys where the function is not differentiable, and gradient based searches slow down at sharp valleys, and often fail. If this non-smooth problem can be converted to a smooth one, powerful gradient based solvers can be employed for finding the solution. Here, we adopt such a conversion used by [69] for a mechanism synthesis problem.

The approach is to incorporate an additional variable z. Using this, the problem can be transformed to

minimize z,

subject to:

$z \geq f_1$, and $z \geq f_2$.

These constraints and objective function are shown in Figure 2.5b. We need to find the value of x and z. Now it can be seen that the problem has become smooth, as all the functions involved are smooth. This approach of transforming to smooth optimization problem, is used in this thesis.

The fact that powerful gradient based optimization solvers could get stuck at non-minimal points of a nonsmooth objective function like the max function, was actually experienced by us when we tried to solve a friction requirement minimization problem for a rover.

2.3 Formulation

The problem addressed here is 'given the parameters and inertia distribution of a rover, and its pose and contact points of wheels with the ground, determine the minimum coefficient of friction needed to maintain equilibrium without slipping'.

$max \left\{ \left| \frac{F_{T_1}}{F_{N_1}} \right|, \left| \frac{F_{T_2}}{F_{N_2}} \right|, \left| \frac{F_{T_3}}{F_{N_3}} \right| \right\}$ is the objective function which is appropriate for minimizing friction requirement. As previously explained, max operator introduces non-smoothness, and in this case absolute values in the component functions also introduce non-smoothness. Hence gradient based searches could fail. In order to overcome this, the problem can be formulated as a smooth optimization problem using the approach discussed in the previous section.

In our formulation, in addition to the existing eight decision variables, the available friction coefficient μ is introduced as a variable. The full set of decision variables is $\{F_{N_1}, F_{T_1}, F_{N_2}, F_{T_2}, F_{N_3}, F_{T_3}, F_1, F_2, \mu\}$. Please refer to Figure 2.4, where the forces are indicated on the two free body diagrams.

Our smooth optimization problem stated in words is, given the parameters and inertia distribution of a rover, and its pose and contact points on the wheels, determine the available friction μ and the eight forces, such that the available friction is minimum, and the rover can maintain static equilibrium without any adhesion or slip between the wheels

and the ground. Mathematically it can be stated as:

$$\text{Determine } \{F_{N_1}, F_{T_1}, F_{N_2}, F_{T_2}, F_{N_3}, F_{T_3}, F_1, F_2, \mu\} \text{ to}$$
$$\text{minimize } \mu,$$

subject to

$$[A]\{x_F\} = \{b\}, \tag{2.8}$$

$$F_{N_i} \geq 0,\ i = 1, 2, 3, \tag{2.9}$$

$$-\mu F_{N_i} \leq F_{T_i} \leq \mu F_{N_i},\ i = 1, 2, 3,\ and \tag{2.10}$$

$$\mu \geq 0. \tag{2.11}$$

Conditions (2.9) are the three inequalities which ensure *non-adhesion* between wheels and ground, conditions (2.10) are the six inequalities which ensure *no slip* between the three wheels and ground, and condition (2.11) ensures that μ is physically meaningful.

It is important to note that our formulation does not insist on either equal contact force ratios or the same sign for traction forces. The above problem was solved at a large number of poses occurring during step climbing. Solutions which violate the equal force ratio criterion were obtained, and are discussed in Section 2.4.3. In that same section, we show solutions where some force ratios can be negative and some positive.

The rocker-bogie suspension rover in [42] was chosen as the nominal rover for our study. Parameter values are given in Table 2.1, and Figure 2.6 shows the nominal rover to scale (Detailed explanation of rover parameters, mentioned in Table 2.1, is given in Chapter 5). Total mass of rover is 17.6 kg, each wheel being 1 kg and the remaining 11.6 kg being associated with body. As mentioned earlier, only half the rover is considered for static analysis (three wheels of 1 kg each and body of 5.8 kg (m_{body})). Acceleration due to gravity, $g = 9.81\ m/s^2$, Global origin is kept at 'O' with X and Y coordinates as marked in Figure 2.6. The body CoM is located above the center of the middle wheel, when the vehicle is resting on a flat horizontal terrain.

The number of poses considered for each wheel, from its first contact with step riser to a pose where the wheel center is vertically above the step corner, is 147. 57 of these are

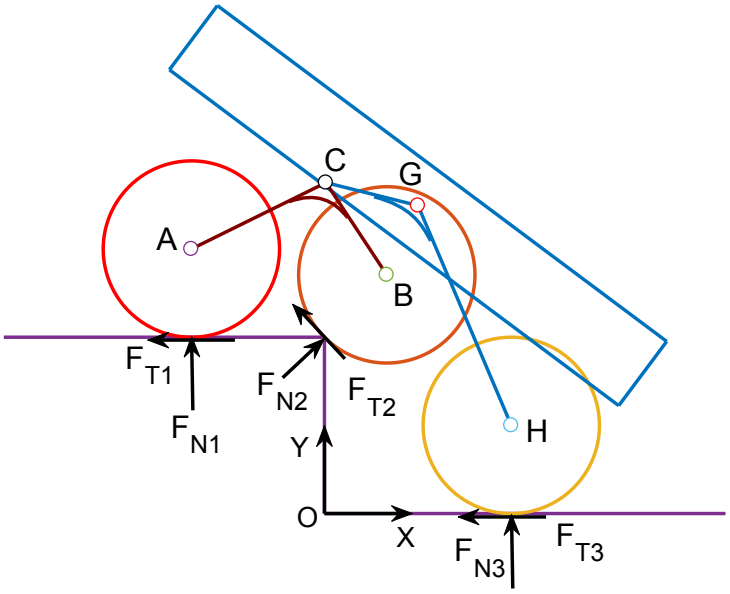

Figure 2.6: Rover climbing a step.

equally separated positions of the wheel on the riser, the remaining 90 are taken at one degree interval of wheel rotation, when climbing the corner of the step. The poses of the three wheels climbing add up to 441 poses. In addition to this several intermediate poses were also considered adding up to a total of 729 poses. For each pose μ was minimized using 'fmincon', an NLP solver based on the SQP algorithm, in MATLAB®. KKT conditions, which are first order necessary conditions for constrained minimum [70], were checked, and found to be satisfied for all solutions.

We generated solutions in two ways. First we generated solution for pose 1 from different random starting points. All of them converged to the same solution. Then for the next pose which is very close to pose 1, we used the solution of pose 1 as guess solution. With this approach, we generated solutions for all the remaining 728 poses. The second approach was to use one randomly selected starting guess for each of the 729 poses. As random guesses, we generated uniformly distributed points in the box $F_{N_1}, F_{N_2}, F_{N_3} \in [0, 100], F_{T_1}, F_{T_2}, F_{T_3}, F_1, F_2 \in [-50, 50], \mu \in [0, 3]$. Optimization searches from the 729 random guesses generated in this fashion (one for each pose) converged to the respective earlier obtained 729 solutions. In the space of decision variables, the starting random guesses were at a mean euclidean distance of 95.1 from their solutions. The minimum and

Table 2.1: Dimensions of nominal rocker-bogie rover.

Parameter	Dimension	Unit
l_1	228	mm
l_2	132.30	mm
θ_2	30	degrees
l_4	347.80	mm
l_5	118.85	mm
α	28.39	degrees
s	110	mm
$r_1 = r_2 = r_3$	55	mm

maximum distances of a starting guess from its solution was 36.5 and 160.9 respectively. This gives us some level of confidence that our solutions are likely to be global minima. It also appears that there are no other local minima for these poses.

2.4 Results

Here we use the term "forward climbing" when the wheels on the bogie is ahead of the wheel on the rocker. "backward climbing" means that the wheel on the rocker is ahead of the wheels on the bogie.

2.4.1 Results for Optimal Forward Climbing

Figure 2.7 plots optimal μ for all 729 poses, while Figure 2.8 plots the corresponding torques. It can be seen that maximum friction requirement of 0.58 occurs when the first wheel just starts climbing the vertical step. The value reported by Thueer [42] is 0.62. The pattern of μ variation is similar to that of Thueer [42]. The results obtained by Thueer [42] also appear to be optimal. The differences in the two results might be due to the fact that there may be some small differences in the parameters used in this thesis and

Thueer [42]. The fact that the variation and values are very close to each other indicates that the results by Thueer [42] and our results confirm each other's validity.

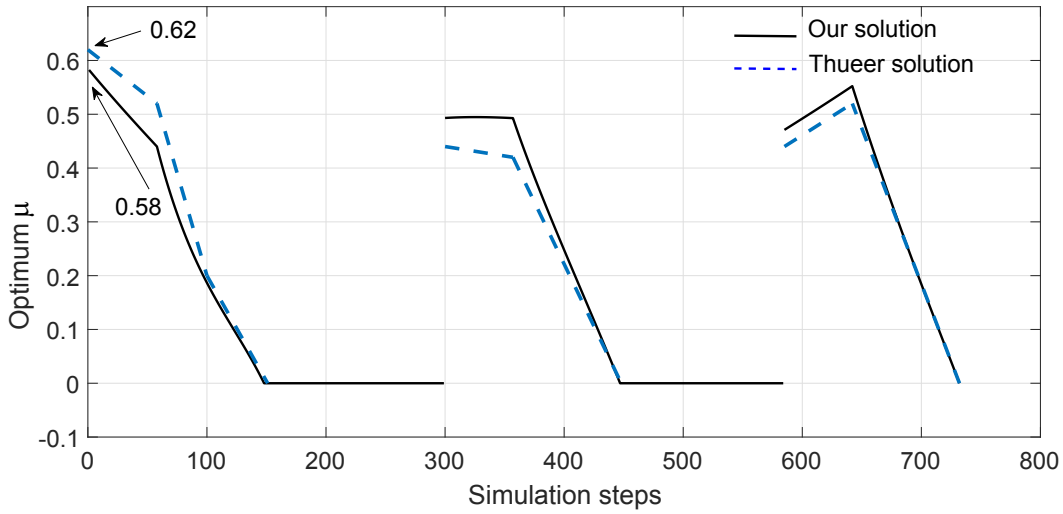

Figure 2.7: Optimal friction coefficient requirement of nominal rocker-bogie rover for forward climbing.

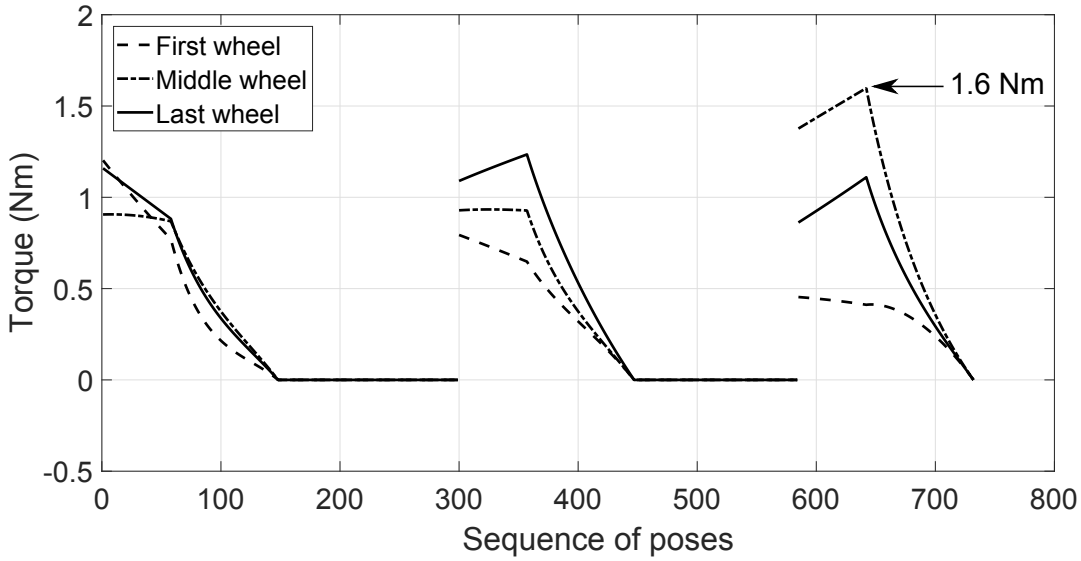

Figure 2.8: Torques of nominal rocker-bogie rover for forward climbing, corresponding to minimal friction requirements.

Maximum normal force is for the middle wheel (53.14 N; 61.56% of total weight). This force occurs when last wheel starts climbing the step. From Figure 2.8 it can be seen that the maximum torque requirement of 1.6 Nm is also for the middle wheel. It happens

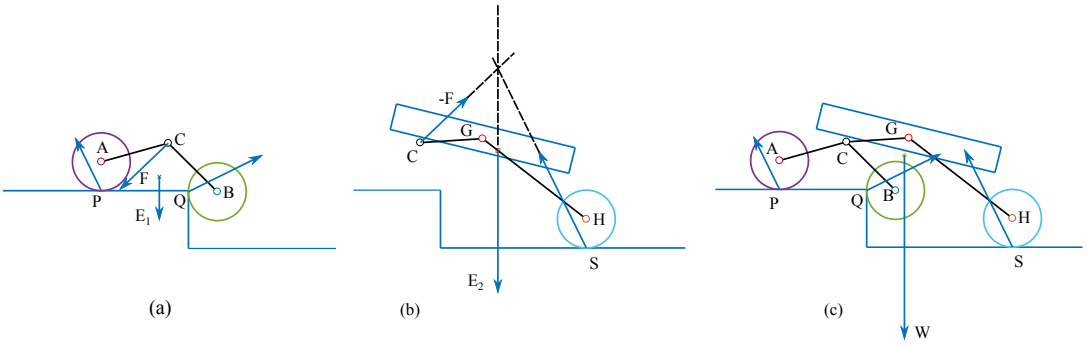

Figure 2.9: External forces on (a) bogie, (b) rocker and body, and (c) entire rover, for optimal solution with three equal contact force ratios, at pose 355.

when the last wheel just reaches the convex corner of the step. This peak torque is 2.6 times the average torque of 0.62 Nm on the wheels during climbing.

The discontinuities in required friction coefficient (Figure 2.7), and torques (Figure 2.8) occur because contact conditions change discontinuously. For example when a wheel just starts climbing the vertical face of a step, contact angle switches discontinuously from 0° to 90°. To handle this in practice, the rover velocity can be brought to zero at the point of contact with the step, and the torque ramped up or down in a finite time interval, using torque/current feedback control.

We now show the equilibrium situation graphically. Figure 2.9 shows external forces corresponding to the optimal solution where the three contact force ratios are equal in magnitude and sign. The contact forces shown acting at the contact points P, Q, and S, are the sum of the normal and traction forces. Force F is the force at pivot 'C', and forces E_1, E_2. and W are the weights acting through the centers of mass. The sets of external forces on the three assemblies are in force and moment equilibrium. The rocker and body being a three force system, the three external forces are concurrent, as can be seen in (b).

Something that surprised us is that the optimal solutions of all the 729 poses were satisfying the equal contact force ratio condition, and all the traction forces had the same sign, while we were expecting solutions which violated these. However, for a rover, optimally designed for climbing a step of height twice the wheel radius (see Figure 2.10), we did get solutions of those kind. Such special cases are discussed later in Section 2.4.3. Optimization of rover for step climbing, and how this optimal rover was obtained, are

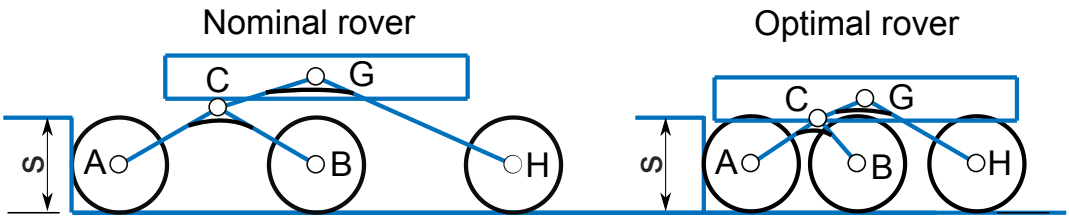

Figure 2.10: Nominal rover, and optimal rover for climbing $h = 2r$ step.

described in detail in Chapter 5.

2.4.2 Results for Optimal Backward Climbing

It is natural to ask the question, 'can the rover climb backward?' In one case it was reported that a rover is not able to climb backward [42]. We determined minimum coefficient of friction required for climbing backwards, at 776 poses in the sequence of backward climbing. Poses were chosen in the same way as described for forward climbing (see Section 2.3). The formulation used was the same as that used in forward climbing.

Variation of minimum μ as the rover climbs backwards is shown in Figure 2.11. The worst μ required for backward climbing is 0.84. This happens when the last wheel just reaches the corner of the step, as shown in Figure 2.12. Thus we can say that the rover considered can climb the given step backwards only if the coefficient of friction is at least 0.84.

In the above set of optimal solutions, the maximum torque needed for climbing was 2.07 Nm, occurring when the first wheel just starts to climb, while the average torque for wheels during climbing is 0.75 Nm. In the case of forward climbing, the maximum torque was lower, at 1.6 Nm. So clearly, the rover considered is better at climbing the given step forward than backward, if the criteria required are friction and torque. Asymmetry in performance in forward and backward climbing is natural to expect in a rover like the rocker-bogie suspension rover, whose configuration is asymmetric. It is preferred to climb down backwards as it will give the same result as when climbing up forward.

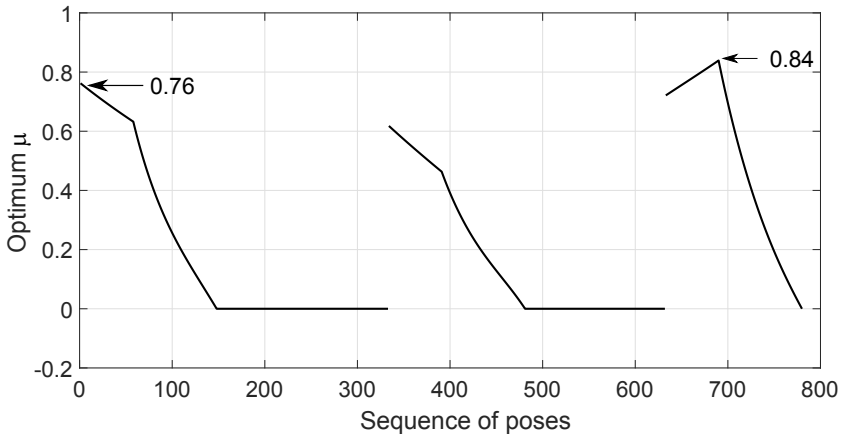

Figure 2.11: Optimal friction coefficient requirement of nominal rocker-bogie rover for backward climbing.

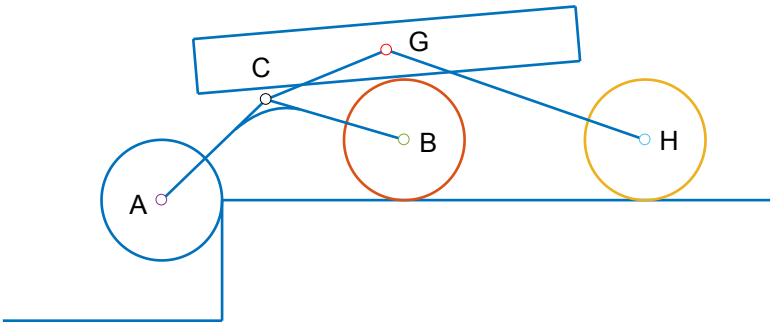

Figure 2.12: Pose in which last wheel just reaches the corner of step during backward climbing.

2.4.3 Special Cases from an Optimally Designed Rover

As already mentioned, optimal solutions of the nominal rover, at all the poses we considered, have equal contact force ratios for the three wheels, and same signs for the torques. We were expecting these conditions to be violated at some poses. We obtained such cases of violation with an optimal rover we describe in Chapter 5, where its parameters and how it was obtained, etc, are discussed. We describe here, the cases were the conditions are violated.

Contact force ratios of the optimal rover are given in Table 2.2 (variation also shown

in Figure 5.8) for the rover climbing a step of height equal to wheel diameter in the forward direction. Only 15 poses were considered for the optimal design of the rover for step climbing (poses are explained in Chapter 5, 'Optimal design for step climbing'). It can be seen from the Table 2.2 that the poses 6 and 11 have contact force ratios with the same magnitude, but with different signs. Pose 5 has nonequal contact force ratios, and one of its ratios is zero. All the remaining 12 poses have the same contact force ratios.

Table 2.2: Contact force ratio at 15 poses - optimal rover.

Pose no.	**First wheel**	**Middle wheel**	**Last wheel**
1	0.4457	0.4457	0.4457
2	0.3230	0.3230	0.3230
3	0.2082	0.2082	0.2082
4	0.0229	0.0229	0.0229
5	0	-0.0640	0.1212
6	0.4457	-0.4457	0.4457
7	0.4457	0.4457	0.4457
8	0.3577	0.3577	0.3577
9	0.1673	0.1673	0.1673
10	0	0	0
11	0.2954	0.2954	-0.2954
12	0.3752	0.3752	0.3752
13	0.4457	0.4457	0.4457
14	0.2392	0.2392	0.2392
15	0	0	0

The three special cases which we discuss below are (a) optimal solutions with reversed torques, (b) optimal solution with unequal contact force ratios, and (c) nonoptimal point with equal contact force ratio.

Case (a): Solutions with Reversed Torques

Although wheel torques are in the same direction at most poses, at poses 6 and 11, they have different directions, though the same magnitude. In pose 6, τ_1 and τ_3 are cw, while

τ_2 is ccw. For pose 11, τ_1 and τ_2 are cw and τ_3 is ccw.

It is intuitive to think that when a rover is climbing forward, all wheels should aid that progression by providing torques in the same direction. This may be true if the rover is accelerating substantially. In our case, were only equilibrium is demanded, the rover may be climbing up or down. Also, in some situations like the front wheel just butting the step during the climbing up sequence, the first two wheels of the nominal rover rotate in one direction, while the last wheel rotates in the opposite direction (see Figure 2.13). So the intuitive feeling could be wrong.

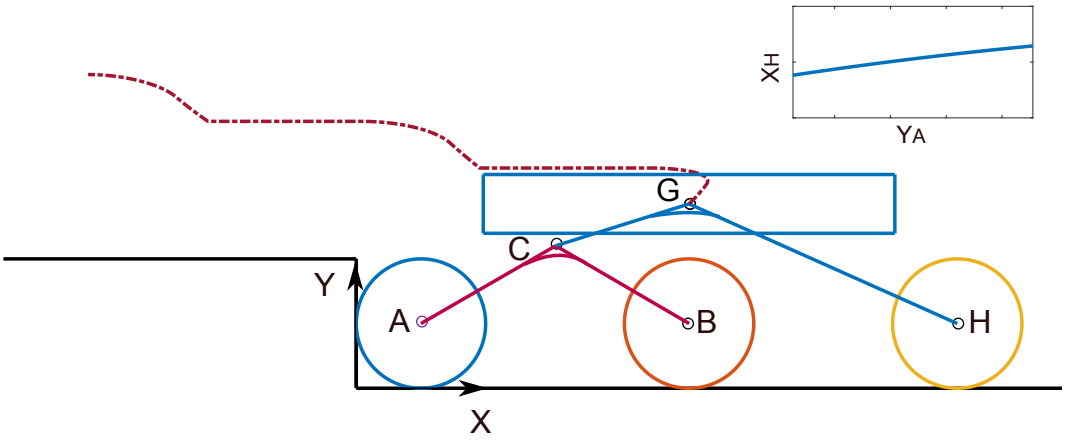

Figure 2.13: Locus of G, and variation of X_H.

If we had solved for pose 6 using the two formulations which demand traction forces with equal direction [28, 39], we would have got the minimum friction requirement as 0.5878, which is higher than the 0.4457 obtained using our formulation. This clearly shows that one should discard the requirement that the three tractions should have the same direction, unless there is some other reason for such a requirement.

We now show the equilibrium situation graphically. Figure 2.14 shows the external forces for the optimal solution in which the three contact force ratios are equal in magnitude, but have different signs. The contact forces at P and S pass through the right side of the respective wheel pivots while the force at Q passes through the left side of the wheel pivot. Hence it is clear that the signs of the contact force ratios of the front and rear wheels are the same, and is different from that of the middle wheel. The forces satisfy the force and moment balance. The rocker and body being a three force system, the three

external forces are concurrent, as can be seen in (b).

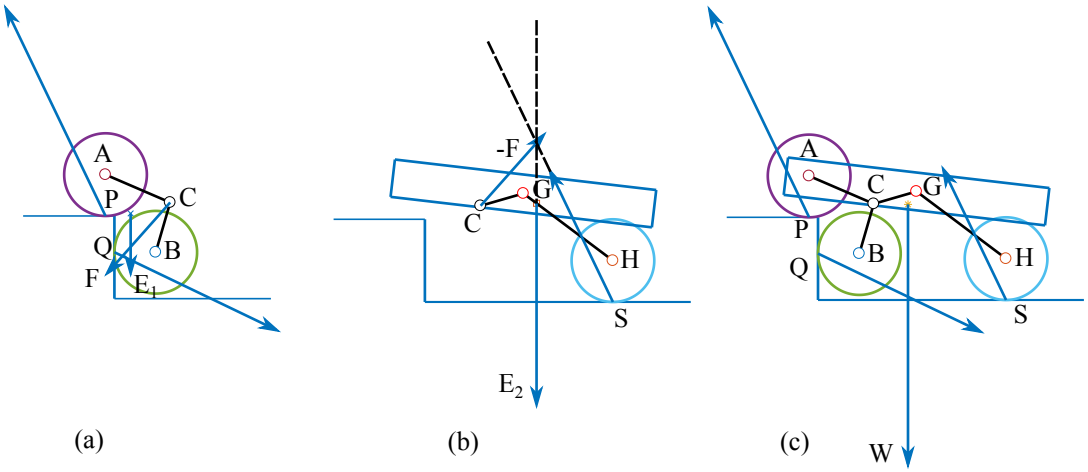

Figure 2.14: External forces on (a) bogie, (b) rocker and body, and (c) entire rover, for optimal solution at pose 156 with equal contact force ratios, with different signs.

A small modification of the second formulation [39] would allow torques in different directions to be considered. If we want to allow the torques to have different signs, we suggest using $\sum_{i=1}^{3}\left((F_{T_i}/F_{N_i})^2 - mean\left\{(F_{T_i}/F_{N_i})^2\right\}\right)^2$ as the objective function, instead of the objective function $\sum_{i=1}^{3}(F_{T_i}/F_{N_i} - mean\left\{F_{T_i}/F_{N_i}\right\})^2$. We used this for pose 6, and obtained the solution we had obtained with our formulation, with optimal friction requirement of 0.4457, and torques in different directions.

However, as shown below in case (b), seeking equal magnitude contact force ratio, even with different signs, would make us miss certain special solutions. We also show in case (c) that, the approach of seeking equal contact force ratio can declare non-minimum points as solutions.

Case (b): Solution with Unequal Contact Force Ratios

At pose 5, when the first wheel has just climbed the step fully, minimization of μ gave rise to different values for the traction to normal force ratios for the three wheels, unlike in all the other 14 poses where the ratios are equal, at least in magnitude. As already mentioned, several earlier formulations [12, 39, 40, 41, 42, 43], use the condition that the

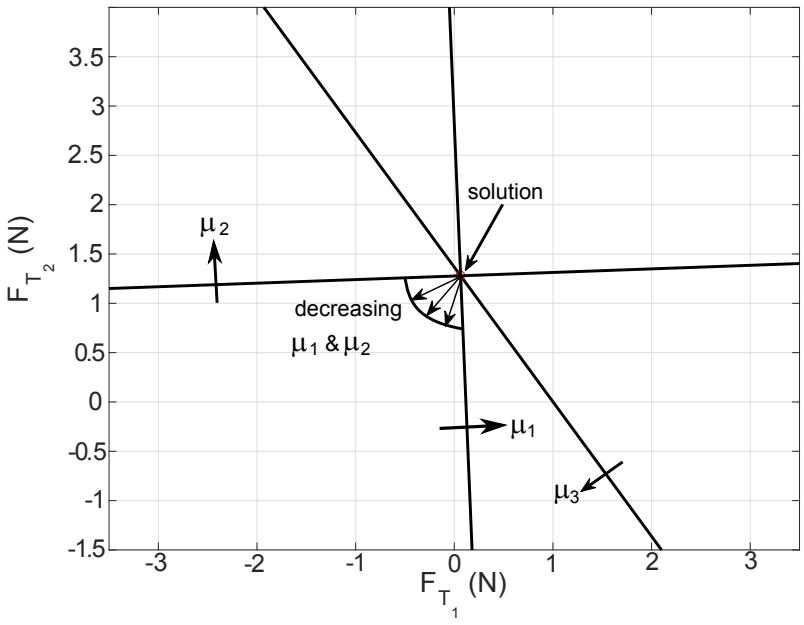

Figure 2.15: Minimax contact force ratio solution at pose 4, during forward climbing, in F_{T_1}-F_{T_2} space.

three force ratios are same at solution. The reason why the condition is violated in pose 5 is explained below. Before considering pose 5, we consider pose 4 where the condition is satisfied.

In Figure 2.15 we show the minimax contact force ratio solution obtained using 'fmincon', with the three contours of $\mu_i = F_{T_i}/F_{N_i} = 0.0229$, i=1,2,3 passing through the solution point in the F_{T_1}-F_{T_2} plane (other six forces being dependent on these two through equilibrium conditions). The increasing directions of the contours are shown. We can see that in all directions in which μ_1 and μ_2 can be decreased (indicated by the cone of arrows), F_{T_3}/F_{N_3} increases, proving that the solution is a local minimum. This is the general case for solutions, while in pose 5, solution does not satisfy the condition of equal μ_i's.

In Figure 2.16, we show the minimax contact force ratio for solution obtained for pose 5, in the F_{T_1}-F_{T_2} plane. At the solution, the optimal μ is equal to μ_3 (0.1212), while $|\mu_2|$ is less than this (0.064). μ_1 is indeterminate as both numerator and denominator are zero, but can be regarded as zero as no traction is required at wheel 1 contact point.

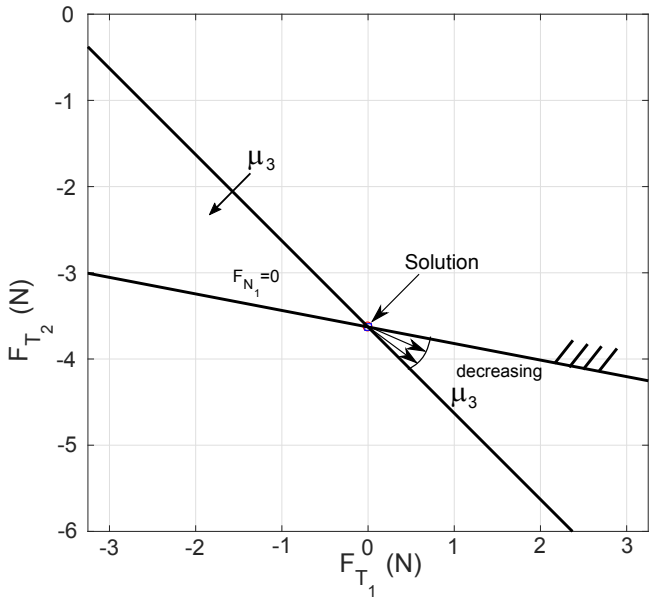

Figure 2.16: Minimax contact force ratio solution at pose 5, during forward climbing, in F_{T_1}-F_{T_2} space.

The solution is at the boundary of the inequality constraint $F_{N_1} \geq 0$. We now ask the question 'can $\mu = \mu_3$ be improved in any direction?'. The cone of directions in which μ_3 can be reduced without violating $F_{N_1} \geq 0$ is shown in Figure 2.16. We can take a finite step along any of these directions to decrease μ_3 without increasing $|\mu_2|$ to a value above 0.1212. However, any finite step from the solution, in any of the directions in the cone, however small, makes μ_1 jump discontinuously from zero to a value in the interval [0.5,∞), which is above the current optimal μ of 0.1212. Thus the solution obtained at pose 5 is a local optimum where $|F_{T_1}/F_{N_1}| \neq |F_{T_2}/F_{N_2}| \neq |F_{T_3}/F_{N_3}| = \mu$. Optimal solution obtained by imposing the condition of equal μ's ($|\mu_1| = |\mu_2| = |\mu_3|$), as done by [12, 39, 40, 41, 42, 43] would give a value of μ = 0.2010, which is not as good as the solution obtained with our formulation ($\mu = 0.1212$). Thus for pose 5, we see that the solution does not satisfy the conditions $|F_{T_1}/F_{N_1}| = |F_{T_2}/F_{N_2}| = |F_{T_3}/F_{N_3}|$, though in the majority of cases these conditions are satisfied. Hence our claim, that equality of contact force ratios is not a necessary condition.

We now show the equilibrium situation graphically. Figure 2.18 shows the external forces for the optimal solution in which $F_{T_1} = F_{N_1} = 0$. They satisfy the force and

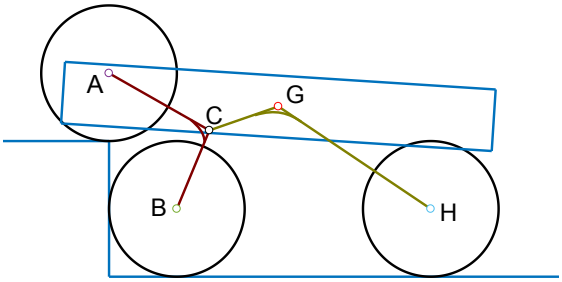

Figure 2.17: Pose 5.

moment balance. All three assemblies are three force systems, and hence the external forces are concurrent. However the points of concurrency are far away.

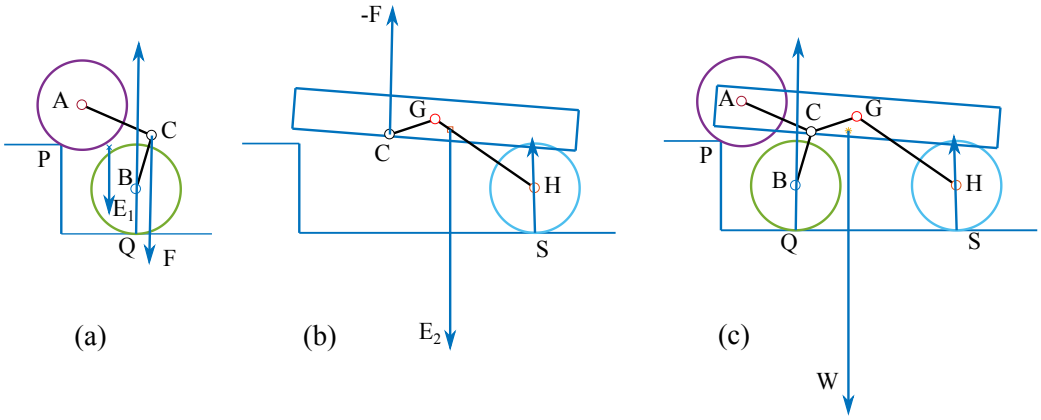

Figure 2.18: External forces on (a) bogie, (b) rocker and body, and (c) entire rover, for optimal solution with $F_{T_1} = F_{N_1} = 0$, at pose 120.

In the special solution for pose 5 discussed above, the optimal solution had $F_{N_1} = 0$. Figure 2.17 shows the rover in pose 5. The front wheel has climbed over the corner of the step and started contacting the landing. The middle wheel appears to be butting against the step in the figure, but is actually contacting the horizontal portion of the ground. An analysis shows that the CoM lies between contact points of wheels 2 and 3. This enables the possibility of the normal reaction on the front wheel being zero. The danger with zero normal force, and how it can be avoided, are discussed in Chapter 3.

Case (c): Nonoptimal Point with Equal Contact Force Ratio

We can also show that equality of contact force ratio magnitude is not a sufficient condition for minimum. For pose 7, we obtained an optimal solution with equal contact force ratio, equal to 0.4457. However, for the same pose, there is another point with equal contact force ratio, equal to 0.4491. This is not even a local minimum of the max objective function, as it does not satisfy KKT conditions. This situation is explained in chapter 3. What it tells us is that, seeking just any equal contact force ratio point, may not give us minimum friction requirement.

2.4.4 Optimal Friction Requirement for Random Poses

Hundred random poses of the optimal rover were generated, and friction requirement minimized. The wheel contact angles of the three wheels were randomly varied between -80° to 80°, and rocker, and bogie angles were randomly varied from -30° to 30°. These hundred random combinations of the five angles are listed in Appendix C.

Friction requirement was minimized for all the hundred random poses. The mean value of optimal contact force ratio was 0.5155, while the highest and lowest values were 2.8934, and 0.0069 respectively. 71 solutions had equal contact force ratios with torques of same sign, 18 solutions had equal contact force ratio magnitudes, but with different signs, and 11 poses did not have even equal contact force ratio magnitudes. These latter 11 solutions had zero as one contact force ratio. This is a clear indication that the type of solutions we had anticipated, namely solutions with different traction force signs, and solutions with unequal contact force ratio magnitudes, could happen on an uneven ground with reasonable probability.

Contact force ratios of four of the solutions are shown in Table 2.3, and their poses in Figure 2.19. In the figures, both contact normal and tangent are shown for the wheels.

Hundred combinations of the five angles mentioned in Appendix C were used to generate hundred random poses for the nominal rover, and the friction requirement minimized for all of them. The mean value of optimal contact force ratio was 0.5027, while

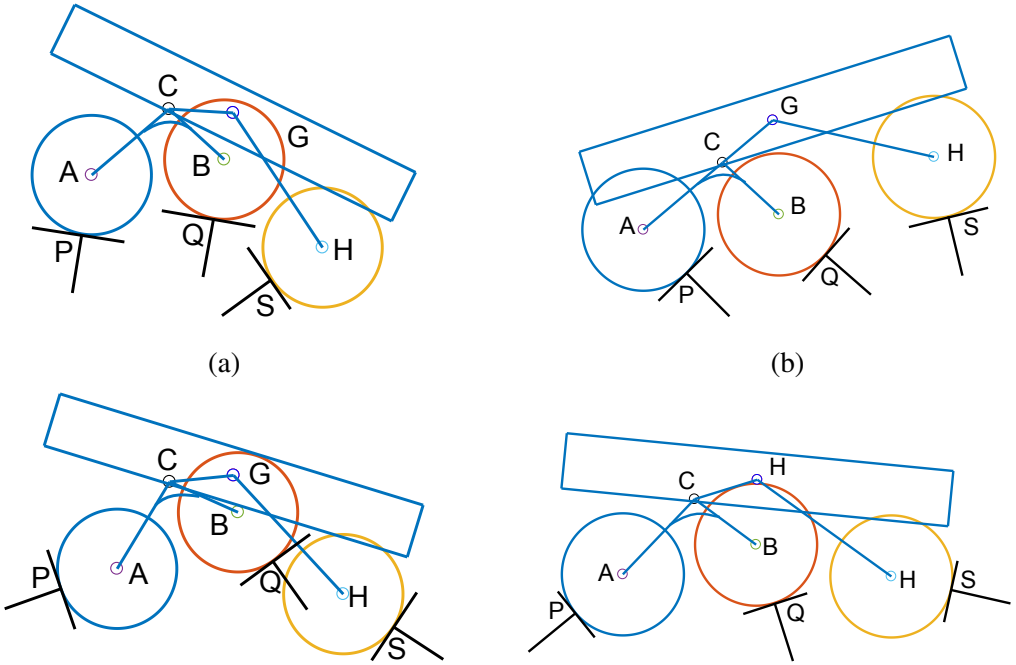

Figure 2.19: Examples from 100 random poses

Table 2.3: Contact force ratio of optimal rover at the four example poses selected from 100 random poses.

Example no.	**First wheel**	**Middle wheel**	**Last wheel**
a	0.4562	0.4562	0.4562
b	-0.7924	-0.7924	-0.7924
c	0.4182	0.4182	-0.4182
d	0.0860	0	-0.4808

the highest and lowest values were 2.2477 and 0.0103 respectively. It was seen that 86 solutions had equal contact force ratios with torques of the same sign, 5 solutions had equal contact force ratio magnitudes, but with different signs, and 9 poses did not have even equal contact force ratio magnitudes. These latter 9 solutions had zero as one contact force ratio.

2.5 Effect of Shifting Centre of Mass

Shifting the center of gravity was used in the Gofor rover [12] to reduce required friction. In this case center of gravity shift was achieved by changing the pose of the rover. Shifting center of gravity using pose change was used by Iagnemma et al. [71] to improve tip over stability of a rover. Shifting of onboard weights to change the normal ground forces, has been discussed by Sandin [72] as a general approach. He describes shifting dedicated weights or payload, and reorienting an onboard manipulator, to enable a robot to step across wide gaps, or climb steeper slopes or higher steps. He points out that the manipulator needs to have reasonable weight for the effects to be significant. Independent of [72], we had also thought of using an onboard manipulator to shift CoM, to reduce the friction required further.

2.5.1 Formulation

A 2 DoF onboard manipulator is attached to the nominal rover, as shown in Figure 2.20. One end of first segment is connected to body using a revolute joint at K, and the other

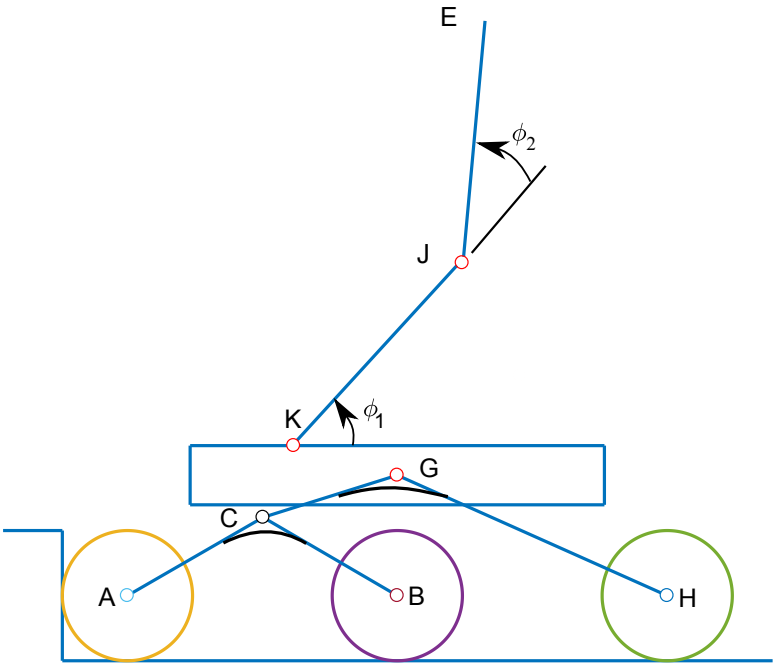

Figure 2.20: Nominal rover with manipulator

end connected to the second segment using a revolute joint J. The motion of the wrist

does not usually change CoM much, and hence not considered. The two segments of the manipulator are positioned using the angles, ϕ_1, and ϕ_2, measured in the ccw, as shown in Figure 5.19. The base revolute joint K, is at a distance of 0.25 times the length of body, measured from the bogie side of rover. The rover body is assumed to have a dimension of 350 mm $\times$ 50 mm. The two segments of manipulator have fixed lengths denoted by l_{m_1} and l_{m_2}, both of which we consider here as 0.2 m. Masses of the two segments, denoted by M_1 and M_2 are taken as equal and as 1 kg here. Center of mass of each segment is assumed to be at the geometric center of each segment.

It can be shown that the important parameter in a shifted CoM is its horizontal position, and not the vertical position. This fact enabled us to use a single parameter x_{manip} for representing the CoM position, instead of ϕ_1 and ϕ_2. Definition of x_{manip}, and its associated local frame is shown in Figure 2.21. A local coordinate frame (x_{lo} y_{lo}) is attached to the body of rover, whose origin coincides with point 'K', and the positive x direction of this local frame aligned with the top surface of body, directed towards the rocker side of rover. The position x_{manip} will fall between the CoMs of the two segments (see Figure 2.21). x_{manip} is related to the manipulator angle ϕ_1 and ϕ_2 by the equation

$$x_{manip} = \frac{M_1 l_{m_1} \cos\phi_1 + M_2 l_{m_2} \cos(\phi_1 + \phi_2)}{M_1 + M_2}. \tag{2.12}$$

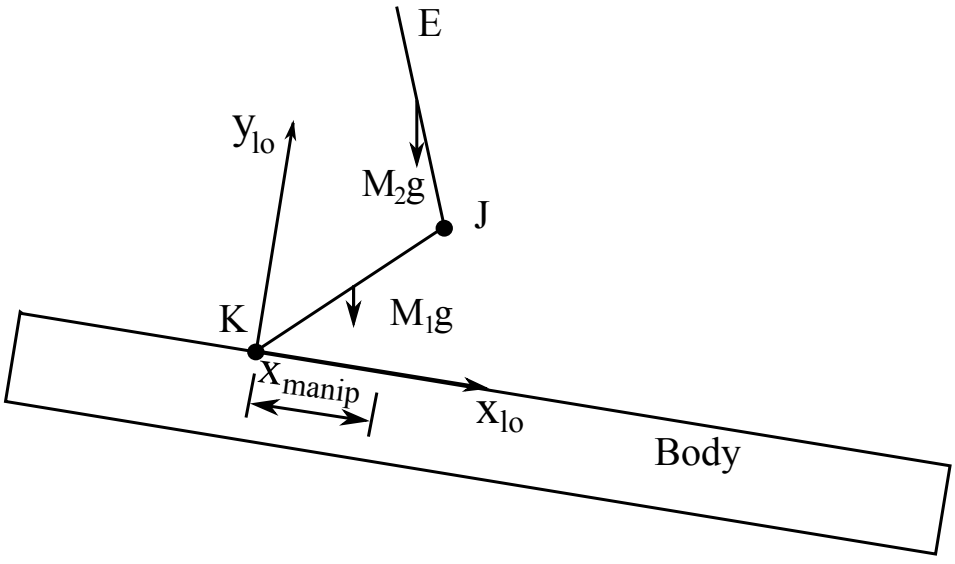

Figure 2.21: Local frame for x_{manip}.

The y coordinate of the CoM of the manipulator is assumed to have zero value in this reference frame. This assumption introduces a small error in our calculations, but this error is small if the angle made by the body with respect to the horizontal is not very high. The limits of x_{manip} can be seen to be $\pm\frac{\left(M_1 l_{m_1}+M_2 l_{m_2}\right)}{(M_1+M_2)}$. Note that if the body of the rover or some feature of terrain does not interfere with the horizontally stretched out pose of the manipulator, this limit is restrictive. Depending on the orientation of the rover body, the limit can be increased on one side. But we do not use that here.

By using x_{manip} as the single manipulator CoM position variable in this fashion, we automatically address the constraint preventing the manipulator from coming below the rover body. Once the optimal x_{manip} value is obtained from solution, in most cases we can have a range of possible corresponding combinations of ϕ_1 and ϕ_2, which the controller can choose appropriately.

The decision variable set consists of x_{manip} in addition to the nine variables as discussed in the formulation for minimizing friction requirement given in Section 2.3. Thus the full set of decision variables are$\{F_{N_1}, F_{T_1}, F_{N_2}, F_{T_2}, F_{N_3}, F_{T_3}, F_1, F_2, x_{manip}, \mu\}$.

The proposed smooth optimization problem stated in words is as follows: Given a pose of the rover and contact points on the wheels, determine the eight forces and x_{manip}, to minimize required coefficient of friction, such that the rover is able to maintain static equilibrium without any adhesion or slip between wheels and ground. Mathematically it can be stated as:

Determine $\{F_{N_1}, F_{T_1}, F_{N_2}, F_{T_2}, F_{N_3}, F_{T_3}, F_1, F_2, x_{manip}, \mu\}$ to

$$\text{minimize } \mu,$$

subject to

$$[A]\{x_F\} = \{b\}, \tag{2.13}$$

$$F_{N_i} \geq 0,\ i = 1, 2, 3, \tag{2.14}$$

$$-\mu F_{N_i} \leq F_{T_i} \leq \mu F_{N_i},\ i = 1, 2, 3, \tag{2.15}$$

$$-\frac{(M_1 l_{m_1} + M_2 l_{m_2})}{(M_1 + M_2)} \leq x_{manip} \leq \frac{(M_1 l_{m_1} + M_2 l_{m_2})}{(M_1 + M_2)},\ and \tag{2.16}$$

$$\mu \geq 0. \tag{2.17}$$

The three non-adhesion conditions, six no slip conditions and the condition for μ are same as that discussed in Section 2.3.

While considering the rover with manipulator for analysis, the free body diagram of the bogie remains same, while the two segment manipulator is also included along with the rocker part, which also contains body and a wheel. The first four equilibrium equations contained in Equation 2.13 are same as that given in the set of equilibrium equations mentioned in Section 2.1. The fifth equilibrium equation will have half the weight of the two segmented manipulator arm, and the sixth equilibrium equation should also include the moment due to the manipulator arm weight.

The constraint Equation 2.16 denotes the range in which the CoM of manipulator arm can be operated. Both the values are the two extreme positions to CoM of the manipulator in the fully stretched out condition, along the top of the body.

Note that our formulation is still smooth and hence we can use gradient based optimization solvers.

For each pose, μ was minimized using 'fmincon' solver in MATLAB®. Randomly selected starting guess for each of the 729 poses were generated as uniformly distributed points in the box $F_{N_1}, F_{N_2}, F_{N_3} \in [0, 100], F_{T_1}, F_{T_2}, F_{T_3}, F_1, F_2 \in [-50, 50], \mu \in [0, 3]$, $x_{manip} \in [-0.5, 0.5]$. The optimal solution obtained for μ was same, when the program was run for multiple times (ten times) with different starting guess solutions.

2.5.2 Results

The effect of shifting CoM was studied on the nominal rover, negotiating a step of height equal to twice the wheel radii. The stretched length of the two segmented manipulator, attached to the nominal rover is about 88% of the wheel base, and its mass is around 12.5% of the rover mass. The rover along with the 2 DoF manipulator considered for study is shown in Figure 2.20.

The variation of coefficient of minimum friction required for the nominal rover to climb a step in forward, and backward directions with and without manipulator are shown

in Figures 2.22 and 2.23 respectively. In the case of forward climbing, the overall peak friction requirement came down only marginally, from 0.5823 to 0.5708, an improvement of only 1.97%. This happened at the pose where the front wheel just buts the step. When the last wheel is negotiating the step, the peak requirement came down more substantially, from 0.5523 to 0.4307, an improvement of 22.02%. The improvements for backward climbing is not substantially different.

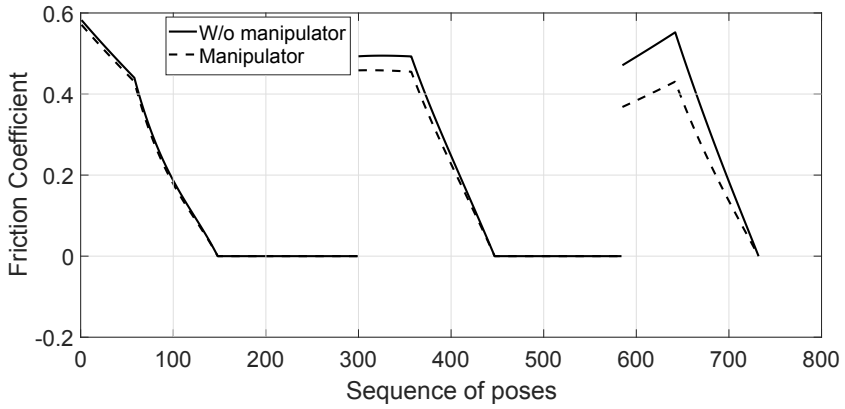

Figure 2.22: Optimal friction coefficient requirement of nominal rocker-bogie rover with and without manipulator for forward climbing.

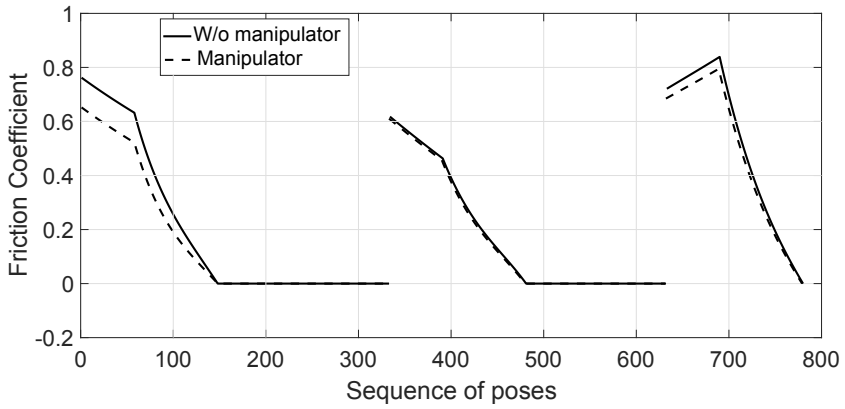

Figure 2.23: Optimal friction coefficient requirement of nominal rocker-bogie rover with and without manipulator for backward climbing.

We show the variation of manipulator arm configuration related parameter x_{manip} , with the sequence of poses during the climbing of a step of height equal to the wheel diameter in the forward direction in Figure 2.24. The three figures below show the poses of the rover with the manipulator pose at three specific poses. The manipulator arm was

extended to the extreme rear end for all the poses from the butting of front wheel with the riser of step, to the pose just before the starting of contact of rear wheel with the riser of step. When rear wheel comes in contact with the step the manipulator arm gets extended to the extreme front end. When the rear wheel is about to touch the step riser, the rover has to be brought to rest in order to avoid impact. This rest can be for a finite interval and used to reconfigure the manipulator, and then the rover can start moving further.

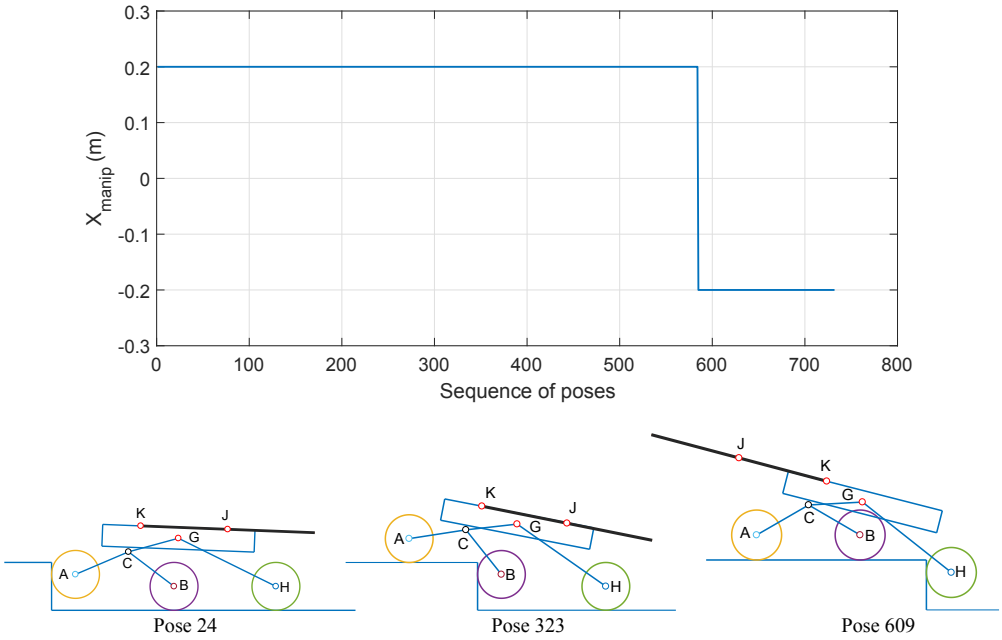

Figure 2.24: Variation of arm configuration related parameter x_{manip}, with the sequence of poses for forward climbing, and rover and manipulator configurations at three specific poses.

We investigated the effect of (a) increasing the manipulator weight by 20%, without changing the segments lengths, and (b) increasing the segment lengths by 20%, without changing the manipulator weight. In case (a), the overall peak optimal requirement improved from 1.97% to 2.34%, while the peak friction requirement during the climbing sequence when the rear wheel climbs the step improved from 22.02% to 25.82%. In case (b), the overall peak optimal requirement improved from 1.97% to 2.71%, while the peak friction requirement during the climbing sequence when the rear wheel climbs the step improved from 22.02% to 25.10%. This clearly shows that as expected, a manipulator with greater weight and greater reach has greater influence on improving the friction

requirement.

There could be a question whether it is a good idea to deploy the manipulator while the rover is moving on an uneven terrain. The manipulator may get subjected to large inertia forces arising from unanticipated shocks and accelerations. This point needs to be taken into account when making a decision. Perhaps in poses where the calculated minimum friction requirement is predicted to cause slip, and the use of CoM shift using manipulator is predicted to prevent that slip, we can think of undocking and using the manipulator.

2.6 Validation of Solutions Using Dynamic Simulation

We could not validate our results, as we did not have access to a rover. Instead, a dynamic analysis was carried out to check the correctness of the optimal solution we obtained using our proposed formulation. Our approach was to apply the torques we obtained from our optimal solution for a pose, to our dynamic model of the rover, assuming that the rover is stationary. The resulting acceleration has to be zero if the torques provide equilibrium, and the resulting reaction forces from the ground have to have the ratios we obtained in our optimization. This would validate the modelling of equilibrium in the formulation of the optimization problem.

The kinematic equations, and dynamic equations of motion (see Appendix A) were derived for the rover, considering the three wheels, the bogie, and the body as free bodies. Thus there are 15 dynamic equations, which contain 14 unknown reaction forces. Kinematic constraints were included considering the wheels to purely roll without slipping on a flat surface, and to purely turn without slipping at the step corner. These kinematic constraints total up to 14.

We considered six segments of motion during step climbing. Segments 1, 3, and 5 represent the front, middle and rear wheels climbing the vertical face of the step. Segments 2, 4, and 6 represent the front, middle and rear wheels climbing the corner of the step. These six segments were required because the kinematic equations are different

when a wheel is on a flat face and when the wheel is at a corner.

We considered the six stationary poses of the nominal rover, numbered as 29, 103, 334, 374, 614, 688, in Section 2.3 and applied the optimal torques obtained as solutions. The resulting accelerations, and deviations of maximum contact force ratio from the optimal friction requirement, are given in Table 2.4. These values can be seen to be equal to zero as expected, within the order of the calculation precision.

Table 2.4: Angular accelerations of front wheel and deviations of maximum contact force ratios from optimal friction when optimal torques are applied.

Pose No.	Angular acceleration of front wheel (rad/s^2)	Max. deviation of μ
29	4.47×10^{-13}	1.78×10^{-15}
103	-2.82×10^{-14}	1.67×10^{-16}
334	-6.05×10^{-14}	1.11×10^{-16}
374	-2.68×10^{-14}	-5.55×10^{-17}
614	1.14×10^{-14}	2.22×10^{-16}
688	5.79×10^{-14}	3.89×10^{-16}

In addition to determining acceleration and ground forces at the above poses, for stationary rover, using forward dynamic calculation, we also simulated the motion of the rover for climbing the step fully, by integrating the equations of motion to validate the formulation in a different way. We describe that, and the results below.

For the six segments mentioned above, we start with the pose at the beginning of the segment, with zero velocity, and apply the torques as functions of the wheel rotation angle. The nominal torques, obtained and interpolated from the results of optimization in Section 2.4.1, as functions of wheel rotation angle, are given in Appendix B. The reason for representing torques as functions of wheel rotation angle is that from our optimal solution, we know torques only as a function of pose. But this has the disadvantage that torque is discontinuous at the junctions of the segments. This is the reason for considering

six segments separately.

We now apply torques in excess of the nominal torques, by 1%, 0.1%, and 0.01%, setting the simulation times to enable the rover to travel the full segment. Figure 2.25 shows how the angular velocity of the first wheel varies with time for 1% excess torque. The maximum angular velocity of 2.078 rad/s with 1% excess torque, comes down to 0.207 rad/s with 0.01% excess torque. The time taken to complete the step climbing sequence increased from 9.637 s to 98.611 s, when the excess torque applied reduced from 1% to 0.01%. This indicates that as excess torque approaches zero, the velocity of the simulated rover also approaches zero. Thus the dynamic aspects of our simulation model (described in Appendix A), are likely to be correct.

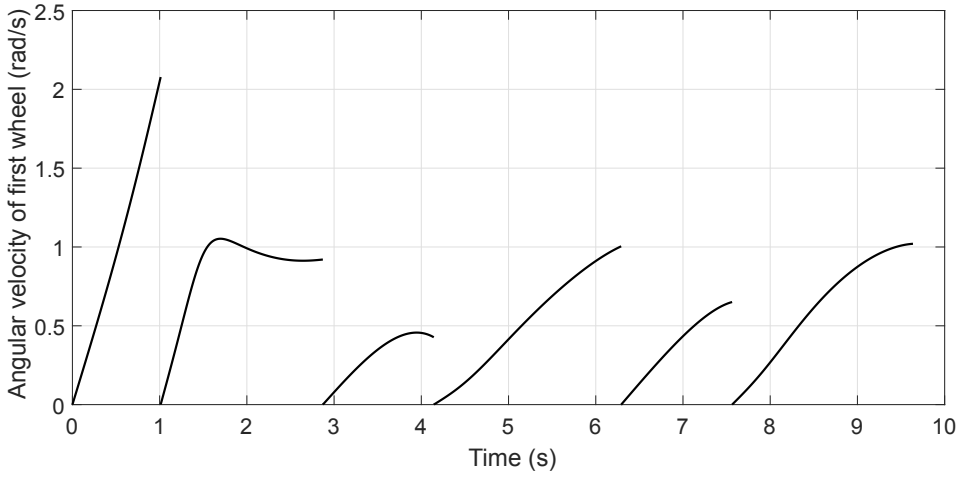

Figure 2.25: Angular velocity of first wheel vs time for 1% excess torque.

Another indication that our dynamic simulation is likely to be correct is the way the normal contact force varies, as the excess torques are reduced. Figure 2.26 shows the difference between normal force for segment 4 when we applied 1% excess torque, and nominal normal force we got for the equilibrium. The fact that these normal forces are different from the nominal normal forces indicate that our dynamic model is different from the equilibrium model. The fact that the magnitude of the maximum difference between actual and nominal normal force came down from 0.1822 N for 1% excess torque to 0.0015 N for 0.01% excess torque, indicates that as excess torque decreases, the rover's dynamic behaviour approaches the equilibrium behaviour.

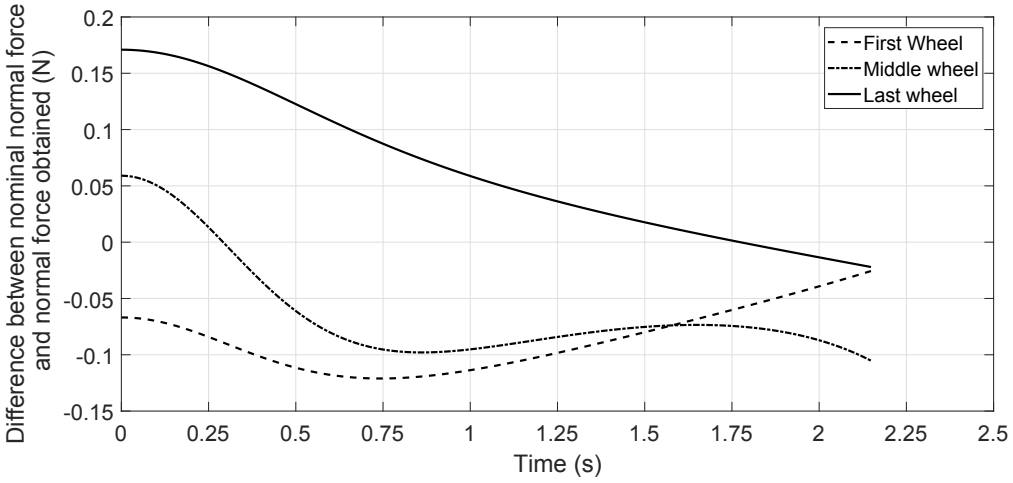

Figure 2.26: Difference between nominal normal force and the normal force obtained while simulating with 1% excess torque.

In the simulation results we used interpolation to locate the poses corresponding to the 147×3 poses we did optimization for, and also obtained interpolated values of the ground reaction forces. We then determined the deviation between the contact force ratios we obtained in simulation and what we obtained in optimization for these 147×3 poses. The maximum deviation of the ratios obtained in simulation from the nominal, are given in the Table 2.5, for the six segments. It can be clearly seen that as the excess torque approaches zero, the deviations in the six segments also approach zero. This shows that it will be possible to make the rover climb with small velocity and acceleration, using torques very close to the nominal, with the friction requirements also being very close to the minimal obtained.

2.7 Conclusion

In this chapter, minimizing the friction requirement, which is the maximum magnitude of contact force ratio, of a six wheeled rover was formulated as a smooth optimization problem. Our formulation yields almost the same result as that of Thueer [42], for the nominal rover. With another rover, and for randomly selected poses for both rovers, our formulation yielded solutions with mixed signs for contact force ratios, and solutions

Table 2.5: Deviation in maximum magnitude of contact force ratios for different values of excess torques.

Excess torque	Deviation in maximum magnitude of contact force ratios					
	Segment 1	Segment 2	Segment 3	Segment 4	Segment 5	Segment 6
1%	5.82×10^{-3}	8.00×10^{-3}	6.03×10^{-3}	6.00×10^{-3}	9.63×10^{-3}	9.43×10^{-3}
0.1%	5.82×10^{-4}	8.34×10^{-4}	6.02×10^{-4}	5.98×10^{-4}	9.55×10^{-4}	9.36×10^{-4}
0.01%	5.82×10^{-5}	8.27×10^{-5}	6.06×10^{-5}	5.97×10^{-5}	9.60×10^{-5}	9.39×10^{-5}

which do not even satisfy equality of magnitudes of contact force ratios. These are solutions which some of the other formulations are not capable of obtaining. We examine the nature of solutions in detail in the next chapter, and propose even more effective non-iterative solution techniques.

The effect of shifting CoM on friction requirement by operating an existing onboard manipulator, was also formulated. The results showed that improvement on maximum friction required was obtained, but was not substantial.

The results obtained based on the proposed formulation were validated using dynamic simulation of the rover.

CHAPTER 3

Analytical Non-iterative Algorithms for Minimizing Friction Requirement

A smooth problem formulation for minimizing friction requirement, without invoking the equal contact force ratios characterization of solutions, was proposed in Chapter 2, and solutions were obtained using a generic numerical solver. This chapter deals with a detailed study of the various ways in which solution can occur, and proposes analytical non-iterative algorithms for solving the problem. Non-iterative algorithms do not have the disadvantage of having to start from suitable guess solutions.

Using the nonsmooth objective function, we can state the problem of minimizing friction requirement as

Determine the six ground reaction forces and the two revolute joint reaction forces to

minimize $max\left\{\left|\frac{F_{T_1}}{F_{N_1}}\right|, \left|\frac{F_{T_2}}{F_{N_2}}\right|, \left|\frac{F_{T_3}}{F_{N_3}}\right|\right\}$

subject to the equilibrium conditions (Equation 2.8), and non-adhesion conditions (inequalities 2.9).

As already mentioned, there have been a few contributions [37, 44] which try to understand the nonsmooth objective function in greater detail, and propose iterative and non-iterative approaches for solution. Our attempt also is to understand the nature of solutions in detail and propose non-iterative solution techniques. We do this for the current version of the problem in which the normal ground reaction forces are bounded below by zero, and also for the problem in which they are bounded below by a positive lower limit. We propose one algorithm each for the two problems, discuss solutions, and compare the speed of our techniques with the iterative approach we described in the previous chapter.

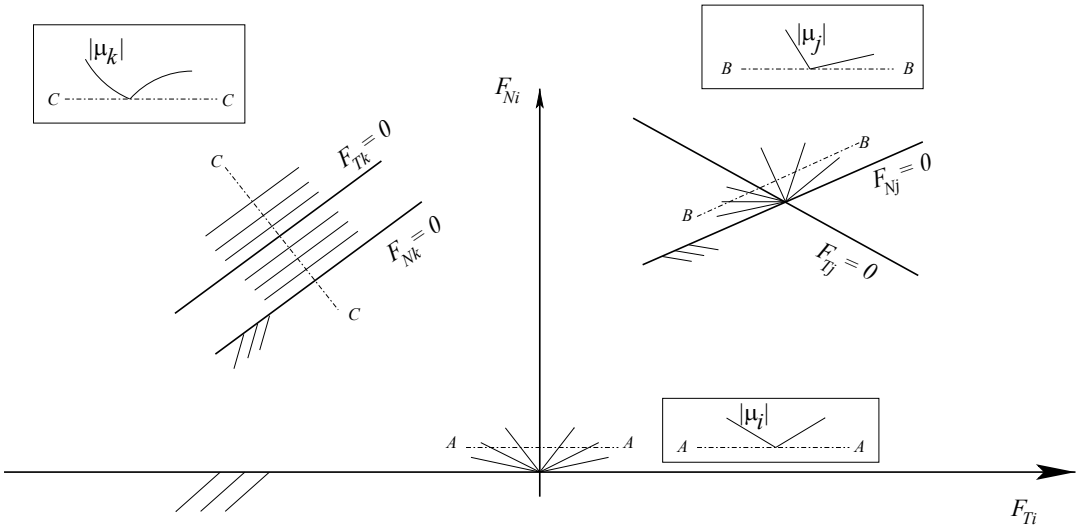

Figure 3.1: Contours of $|\mu_i|$'s.

3.1 Nature of optima: Non-negative Normal Forces

Firstly, the nature of the functions $|\mu_1|$, $|\mu_2|$, and $|\mu_3|$ need to be studied. In the following discussion, we use indices i, j, and k, instead of 1, 2, and 3, in order to prevent perception of preference to any specific wheel. So i, j, and k can be any of 1 or 2 or 3, provided they are not the same.

As there are six equilibrium equations, with 8 unknowns, F_{T_i} and F_{N_i} are assumed as independent free variables. The contours of $|\mu_i|, |\mu_j|, |\mu_k|$ can be represented in the plane of F_{T_i} and F_{N_i}, as shown in Figure 3.1.

From the fact that μ_is are ratios of functions which are linear in F_{T_i} and F_{N_i}, it follows that their contours are straight lines in the decision variable plane. Figure 3.1 shows two ways in which this can occur. In the case of μ_i and μ_j, the contours radiate from the point where the corresponding tangential and normal forces are zero. In the case of μ_k, as there is no point where F_{T_k} and F_{N_k} are simultaneously zero (as $F_{T_k} = 0$ and $F_{N_k} = 0$ lines are parallel), the contours of μ_k are parallel straight lines. Thus the functions μ_is are ruled surfaces. We also note that μ_js are identically zero on the straight lines $F_{T_j} = 0$ for j=1, 2, 3.

To understand the nature of $|\mu_i|$s, we show their variations on certain straight lines

which intersect their contours. The insets (in Figure 3.1) show the variation of $|\mu_i|$s, while we are moving on each of the lines $A-A$, $B-B$ and $C-C$. For $|\mu_i|$ and $|\mu_j|$, these straight lines are $A-A$ and $B-B$ respectively (see Figure 3.1). Both functions reach zero and then change slopes discontinuously. This is expected as we are plotting $|\mu_i|$ and not μ_i. On the entire line $F_{T_i}=0$, $|\mu_i|$ is non-differentiable. Similar behaviour is seen for $|\mu_k|$ on the line $C-C$ which is perpendicular to the contours. An additional fact to note in this case is that the value of $|\mu_k|$ blows up as the point $F_{N_k}=0$ is approached. On the entire line $F_{N_i}=0$, $|\mu_i|$ has a singularity, and is indeterminate. At the point $F_{T_i}=0$ and $F_{N_i}=0$ also, $|\mu_i|$ is indeterminate, but we define the value to be zero. Thus the point $F_{T_i}=0$ and $F_{N_i}=0$ is a singularity and has discontinuity. Such points could be in the feasible space, and could even be a solution, as we saw in the last chapter. In our analysis, we deal with such points specifically.

Note that we do not consider cases where the normal and tangential forces are constant with respect to the independent decision variables.

We now consider the possibility of occurrence of the following types of isolated local minima. Let us call the optimum value as $\mu^* = \min\ (\max\{|\mu_i|, |\mu_j|, |\mu_k|\})$

- Case 1: $\mu^* = |\mu_i| > |\mu_j|, |\mu_k|$.
- Case 2: $\mu^* = |\mu_i| = |\mu_j| > |\mu_k|$.
- Case 3: $\mu^* = |\mu_i| = |\mu_j| = |\mu_k|$.

In addition to the above three cases, we examine whether the special points $F_{T_i} = 0,\ F_{N_i} = 0$ can be isolated local minima. This is case 4.

3.1.1 Case 1: $\mu^* = |\mu_i| > |\mu_j|, |\mu_k|$

The way an isolated local minimum of this type can happen, is for μ_i (or $-\mu_i$) to attain an isolated minimum. Thus the point has to be a minimum of the function μ_i (Figure 3.2 shows this conceptually).

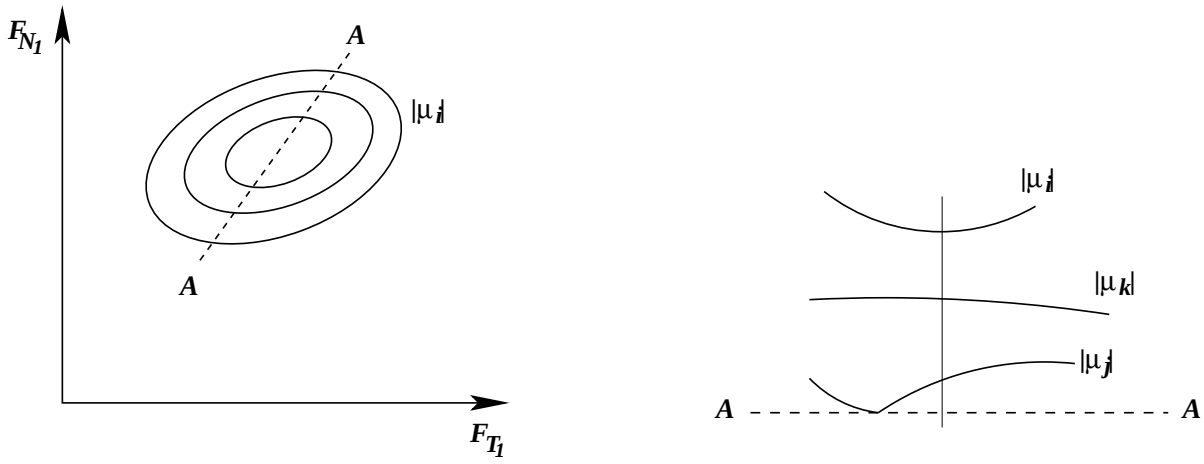

Figure 3.2: (a) Contours of $|\mu_i|$ for case 1, (b) variation of $|\mu_i|, |\mu_j|, |\mu_k|$ on $A - A$.

Without loss of generality, let us consider F_{T_1} and F_{N_1} to be the independent variables. For the pose under consideration, using the equilibrium equations, we can write $F_{T_i} = a_1 F_{T_1} + b_1 F_{N_1} + c_1$, and $F_{N_i} = a_2 F_{T_1} + b_2 F_{N_1} + c_2$. Here $a_1, b_1, c_1, a_2, b_2, c_2$ are specific numerical values obtained from the equilibrium equations, as explained later. Now μ_i can be expressed as

$$\mu_i = \frac{F_{T_i}}{F_{N_i}} = \frac{a_1 F_{T_1} + b_1 F_{N_1} + c_1}{a_2 F_{T_1} + b_2 F_{N_1} + c_2}. \tag{3.1}$$

To find where μ_i attains stationarity, we equate the gradient $\nabla \mu_i$ to the null vector. From this we find that stationarity happens at the point

$$F_{T_1} = \frac{c_1 b_2 - c_2 b_1}{a_2 b_1 - a_1 b_2}, \tag{3.2}$$

$$F_{N_1} = \frac{a_1 c_2 - a_2 c_1}{a_2 b_1 - a_1 b_2}. \tag{3.3}$$

But the above is precisely the point where $F_{T_i} = F_{N_i} = 0$. At this point μ_i is indeterminate. However, we define $\mu_i = 0$, as $F_{T_i} = 0$. Hence $|\mu_i|$ cannot be greater than μ_j or μ_k at this point. Hence an isolated minimum of the type in case 1 cannot occur. Note that at the point $F_{T_i} = F_{N_i} = 0$, the gradient of μ_i is not defined, as it involves a division of zero by zero.

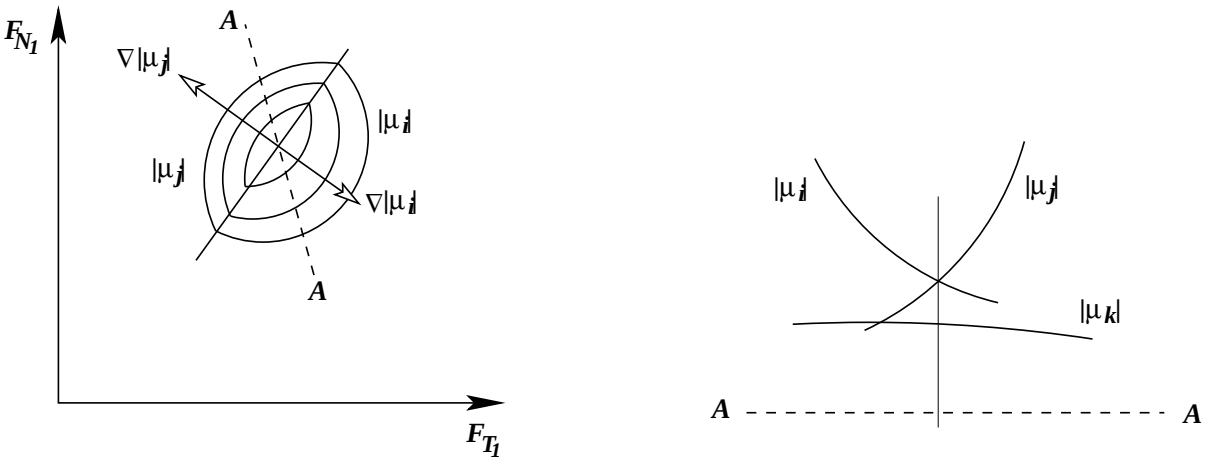

Figure 3.3: (a) Contours of $|\mu_i|$ and $|\mu_j|$ for case 2, (b) variation of $|\mu_i|, |\mu_j|, |\mu_k|$ on $A - A$.

The fact that $|\mu_i|$ cannot have an isolated minimum other than perhaps at $F_{T_i} = F_{N_i} = 0$, is evident from Figure 3.1, and the associated discussion on variation of $|\mu_i|$s.

3.1.2 Case 2: $\mu^* = |\mu_i| = |\mu_j| > |\mu_k|$

Figure 3.3 visualizes how this case could occur. In Figure 3.3a we see the contours of $|\mu_i|$ and $|\mu_j|$ on the F_{T_1}, F_{N_1} plane. Variation of all three contact force ratios are shown in Figure 3.3b, on a line segment A-A which passes through the possible optimum. It can be seen that there is a gradient discontinuity at the optimum.

Now we consider the algebraic condition for the above point to be an optimum. At a local minimum which satisfies this case, the two gradients $\nabla|\mu_i|$ and $\nabla|\mu_j|$ have to be parallel and in opposite directions, as shown in Figure 3.3a. We can now write an expression for μ_j. Using the equilibrium equations, treating F_{T_1} and F_{N_1} to be the independent variables like before, we can write $F_{T_j} = d_1 F_{T_1} + e_1 F_{N_1} + f_1$, and $F_{N_j} = d_2 F_{T_1} + e_2 F_{N_1} + f_2$. Here $d_1, e_1, f_1, d_2, e_2, f_2$ are specific numerical values obtained from the equilibrium equations, as explained later. Now μ_j can be expressed as

$$\mu_j = \frac{F_{T_j}}{F_{N_j}} = \frac{d_1 F_{T_1} + e_1 F_{N_1} + f_1}{d_2 F_{T_1} + e_2 F_{N_1} + f_2}. \tag{3.4}$$

Now the condition of equality of μ_i and μ_j, and the condition that the gradients $\nabla\mu_i$ and $\nabla\mu_j$ are parallel, can be written as

$$\frac{a_1F_{T_1} + b_1F_{N_1} + c_1}{a_2F_{T_1} + b_2F_{N_1} + c_2} = \frac{d_1F_{T_1} + e_1F_{N_1} + f_1}{d_2F_{T_1} + e_2F_{N_1} + f_2}, \tag{3.5}$$

$$\frac{(a_1b_2 - a_2b_1)F_{N_1} + (a_1c_2 - a_2c_1)}{(a_2b_1 - a_1b_2)F_{T_1} + (c_2b_1 - c_1b_2)} = \frac{(d_1e_2 - d_2e_1)F_{N_1} + (d_1f_2 - d_2f_1)}{(d_2e_1 - d_1e_2)F_{T_1} + (f_2e_1 - f_1e_2)}. \tag{3.6}$$

The first of the above, when cross multiplied, is quadratic in the unknowns F_{T_1} and F_{N_1}, and we can see that the corresponding curve passes through the two points $F_{T_i} = F_{N_i} = 0$, and $F_{T_j} = F_{N_j} = 0$. The second condition reduces to the following linear equation

$$lF_{T_1} + mF_{N_1} + n = 0 \tag{3.7}$$

where $l = ((a_1c_2 - a_2c_1)(e_1d_2 - e_2d_1) - (d_1f_2 - d_2f_1)(b_1a_2 - b_2a_1))$,
$m = ((a_1b_2 - a_2b_1)(e_1f_2 - e_2f_1) - (d_1e_2 - d_2e_1)(b_1c_2 - b_2c_1))$,
$n = ((a_1c_2 - a_2c_1)(e_1f_2 - e_2f_1) - (b_1c_2 - b_2c_1)(d_1f_2 - d_2f_1))$,

which represents a straight line through the points $F_{T_i} = F_{N_i} = 0$, and $F_{T_j} = F_{N_j} = 0$. The above two equations can be reduced to a single quadratic in either F_{T_1} or F_{N_1} and solved. On solving, it can be seen that the two solutions correspond to the points $F_{T_i} = F_{N_i} = 0$ and $F_{T_j} = F_{N_j} = 0$.

It is easy to see why we got the above points as solutions. At the point $F_{T_i} = F_{N_i} = 0$, both μ_i and its gradient are indeterminate, involving division of zero by zero. The cross multiplications involved in reducing the conditions makes us multiply deterministic values of μ_j and its gradient by zero, and hence the conditions become satisfied at the point $F_{T_i} = F_{N_i} = 0$. The same arguments can be made for the point $F_{T_j} = F_{N_j} = 0$. As the two points actually do not satisfy our original conditions, and no other point also satisfies them, we can conclude that in general, there are no points which satisfy the conditions of case 2.

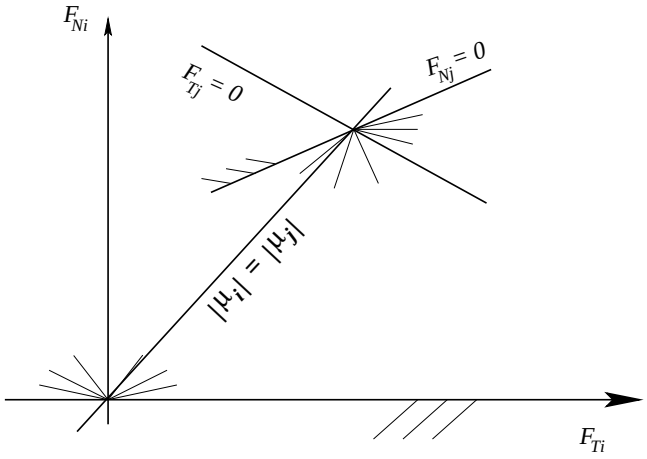

Figure 3.4: $|\mu_i| = |\mu_j|$ straight line satisfying the condition for minimum.

A special case can occur when the quadratic arising from equality of μ_i and μ_j degenerates into a straight line. This would happen when the value of $|\mu_i|$ at the point $F_{T_j} = F_{N_j} = 0$ becomes equal to the value of μ_j at $F_{T_i} = F_{N_i} = 0$. When this happens, the entire straight line through the two points satisfies the two conditions. This situation is illustrated in Figure 3.4. This is a very special situation. We do not consider such special cases for developing our current algorithms.

3.1.3 Case 3: $\mu^* = |\mu_i| = |\mu_j| = |\mu_k|$

As mentioned earlier, most researchers use the condition $\mu_1 = \mu_2 = \mu_3$ to characterize optima, and have obtained solutions of this type. Hence we do not attempt to prove its existence. As there are two independent decision variables, and as cases 1 and 2 have been shown to not exist, the general solution can be expected to be of this type, which satisfy two equality conditions. In fact one of the main contributions of this work is to obtain such solutions analytically. This analytical procedure will be described later in detail.

We now describe the conditions under which points with equal magnitudes of the three contact force ratios are local minima. Let a point satisfying the condition of case 3 be in feasible space. The condition for such a point to be a local minimum is that the convex hull of the subgradients of μ contains the null vector [73]. This condition is

easily stated mathematically as follows. Let $\nabla|\mu_i|,\ i = 1, 2, 3$. Then the point is a local minimum if

$$\alpha_1 \nabla|\mu_1| + \alpha_2 \nabla|\mu_2| + \alpha_3 \nabla|\mu_3| = \phi, \tag{3.8}$$

$$\alpha_1 + \alpha_2 + \alpha_3 = 1, \tag{3.9}$$

$$\alpha_i > 0, i = 1, 2, 3.$$

We can solve the above three equations (first equation (3.8) is a vector equation of dimension 2) to obtain $\alpha_1, \alpha_2, \alpha_3$. If all of them are positive, the point is a local minimum. If any of them is negative, the point is not a local minimum. If the three of them are non-negative, and one or more is zero, then we need to determine the higher derivatives to come to a conclusion.

For example, consider pose 7 of optimal rover discussed as case (c) in Subsection 2.4.3. At that pose, we stated that a point with $\mu = 0.4491$, has equal contact force ratio magnitudes, but is not a local minimum. By applying the condition for optimality, (3.8) and (3.9), the values of the multipliers are $\alpha_1 = -0.0615$, $\alpha_2 = 0.0505$, and $\alpha_3 = 1.0110$. As one of them is negative, this point with equal contact force ratio magnitudes, is not a local minimum.

3.1.4 Case 4: $F_{T_i} = F_{N_i} = 0$

There are two possible ways in which this point can be a local minima.

- $F_{T_i} = F_{N_i} = 0,\ \mu^* = |\mu_j| > |\mu_k|$
- $F_{T_i} = F_{N_i} = 0,\ \mu^* = |\mu_j| = |\mu_k|$

The latter one will occur only with zero probability, and hence is not considered here. Let us consider the first case.

$F_{T_i} = F_{N_i} = 0,\ |\mu_j| > |\mu_k|$:

Let us call this 'special point'. As already mentioned, μ_i is indeterminate at the special point. We assign it the value zero, as the traction force required, $F_{T_i} = 0$. Arbitrarily close to the special point, $|\mu_i|$ can discontinuously jump to any value in $[0, \infty]$, depending on the direction. Based on this special behaviour, how this point can be an isolated minimum, was explained in Section 2.4.3.

We now describe a way to check whether this special point $F_{T_i} = F_{N_i} = 0$ is a local minima or not, assuming that it is feasible for the constraints $F_{N_j} \geq 0$, and $F_{N_k} \geq 0$

The key idea is to check whether in some feasible descent direction of $|\mu_j|$, $|\mu_i|$ will be less than $|\mu_j|$. In that case we can decrease $|\mu_j|$ at least for some distance in that direction, with $|\mu_i|$ and $|\mu_k|$ staying below $|\mu_j|$, and hence the special point is not a local minimum. If such a direction does not exist, i.e., in all feasible descent directions for $|\mu_j|$, $|\mu_i|$ has a higher value than $|\mu_j|$ value at the special point, then it is a local minimum.

There are two cases to be considered, illustrated in Figure 3.5, as (a) and (b). The figure shows the special point which is the intersection of straight lines $F_{N_i} = 0$ and $F_{T_i} = 0$. The contour of $|\mu_j|$ through this point, and the gradient $\nabla|\mu_j|$ are also shown. In case (a), the line $F_{T_i} = 0$ is in the cone of feasible descent directions of μ_j. In this case, the special point is not a local minimum, as $|\mu_j|$ can be decreased in the direction of the line $F_{T_i} = 0$, without becoming lower than $|\mu_k|$.

In case (b), the line $F_{T_i} = 0$ is not in the cone of feasible descent directions. In that case, the least value of $|\mu_i|$ is in the feasible direction in which $|\mu_j|$ is stationary. If this lowest value of $|\mu_i|$ is lower than the value of $|\mu_j|$ at the special point, then the point cannot be a local minimum, as $|\mu_j|$ can be decreased in that direction. If this lowest value of $|\mu_i|$ is higher than the value of $|\mu_j|$, then the special point is a local minimum.

Later we will show examples of special points which are examples of the above two cases.

The pseudocode for an algorithm for checking whether a point with $F_{N_i} = F_{T_i} = 0$ is a local minimum or not, is given below.

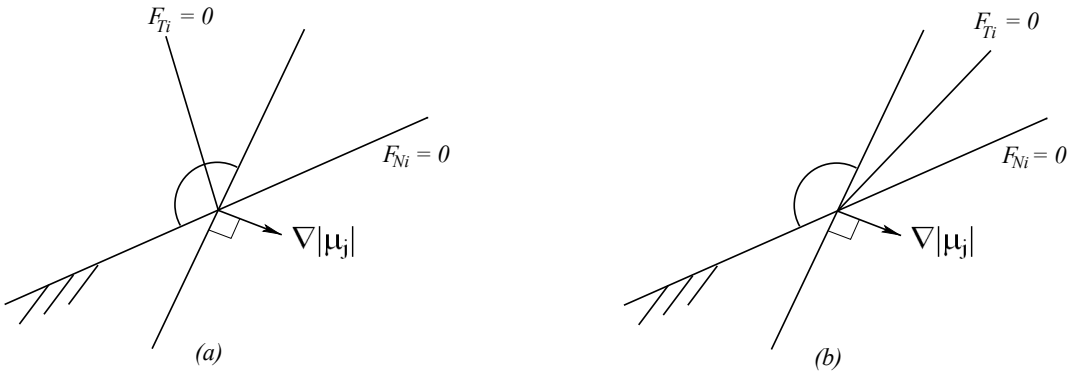

Figure 3.5: Two cases of special point. (a) the line $F_{T_i} = 0$ is in the cone of feasible descent directions, (b) the line $F_{T_i} = 0$ is not in the cone of feasible descent directions.

Without loss of generality, we assume $\mu^* = |\mu_j| > |\mu_k|$.

Let

$F_{T_i} = a_1 F_{T_1} + b_1 F_{N_1} + c_1$,

$F_{N_i} = a_2 F_{T_1} + b_2 F_{N_1} + c_2$,

$\bigtriangledown|\mu_j| = \{d, e\}^T$,

$|\mu_i|_{min}$: the smallest nonzero value of $|\mu_i|$, arbitrarily close to the point $F_{N_i} = F_{T_i} = 0$, in the feasible region.

Step 1: Check whether the straight line $F_{T_i} = 0$ is in the cone of directions which are feasible for $F_{N_i} > 0$, and descent for $|\mu_j|$ (case shown in Fig. 3.5a). This is true if $(\{-b_1, a_1\}\{a_2, b_2\}^T)(\{-b_1, a_1\} \bigtriangledown |\mu_j|) < 0$. In that case, declare that point $F_{T_i} = F_{N_i} = 0$ is not a local minimum and stop. Else proceed.

Step 2: Calculate $|\mu_i|_{min} = \left| \dfrac{-a_1 e + b_1 d}{-a_2 e + b_2 d} \right|$.

Step 3: If $|\mu_i|_{min} > \mu^*$, the special point is a local minimum.

If $|\mu_i|_{min} < \mu^*$, the special point is not a local minimum.

Note: We have not considered the special zero probability cases, where the above strict inequalities do not hold.

3.2 Analytical Determination of Equal Force Ratio Points

As already discussed, there are six equilibrium equations which are linear in the eight unknowns (normal reactions F_{N_1},F_{N_2},F_{N_3}, traction forces F_{T_1},F_{T2},F_{T_3}, and components of force at joint 'C', F_1, F_2). Two free variables can be chosen from the eight unknowns, as independent variables. The six equilibrium equations can be re-written in matrix form with two free variables moved to the right hand side.

$$[A^*]\{V_1\} = \{F\} - [G]\{V_2\} \tag{3.10}$$

where $\{V_1\}$ is a column vector of the six dependent variables, $[A^*]$ is a 6×6 matrix which consists of the coefficients of the six variables chosen in $\{V_1\}$ matrix, $\{F\}$ the column vector in Equation. 2.1, $[G]$ the coefficients of the two free variables and $\{V_2\}$ the two free variables. In our case the free variables chosen are F_{T_1} and F_{N_1}.

While choosing the two free variables, rank of $[A^*]$ needs to be six. If the rank of $[A^*]$ is less than six, then there can be solution only if the columns of $\{F\}$ and $[G]$ are in the subspace spanned by the columns of $[A^*]$.

Multiplying with the inverse of $[A^*]$ on both sides of Equation 3.10, we get

$$\{V_1\} = [c] + [a\ b]\{V_2\} \tag{3.11}$$

where $[c] = [A^*]^{-1}\{F\}$, $[a\ b] = -[A^*]^{-1}[G]$
The system of Equations (3.11) can be written as

$$
\begin{aligned}
F_{T_2} &= a_1 F_{T_1} + b_1 F_{N_1} + c_1; \quad & F_{N_2} &= a_2 F_{T_1} + b_2 F_{N_1} + c_2; \\
F_{T_3} &= a_3 F_{T_1} + b_3 F_{N_1} + c_3; \quad & F_{N_3} &= a_4 F_{T_1} + b_4 F_{N_1} + c_4; \\
F_1 &= a_5 F_{T_1} + b_5 F_{N_1} + c_5; \quad & F_2 &= a_6 F_{T_1} + b_6 F_{N_1} + c_6;
\end{aligned} \tag{3.12}
$$

We are seeking points in space of $F_{T_1} - F_{N_1}$ where the force ratio $\mu_i = \dfrac{F_{T_i}}{F_{N_i}}$ is same in magnitude for all the wheels. In terms of equations:

$$
\pm\frac{F_{T_1}}{F_{N_1}} = \pm\frac{F_{T_2}}{F_{N_2}} = \pm\frac{F_{T_3}}{F_{N_3}}
$$

Positive and negative signs for traction force are possible, because the wheel torque can be applied in forward or backward directions at any pose, to put the entire system in equilibrium. Positive sign is assigned for torques applied in the counter-clockwise direction.

We introduce a variable t and write the above two equations as three equations.

$$
\frac{F_{T_i}}{F_{N_i}} = s_i t, \; i = 1, 2, 3 \tag{3.13}
$$

where $s_i = \pm 1, i = 1, 2, 3$.

Writing $F_{T_i}, F_{N_i}, \; i = 2, 3$ in terms of F_{T_1} and F_{N_1}, and eliminating F_{T_1} and F_{N_1}, we obtain the following cubic equation in t.

$$
P_3 t^3 + P_2 t^2 + P_1 t + P_0 = 0, \tag{3.14}
$$

where the coefficients P_3, P_2, P_1, P_0 are

$$
\begin{aligned}
P_3 &= s_1 s_2 s_3 (c_4 a_2 - c_2 a_4); \\
P_2 &= s_1 s_2 (c_2 a_3 - c_3 a_2) + s_1 s_3 (a_4 c_1 - c_4 a_1) + s_2 s_3 (b_2 c_4 - b_4 c_2); \\
P_1 &= s_1 (c_3 a_1 - c_1 a_3) + s_2 (c_2 b_3 - c_3 b_2) + s_3 (b_4 c_1 - c_4 b_1); \\
P_0 &= c_3 b_1 - c_1 b_3.
\end{aligned} \tag{3.15}
$$

Note that coefficients a_i, b_i, c_i, etc are described in Equation 3.12 and are obtained from Equation 3.11. We solve the cubic equation to obtain solutions for t. Then using two of the equations in Equation (3.13) we obtain F_{N_1}, and F_{T_1}. Once the two forces (F_{N_1}, F_{T_1}) are known, all the remaining forces can be obtained from Equation 3.12. The roots of the cubic polynomial were obtained explicitly by the solution procedure described in [74].

As already mentioned, traction forces can have positive or negative sign. This will result in eight combinations of equal force ratios. Out of the eight combinations, only four cases need to be considered (while the other four are equivalent to them). They are listed as follows.

- Case 1: $\mu_1 = \mu_2 = \mu_3$ same as $-\mu_1 = -\mu_2 = -\mu_3$
- Case 2: $\mu_1 = \mu_2 = -\mu_3$ same as $-\mu_1 = -\mu_2 = \mu_3$
- Case 3: $\mu_1 = -\mu_2 = \mu_3$ same as $-\mu_1 = \mu_2 = -\mu_3$
- Case 4: $\mu_1 = -\mu_2 = -\mu_3$ same as $-\mu_1 = \mu_2 = \mu_3$

We can see that without loss of generality, we can assume $s_1 = +1$, with s_2 and s_3 taking the four possible combinations of values. Each case can have a maximum of 3 real solutions, and hence altogether, a maximum of 12 solutions can be obtained. Complex solution corresponds to a situation which is not feasible. Of these, real solutions with non-negative values for the three normal forces, are the feasible points with equal contact force ratio magnitudes. All of them need not be local minima.

3.3 Algorithm 1 and Solutions

Based on the above discussion, we propose the following non-iterative algorithm for finding the global minimum of μ, subject to $F_{N_i} \geq 0,\ i = 1, 2, 3$.

3.3.1 Algorithm 1

Step 1: Determine the 12 points of the type $\frac{F_{T_1}}{F_{N_1}} = s_2\frac{F_{T_2}}{F_{N_2}} = s_3\frac{F_{T_3}}{F_{N_3}}$, $s_2, s_3 = \pm 1$, and from them collect all the real solutions which are feasible $(F_{N_i} \geq 0,\ i = 1, 2, 3)$.

Step 2: Determine special points of the type $F_{T_i} = F_{N_i} = 0,\ i = 1, 2, 3$, and from them collect the feasible points.

Step 3:

if feasible sets in steps 1 and 2 are empty **then**

declare "no feasible solution", and stop.

else

from the feasible points identified in steps 1 and 2, declare the one with lowest μ as global minimum, and stop.

end

Note that as we are selecting the best point from amongst the feasible equal force ratio points and special points, there is no need to waste time in checking whether it is a local minimum.

This algorithm does not address the special cases of solution, like that mentioned in Case 3.1.2, where an entire line segment can be the solution.

3.3.2 Results and Discussion

544 poses of the optimal rover of Chapter 5 were solved using the proposed algorithm 1. Among the 544 poses, 100 poses are randomly selected (see Section 3.6, and Appendix C), and the remaining 444 poses correspond to the sequence of rover climbing step equal to the diameter of wheel, mentioned in Chapter 2. Among the 544 poses solved, equal contact force ratio solution was obtained for 500 poses, and the remaining 44 poses had special points with one wheel having $F_{T_i} = F_{N_i} = 0$, as solutions.

Two poses from the optimally designed rover were selected for discussing the solutions. These poses are designated as pose numbers 225 and 120, and are shown in Figures 3.6a, and 3.6b.

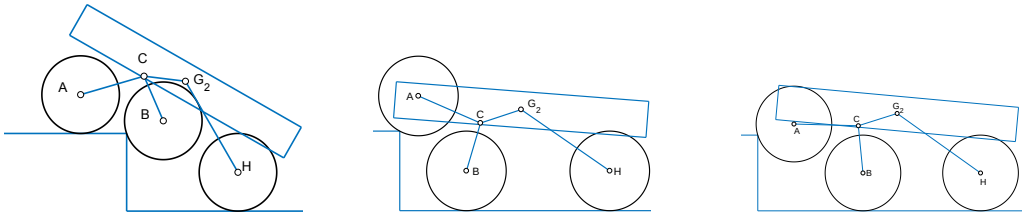

(a) Rover pose 225. (b) Rover pose 120. (c) Rover pose 75.

Figure 3.6: Different poses of optimal rover considered.

These poses were chosen because, for pose 225 the global minimum is a point with equal force ratio magnitudes, and for pose 120 the global minimum is a point where the tangential and normal forces on one wheel are zero.

Solution for pose 225

Here the middle wheel is at the step corner (shown in Figure 3.6a). Various points obtained and solution are analysed below, in detail.

- Of the 12 points obtained using equal contact force ratio condition, four are imaginary and four have negative normal forces. Remaining four points are real and feasible, and out of them only one is a local minimum and is the global solution with objective function value of 0.2660. The other three which are not local minima, have objective function values close to this.
- Of the three points with $F_{T_i} = F_{N_i} = 0,\ i = 1, 2, 3$, one is infeasible while the other two are not local minima.

Contour plot of max contact force ratio μ in the decision variable space $F_{T_1} - F_{N_1}$ for pose 225 is shown in Figure 3.7. The right hand side of the line $F_{N_2} = 0$, is the feasible region in the window shown in figure. All four feasible equal contact force ratio points are shown, denoted by letters, A, B, C, and D. The point A is the global minimum. Of the two feasible points of the type $F_{T_i} = F_{N_i} = 0$, one of them, E appears on the plot.

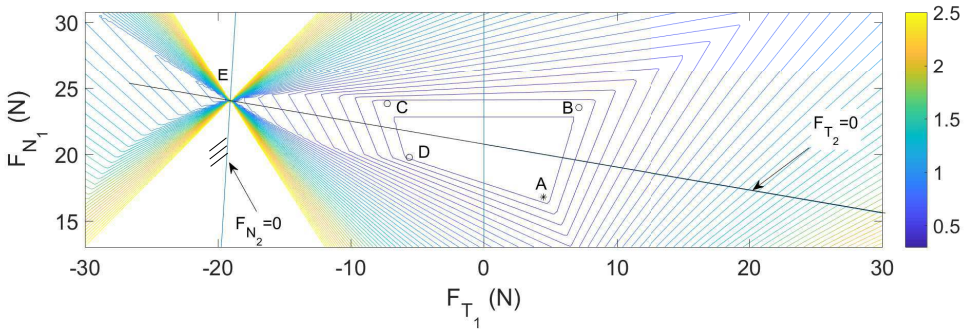

Figure 3.7: Contour plot of contact force ratios for pose 225.

The global minimum A, and the point E with $F_{T_2} = F_{N_2} = 0$, but not a local minimum, are shown separately in Figure 3.8.

From Figure 3.8a, it is evident that point A has equal values for $|\mu_1|, |\mu_2|, |\mu_3|$. From the directions of the gradients $\bigtriangledown|\mu_1|, \bigtriangledown|\mu_2|, \bigtriangledown|\mu_3|$, it is possible to see that the null vector is inside the convex hull of the three gradients. For the point A, all the three multipliers in the condition for optimality, (3.8), and (3.8), are positive ($\alpha_1 = 0.0267$, $\alpha_2 = 0.0626$, and $\alpha_3 = 0.9107$), and hence A is an isolated local minimum of μ.

At point E where $F_{T_2} = F_{N_2} = 0, \mu = |\mu_1|$ (Figure 3.8b). As the line $F_{T_2} = 0$ is inside the cone of feasible directions, it is evident that we can move from E along this line for a finite distance, decreasing μ. Hence E cannot be a local minimum.

It has to be noted that apart from A, even though three more feasible equal contact force ratios are also available (B, C, and D), none of these points are local minima. Thus, as already demonstrated when discussing type 3 points, it is not necessary that all equal contact force ratio points are local optima. Looking at Figure 3.7, one might think that only two ratios are equal at points B, C, and D. Let's consider point B. Figure 3.9 shows a closer view of point B, along with the dominant μs at each region. We have taken contours, which are closer than in Figure 3.7. From this it is clear that point B is an intersection of three equal μ_is. Similar finer contour plots can also be taken at points C, and D, to show that they are also intersections of three equal μ_is.

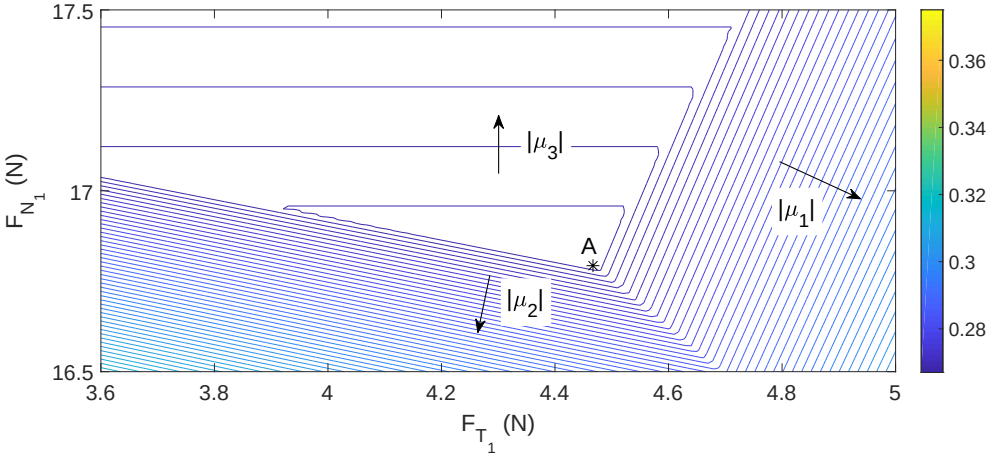

(a) Contour around A.

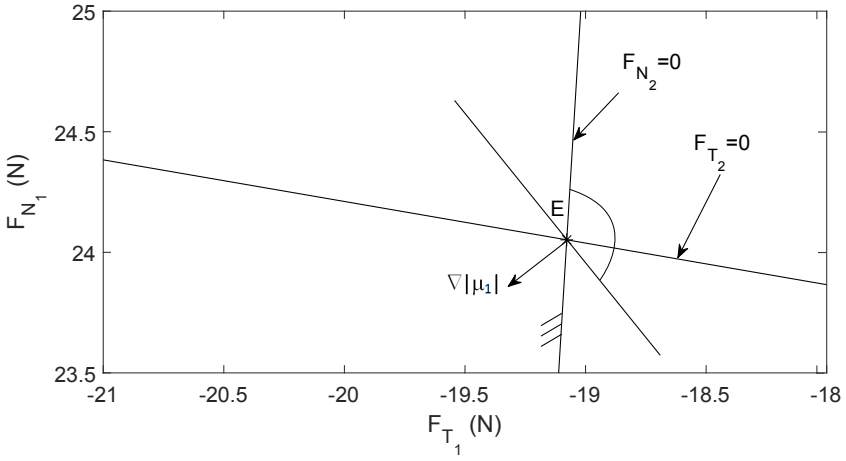

(b) Contour around E.

Figure 3.8: Close up view of points A, and E for pose 225.

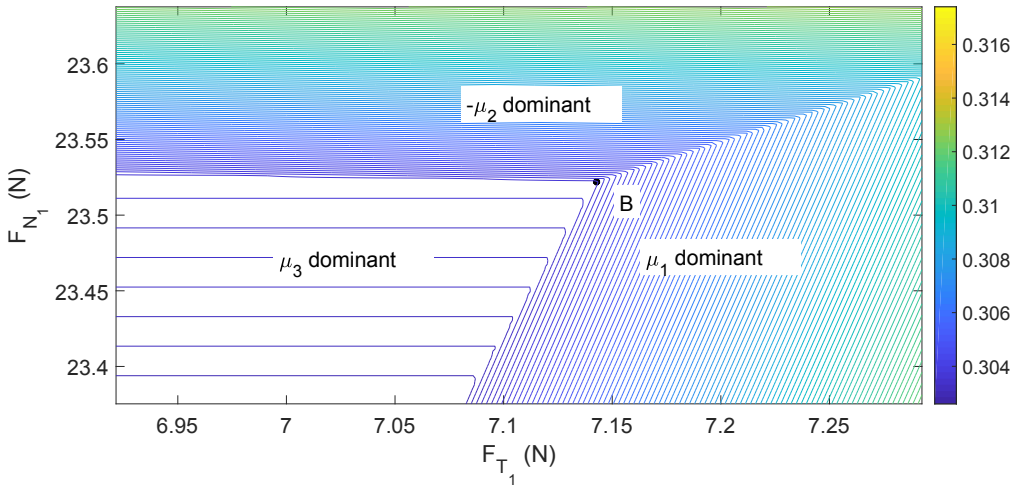

Figure 3.9: Close up view of point B for pose 225.

Solution for pose 120

Here the first wheel is at the corner of the step (see Figure 3.6b). Various points obtained and solution are analysed below, in detail.

- All the 12 points obtained with equal contact force ratios are real, but only three are feasible. None of them are local minima. Lowest value for objective function amongst the three is 0.3821.
- Of the three points satisfying the condition $F_{T_i} = F_{N_i} = 0$, two are feasible. Among the two feasible points, one is a local minimum with objective function value of 0.0288. The other is not a local minimum and has an higher value of objective function.
- Thus we see that the best feasible point with equal contact force ratio, is not even a local minimum, and has a μ value of 0.3821 which is much higher than 0.0288, the μ of the global minimum.

Contour plot of objective function μ for pose 120 is shown in Figure 3.10, in F_{T_1}-F_{N_1} space. The upper part of the line $F_{N_1} = 0$, is the feasible region, within the selected plot window. Two of the feasible equal contact force ratio points are shown in this plot

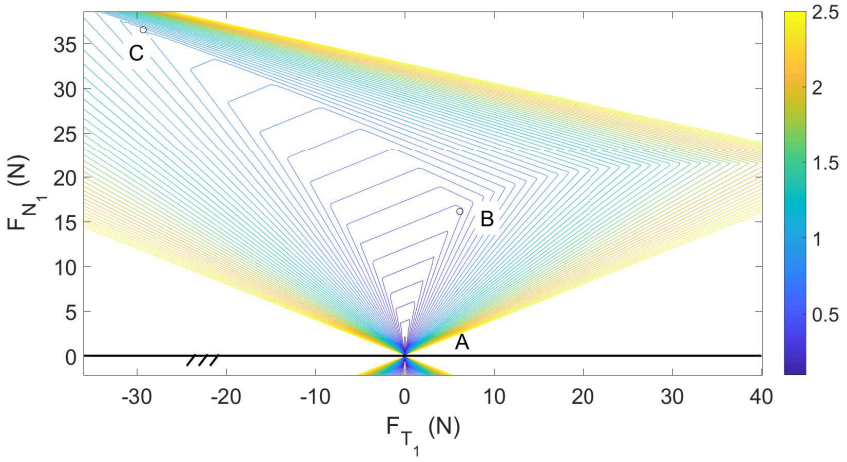

Figure 3.10: Contour plot of contact force ratios for pose 120.

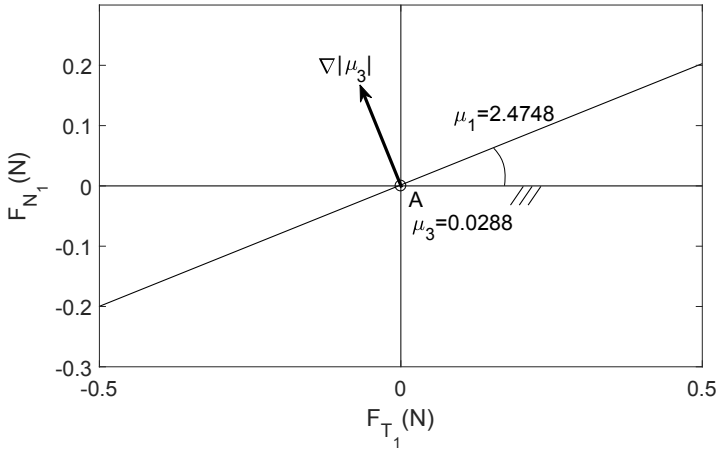

(a) Contour around A.

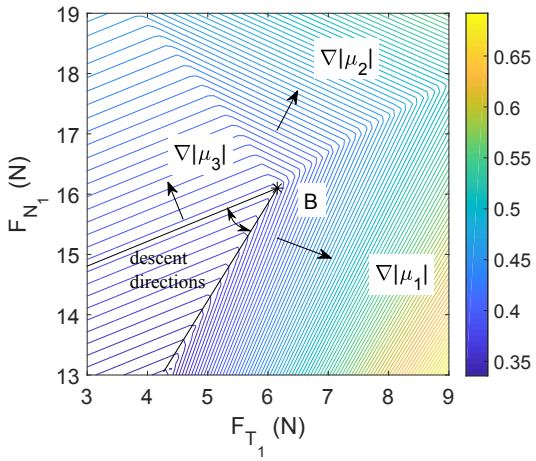

(b) Contour around B.

Figure 3.11: Close up view of points A, and B for pose 120.

as B, and C. The third feasible equal contact ratio point is not in the plot. The point A has $F_{T_1} = F_{N_1} = 0$, and is the global minimum with $\mu = 0.0288$. The point with $F_{T_2} = F_{N_2} = 0$, which is also feasible, lies outside the plot.

Points A and B are shown with more detail in Figure 3.11. Figure 3.11a shows the global minimum A, where $F_{T_1} = F_{N_1} = 0$, and $\mu = |\mu_3|$. We can see that the line $F_{T_1} = 0$ is not in the cone of feasible descent directions, and hence the point can be a local minimum. We then look at the value of $|\mu_1|$ on the line perpendicular to the gradient $\nabla|\mu_3|$. We find that on this line $|\mu_1| = 2.47 > \mu^* = 0.0288$. In all other feasible directions $|\mu_1|$ will be even higher. Hence A is a local minimum.

Figure 3.11b shows the point B which has equal contact force ratio magnitudes, as can be seen from contours of μ. However, from the gradients $\nabla|\mu_i|, i = 1, 2, 3$ shown in figure, we can make out that the convex hull of the gradients does not contain the null vector. This is indicated by the fact that the multipliers in the condition for optimality, (3.8), and (3.9), are $\alpha_1 = 0.2849$, $\alpha_2 = -0.4719$, $\alpha_3 = 1.1870$, with one of them being negative. Hence B is not a local minimum. The cone of feasible descent directions is marked on Figure 3.11b.

The two numerical examples show that global minimum of both types which we anticipated occur. Also, several points obtained with equal force ratio magnitudes are not local minima.

We did not get a case where there is no feasible region. In our algorithm we do not explicitly check optimality condition for local minimum, because of the assumption that the point with lowest μ obtained in our algorithm will be the global minimum. This assumption was not violated in the 544 poses and contact point combinations for which we generated solutions using algorithm 1.

When we examine the points of the type $F_{T_i} = F_{N_i} = 0$, obtained for pose 120, we realise that if these torques are applied, either the rover could be near to toppling, or the bogie could be near to turning over in an uncontrolled fashion. A small error in control could make this happen, as was pointed out in [44] too. Even if the error in controlling torques does not make the bogie or rover turn over, it will make the required μ jump

discontinuously to a higher value than the optimum. To ensure that the rover does not get close to such a nonrobust situation, it is useful to pose a positive lower limit to the normal forces on all wheels. Hence we now address the problem of minimizing μ with the condition $F_{N_i} \geq F_{N_{min}},\ i = 1, 2, 3$, for some specified $F_{N_{min}} > 0$.

3.4 Positive Lower Bounds on Normal Forces

The problem to be solved is, minimize $\mu = max\left\{\left|\frac{F_{T_1}}{F_{N_1}}\right|, \left|\frac{F_{T_2}}{F_{N_2}}\right|, \left|\frac{F_{T_3}}{F_{N_3}}\right|\right\}$ subject to

$$F_{N_i} \geq F_{N_{min}} > 0,\ i = 1, 2, 3. \tag{3.16}$$

In the previous analytical formulation, the special points $F_{T_i} = F_{N_i} = 0,\ i = 1, 2, 3$ were considered as possible solutions. In this formulation, we need not consider them as candidate solutions, as they are outside the feasible region. But we need to additionally look for solutions on the boundaries of the inequalities (3.16).

The following observations can be made about the nature of optima for the above problem.

(a) If global minimum occurs inside the feasible region, three contact force ratios will be equal in magnitude, and it will be a local minimum.

(b) Even if the best equal contact force ratio point occurs inside the feasible region, it need not be the global minimum if a point of the type $F_{T_i} = F_{N_i} = 0$, $F_{N_j}, F_{N_k} > 0$, has better μ than that.

(c) A local minimum on an edge of the boundary (not at a vertex), cannot have only one dominant $|\mu_i|$. On a boundary $F_{N_i} = F_{N_{min}}$, $\mu_j s$ have singularity at $F_{N_j} = 0$, and on either side of the singularity, approach a specific value monotonically and asymptotically. Hence μ_j has no stationary point on the lines $F_{N_i} = F_{N_{min}}$. This can be shown algebraically by equating the directions of gradient of μ_j and F_{N_i},

and using the fact that $F_{N_i} = F_{N_{min}}$. As

$$\mu_j = \frac{F_{T_j}}{F_{N_j}} = \frac{d_1 F_{T_1} + e_1 F_{N_1} + f_1}{d_2 F_{T_1} + e_2 F_{N_1} + f_2}, and \tag{3.17}$$

$$F_{N_i} = a_2 F_{T_1} + b_2 F_{N_1} + c_2 = F_{N_{min}}, \tag{3.18}$$

this means that the condition

$$(e_2 d_1 - e_1 d_2)\,(F_{N_{min}} - c_2) = f_2 e_1 a_2 - f_1 e_2 a_2 - f_2 d_1 b_2 + f_1 d_2 b_2 \tag{3.19}$$

has to be satisfied.

This means that only for specific values of $F_{N_{min}}, a_2, b_2, c_2, d_1, d_2, e_1, e_2, f_1, f_2$, can stationary points be obtained.

A minimum point on an edge of the boundary (not at a vertex) will have typically two equal and dominant $|\mu_i|$s. Determination of points of two equal dominant $\mu_i s$ on boundary is easily reduced to solution of a quadratic equation.

(d) A vertex of the feasible region boundary, if a local minimum, could have a single dominant $|\mu_i|$ typically.

(e) An entire line $F_{N_i} = F_{N_{min}}$ could be infeasible. If so, it can be ignored when searching for minimum points.

(f) The global minimum is the one with the best μ amongst feasible points of the type (i) with equal contact force ratio magnitudes and inside feasible region (not on boundary), (ii) on a feasible edge of the boundary (not at a vertex) with two equal and dominant $|\mu_i|$s, and (iii) at a feasible vertex of the boundary. The best point amongst them will also be a local minimum, and hence we need not check for local minimum condition, if one or more points of the three types are obtained.

3.5 Algorithm 2 and Solutions

Based on the above observations, the following non-iterative algorithm (Algorithm 2) was proposed. The approach is to seek feasible equal force ratio points within the feasible region, and also seek solutions on the edges and vertices of the boundaries of the feasible space, and choose the best amongst them.

3.5.1 Algorithm 2

Step 1: Determine the three vertices $F_{N_i} = F_{N_j} = F_{N_{min}},\ i, j = 1, 2, 3,\ i \neq j$, and check whether they are feasible, ie., whether $F_{N_k} \geq F_{N_{min}}, k \neq i, j$.

if all three are infeasible, **then**

declare "no feasible solution", and **stop**.

else

determine $\mu' s$ of feasible vertices, and proceed to step 2.

end

Step 2: Determine all points of the type $|\mu_1| = |\mu_2| = |\mu_3|$ (both feasible and infeasible), and find their $\mu' s$.

Step 3: Determine the three special points of the type $F_{T_i} = F_{N_i} = 0,\ i, = 1, 2, 3$ (both feasible and infeasible), and find their $\mu' s$.

if best point of step 2 is feasible and better than the best point of step 3, **then**

declare this point as global minimum, and **stop**.

else

proceed to step 4.

end

Step 4: Determine all feasible points on the boundary (not vertex) with two equal and dominant $|\mu_i|$s, and find their μs.

Step 5: Declare as global minimum, the point with lowest μ from amongst

(a) the feasible vertices found in step 1,

(b) the feasible equal $|\mu_i|$ points found in step 2, and

(c) the feasible points found on edges in step 4, with two equal dominant $|\mu_i|$s.

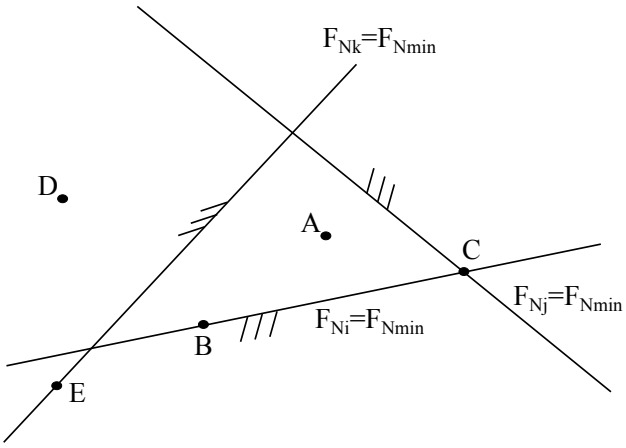

Figure 3.12: Feasible region: Type 1

The kernel of algorithm 2 can be understood from Figure 3.12, and Figure 3.13, which shows the ways in which the feasible region can occur for these problems. The points we are considering can be like point 'A' (inside a feasible region), 'B' (on a feasible edge of boundary), or 'C' (feasible vertex of the boundary) as shown in Figure 3.12. Point 'D', and 'E' (shown in Figure 3.12) can be neglected as they are outside the feasible region.

The line $F_{N_i} = F_{N_{min}}$, shown in Figure 3.13 need not be considered for searching the minimum point, as it is outside the feasible region.

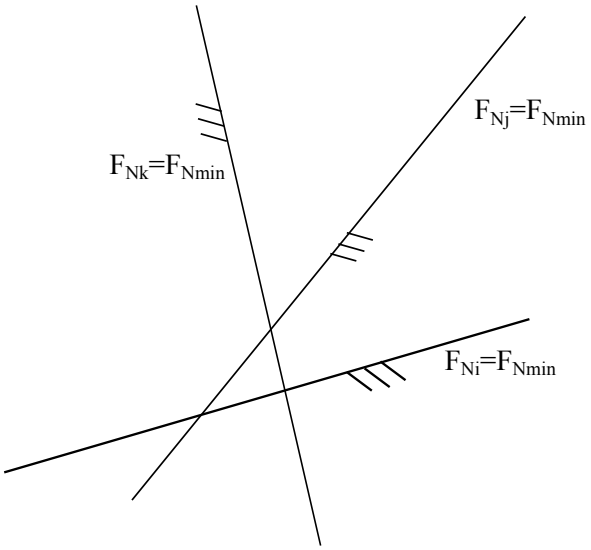

Figure 3.13: Feasible region: Type 2

The following two points need to be noted, while implementing algorithm 2 on a

controller.

1. Steps 2 and 3 could help us avoid the determination of candidate points on the boundaries.

2. If two vertices are infeasible (step 1), then their common edge need not be considered in step 4.

3.5.2 Results and Discussion

The same 544 poses mentioned earlier were solved using algorithm 2, and among them equal contact force ratio solution was obtained for 433 poses. 80 poses had the solution on the boundary with two contact force ratio magnitudes being equal, and the remaining 31 poses had solution on a vertex, with a single dominant contact force ratio.

For illustrating different types of points and solutions, the poses mentioned earlier as number 225 and 120 are used, and in addition, pose number 75 from the same solution set of optimally designed rover in Chapter 5 is also used (see Figure 3.6c for the pose).

For minimum normal force, any positive non-zero value, which is reasonable, considering the rover weight can be used. Here, we used values of $20N$ and $60N$, for obtaining different types of solutions.

Solution for Pose 225

The Figure 3.6a shows the corresponding pose. Lower bound of normal force, $F_{N_{min}} = 20N$ was used. Contours of μ near the solution are shown in Figure 3.14.

- Vertices: In this pose, two out of the three vertices are feasible, while the third one is infeasible. One feasible vertex is shown as D in Figure 3.14, and it has a μ of 0.2848. The other feasible vertex has very high μ and does not fall within the region shown in Figure 3.14. We can also conclude that all the three edges of boundary have feasible segments, and that the feasible region is unbounded.

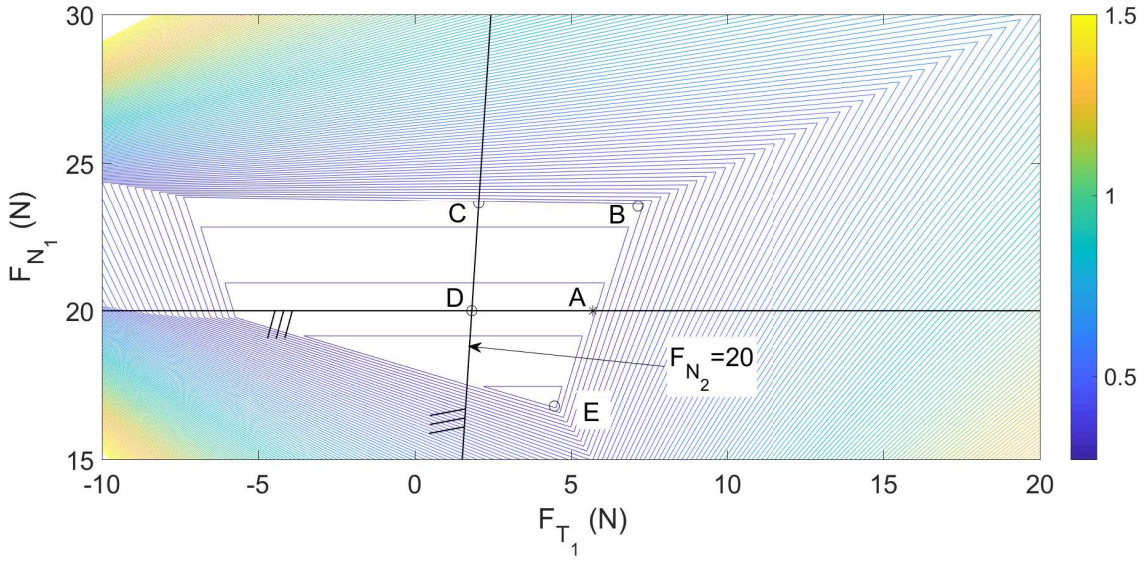

Figure 3.14: Contour plot of pose 225 for $F_{N_{min}} = 20$.

- Points with equal contact force ratio: The best of such points has μ of 0.2660 (point E), but is infeasible. Hence solution is expected to lie on the boundary. Only one equal ratio point is feasible, and is shown in Figure 3.14 as B. It has μ of 0.3037.

- Candidate points on edges: A total of only two feasible points of this type resulted and are shown in Figure 3.14 as A, and C. Their $\mu's$ are 0.2848, and 0.3042 respectively. The point A lies on the line $F_{N_1} = 20$, while C lies on the line $F_{N_2} = 20$.

Thus algorithm 2 will declare two points, namely A and D as optimal, with equal values of μ. In this problem it turned out that an entire segment, AD on edge $F_{N_1} = 20N$ has the global minimum μ. This happened because the contours of the dominant $|\mu_i|$ are parallel to this edge. This is a low probability situation and hence not considered separately in our algorithm.

If the value of lower bound on normal force is reduced to $15N$ ($F_{N_{min}} = 15N$), the solution will be the point E shown in Figure 3.14, which is an unconstrained global minimum of the type $|\mu_1| = |\mu_2| = |\mu_3|$ with μ of 0.2660.

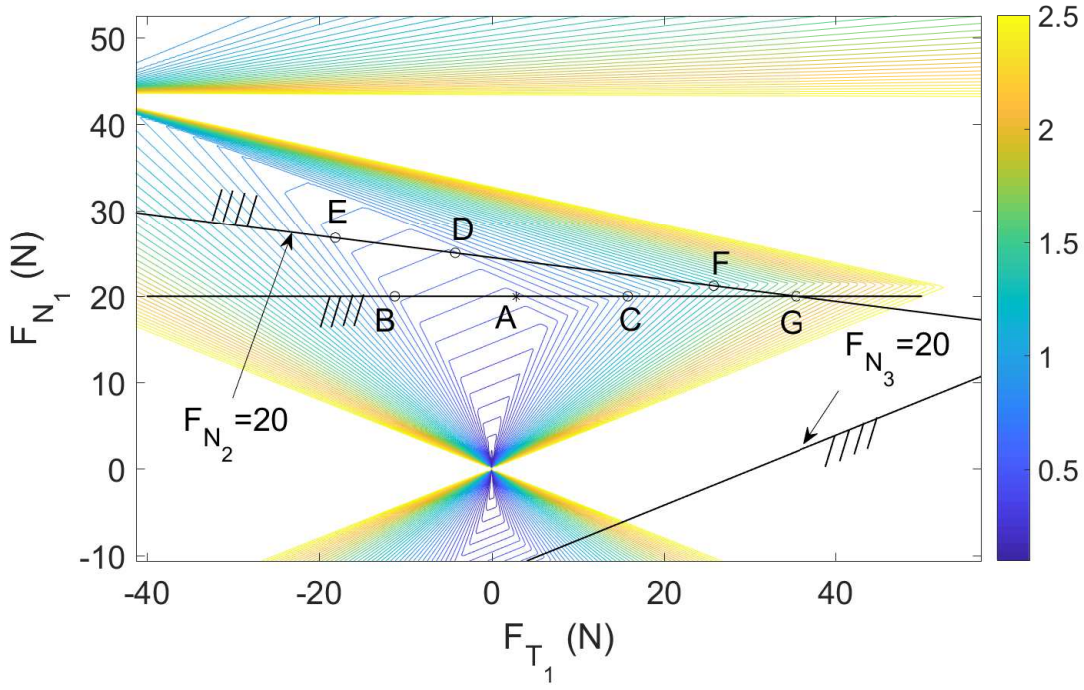

Figure 3.15: Contour plot of pose 120 for $F_{N_{min}} = 20$.

Solution for Pose 120

A lower bound of $F_{N_{min}} = 20$ for normal force is used, and the corresponding pose can be seen in Figure 3.6b . Contour plots of μ near the solution are shown in Figure 3.15.

- Vertices: In this pose, two out of the three vertices are infeasible and only one is feasible, indicating one entire edge ($F_{N_3} = 20N$) is infeasible. The feasible vertex, shown as G in Figure 3.15, has μ of 1.7669. Figure 3.16a shows G in greater detail, with gradients of the two inequality constraints, and the gradients of μ. It is easy to see that KKT conditions are not satisfied. The cone of feasible descent directions is shown in figure.

- Points with equal contact force ratio: The best point has μ of 0.3821, but is infeasible. Hence solution is expected to lie on the boundary. None of the equal ratio points are feasible.

- Candidate points on edges: A total of seven feasible points of this type were obtained. Three of them lie on $F_{N_1} = 20$, and are shown as A, B, and C in Fig-

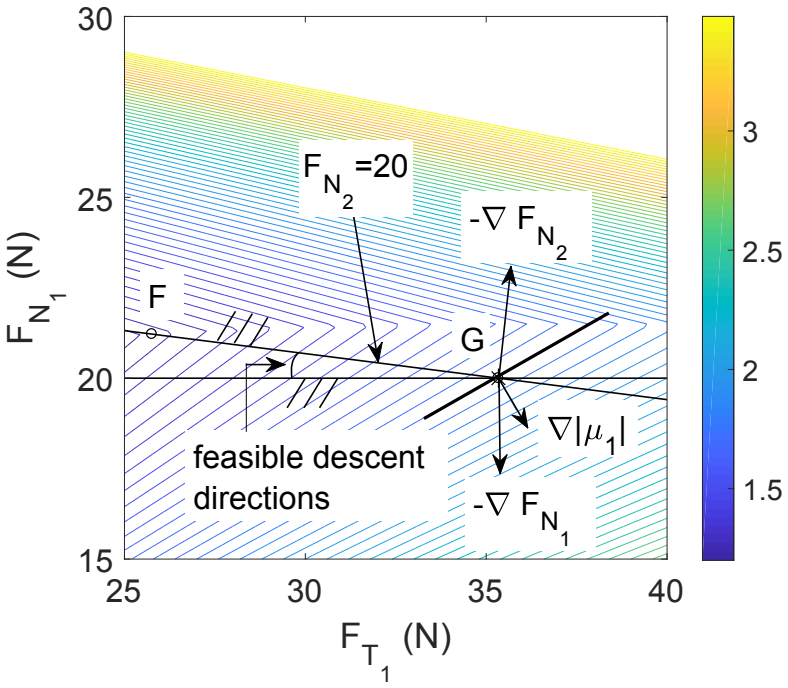

(a) Contour around G.

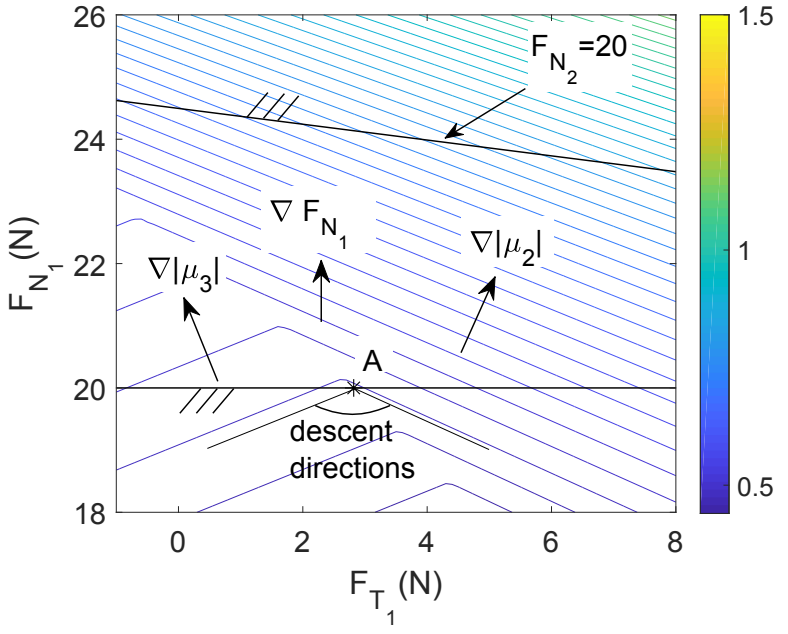

(b) Contour around A.

Figure 3.16: Close up of contours for pose 120.

ure 3.15. The best point A has μ of 0.4763. The point A is shown in more detail in Figure 3.16b, with the gradients of the two dominant μ_is and gradient of the inequality constraint. We can see that the entire cone of descent direction is infeasible. Four of the seven points lie on the line $F_{N_2} = 20$, and three of them, which appear in the figure, are shown as points D, E, and F in Figure 3.15. The best point of the four, F has a μ value of 0.5907.

Of all the feasible special points obtained, point A has the best μ, and is a local minimum. It is also the global minimum.

Solution for Pose 75

The pose 75 is shown in Figure 3.6c. In order to demonstrate the occurrence of solution at a vertex, a higher value of $60N$ was used for $F_{N_{min}}$. Contours of μ are shown near the solution in Figure 3.17.

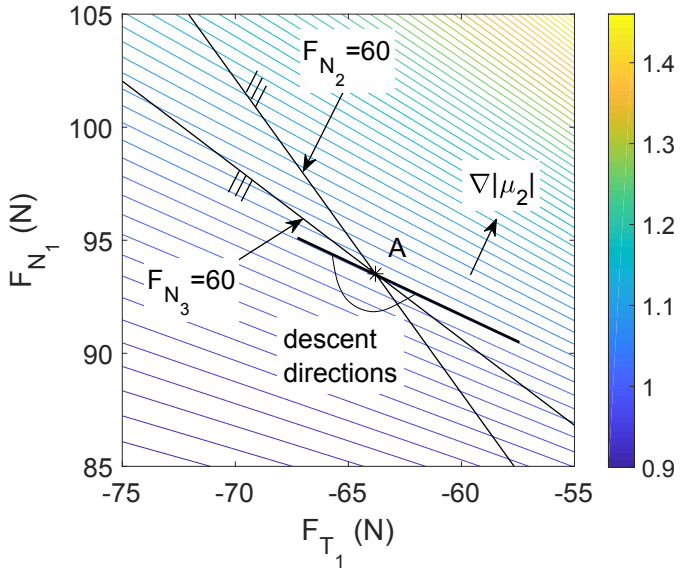

Figure 3.17: Close contour of point A, pose 75 for $F_{N_{min}} = 60N$.

- Vertices: In this pose, two out of the three vertices are infeasible, indicating that one entire edge ($F_{N_1} = 60$) is infeasible. The feasible vertex has a μ of 1.0316 and is the intersection of edges $F_{N_2} = 60$N, and $F_{N_3} = 60$N. It is marked as point A in

Figure 3.17. It can be seen that point A is a local minimum, as there is no descent direction into the feasible region.

- Points with equal contact force ratio: The best point has μ of 0.1142, but is infeasible, indicating the solution can be expected to lie on the boundary. None of the equal ratio points are feasible, as they have F_{N_i}, lower than 60N.
- Candidate points on edges: No feasible candidate point exists on edges.

With a high $F_{N_{min}}$ of $60N$, about 66.89% of rover weight, no feasible point of the three or two equal force ratio type occurred. The sole vertex point A is a local minimum and is the global solution with a high μ of 1.0316.

3.6 Comparison of Speed with a general NLP solver

The powerful SQP based NLP solver 'fmincon' of MATLAB® was used in Chapter 2, for minimizing friction requirement of the rover, after formulating it as a smooth optimization problem. Here the performance of algorithms 1 and 2 were compared with that of this solver.

Two sets of poses were considered for performance evaluation. Firstly, 444 poses of an optimal rover climbing a single step of height equal to the diameter of wheel (Chapter 5), and secondly 100 random poses with wheel contact angle varying between -80° to 80°, and rocker, and bogie angles varying from -30° to 30° (see Appendix C). This study was done on a computer with 1.60 GHz processor, and 12 GB RAM.

In the first comparison, the 444 step climbing poses were solved with $F_{N_i} \geq 0, i = 1, 2, 3$. The solver 'fmincon' of MATLAB® was used, with (a) randomly chosen guess solutions, and (b) the optimal solution obtained for the just previous pose during climbing. The same 444 poses were optimised using algorithm 1 proposed in this thesis. The mean, maximum and minimum times needed for determining solution with the above three are given in Figure 3.18, as a bar chart. Algorithm 1 clearly outperforms 'fmincon' from both sets of guess solutions. The mean time with algorithm 1 is only 5.87% of

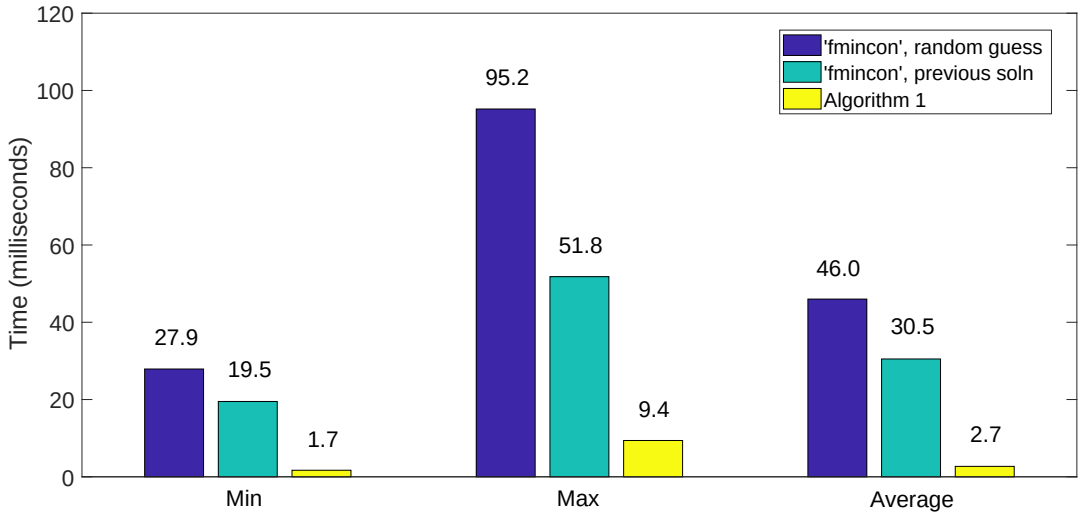

Figure 3.18: Solution time for step climbing with $F_{N_i} \geq 0$.

the mean time used by 'fmincon' from random guesses, and 8.85% of mean time from solution of previous pose as guess solution.

In the second comparison, the 444 poses described above were solved with the constraints $F_{N_i} \geq 5N$, $i = 1, 2, 3$. In this case, algorithm 2 was used. Results are shown in Figure 3.19. Algorithm 2 performed better than 'fmincon'. Its mean time for solution was 13.12% of mean time of solution with 'fmincon' from random guesses, and 17.55% of mean time from solution of previous pose as guess solution.

In the third comparison, hundred randomly selected poses and wheel contact points with constraint $F_{N_i} \geq 0, i = 1, 2, 3$ were solved using 'fmincon', from randomly selected guess solutions, and also using algorithm 1. The time for solving is shown in Figure 3.20. It can be seen that algorithm 1 is much faster, taking only 2.70% of the time taken by 'fmincon', on the average.

In the fourth comparison, the above set of hundred random poses with constraint $F_{N_i} \geq 5N$, $i = 1, 2, 3$ were solved using 'fmincon' and algorithm 2, and time taken shown in Figure 3.21. Algorithm 2 is much faster, taking only 8.57% of the time taken by 'fmincon', on the average.

The time estimates above are not the times for solutions alone as other threads were

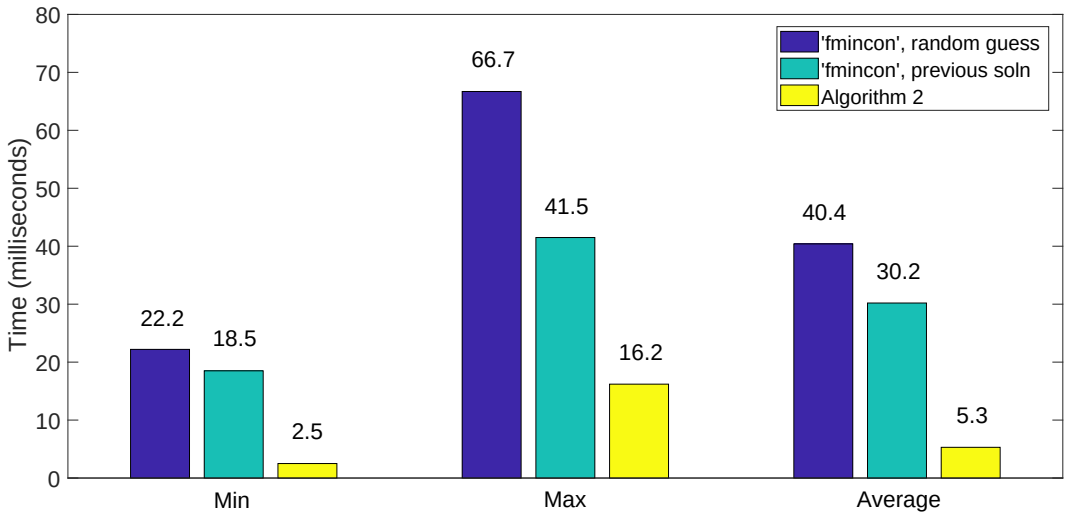

Figure 3.19: Solution time for step climbing with $F_{N_i} \geq F_{N_{min}}$.

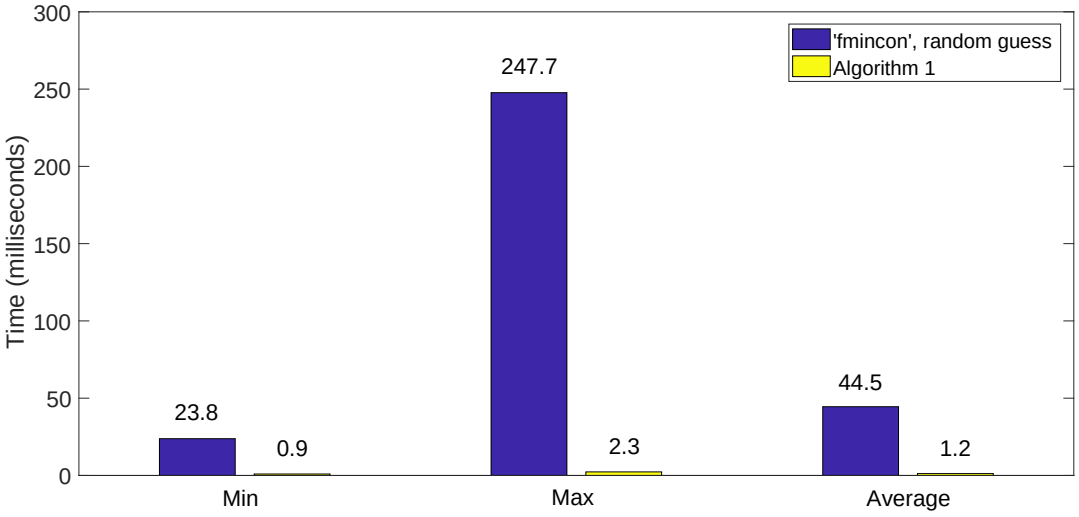

Figure 3.20: Solution time for 100 random poses with $F_{N_i} \geq 0$.

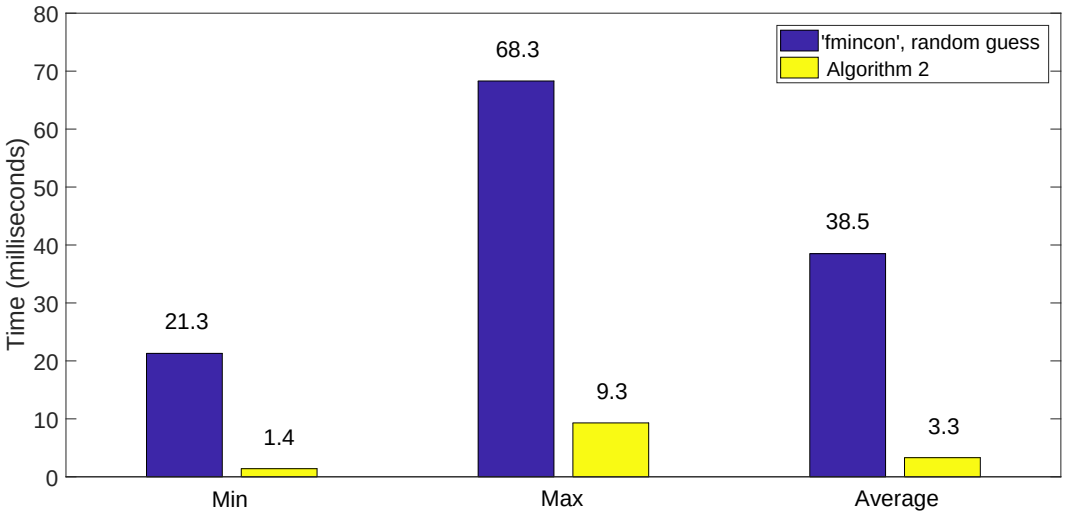

Figure 3.21: Solution time for 100 random poses with $F_{N_i} \geq F_{N_{min}}$.

also running. Solving the same problem at different times gives different execution times. When we analysed the time by running the same solution search 200 times for a particular pose, we found that the time we used for plotting the bar graphs are near but not exactly the same as the mean time of 200 runs. But the trend is a clear indicator of the superior speed of algorithms 1 and 2.

An important observation is that for all the 1088 problems solved, the solutions obtained by algorithm 1 and algorithm 2 were identical to the solutions obtained using 'fmincon'.

The algorithms 1 and 2, are much easier to implement in a controller than a sophisticated algorithm like 'fmincon'. These algorithms are as good as 'fmincon' for finding global minima, but does it much faster than 'fmincon'. In good processors, coded in C or C++, the execution times are expected to be much better than the execution time for MATLAB® codes, which we have reported.

3.7 Conclusion

Based on the results obtained, we can conclude that our two algorithms are capable of obtaining global minima without failure, for the respective problems addressed by them. Both of them take much less time than a powerful SQP based NLP solver when the latter solves smooth versions of the two problems. Our algorithms are quite simple and easy to code, and is likely to be more easily implementable in a rover's controller.

We believe that our understanding of how solutions can occur, for both the categories of problems, is quite comprehensive, and represents an advance in research on rovers of this type.

CHAPTER 4

Optimum Performance on Partially and Fully Known Terrains

The context of the problem we addressed so far, is that the coefficient of friction available from the ground is not known, and hence minimizing friction requirement in order to minimize the possibility of slip, was relevant. Now we ask the question, suppose the coefficient of friction is partially known, in the sense that there are some patches where it is known. Or suppose the coefficient of friction is known everywhere on the ground. Here we consider these two situations, and formulate the problem of optimal operation of the rover, and solve these problems numerically.

4.1 Optimal Performance on Partially Known Terrain

For a partially known terrain, we pose the problem of optimal operation as 'given the pose of the rover, the contact points, and the available coefficient of friction between the wheel and ground for one of the wheels (a patch), minimize the coefficient of friction required at the remaining two wheels'. As already stated in Chapter 2, the motivation for choosing required coefficient of friction as the objective function, is to minimize the possibility of wheel slip, when the coefficient of friction on all wheels are not known. Other objective functions could have been considered. If we are able to obtain good formulations for required friction, we believe it would be possible to use similar approaches for other objective functions too. Hence we do not consider other objective functions for this situation here.

The scenario where we might know the coefficient of friction in some regions and not others occur as follows. If the wheels have slip and force sensors, the coefficient of friction can be estimated when there is a slip. Thus in this scenario, the lower coefficient

of friction would be known once slip happens, and then replanning of torque application can be done.

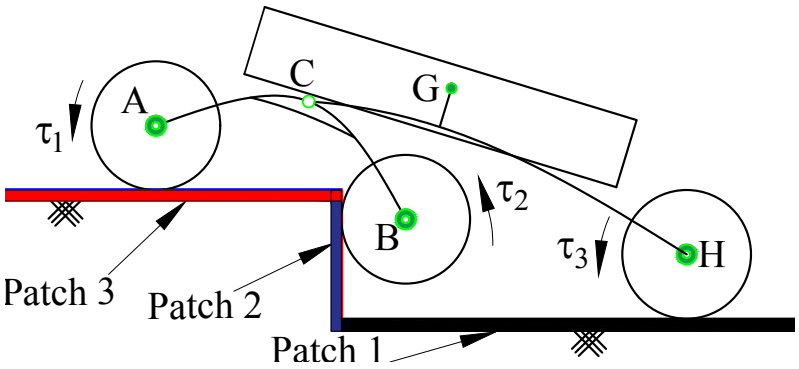

Figure 4.1: Rocker-bogie rover climbing a different patch step

4.1.1 Formulation

Let the coefficient of friction available for a particular portion (patch) of terrain be denoted as μ_{avl_p}, where $p = 1\ or\ 2\ or\ 3$ denotes the patch number. The goal of optimization is to determine the values of wheel torques, which minimize μ required between the terrain and the other two wheels whose friction coefficients with ground are unknown.

$\{F_{N_1}, F_{T_1}, F_{N_2}, F_{T_2}, F_{N_3}, F_{T_3}, F_1, F_2, \mu\}$ is the full set of decision variables which need to be determined.

Mathematically, the problem can be stated as:
Determine $\{F_{N_1}, F_{T_1}, F_{N_2}, F_{T_2}, F_{N_3}, F_{T_3}, F_1, F_2, \mu\}$ to

minimize μ,

subject to

$$[A]\{x_F\} = \{b\}, \tag{4.1}$$

$$F_{N_i} \geq 0,\ i = 1, 2, 3, \tag{4.2}$$

$$-\mu_{avl_p} F_{N_n} \leq F_{T_n} \leq \mu_{avl_p} F_{N_n},\ n = 1\ or\ 2\ or\ 3, \tag{4.3}$$

$$-\mu F_{N_i} \leq F_{T_i} \leq \mu F_{N_i},\ i = 1, 2, 3,\ i \neq n,\ and \tag{4.4}$$

$$\mu \geq 0. \tag{4.5}$$

First slip constraint shown in Equation 4.3, corresponds to the patch whose coefficient of friction is known, and the value of n can be 1, or 2 or 3 depending on which wheel is in contact with the patch (p in Equation 4.3 refers to patch number). While, the second set of slip constraints (Equation 4.4), corresponds to the other two wheels.

Six wheeled nominal rover with rocker-bogie suspension, climbing a single step of height equal to wheel diameter, is considered as the terrain for this study. Figure 4.1 shows the different patches on a step. The bottom horizontal portion of step, is named as 'patch 1'. The vertical rise of step along with its convex corner is named as 'patch 2', and the tread (top landing) of step is named as 'patch 3'. Every wheel will move from patch 1 to patch 3, through patch 2. Similar to the previous sections, 'fmincon' is used for finding the optimal friction requirement.

Poses Considered

The poses in the sequence of the rover climbing the step, discussed in Chapter 2, and whose optimal solutions are shown in Figure 2.7 are considered. From amongst these poses, those requiring zero traction forces on the three wheels, were not considered.

We can identify three regimes during the climbing of the step, where a single wheel is on a patch with known coefficient of friction. They are as follows.

- Regime 1 (coefficient of friction of patch 1, μ_{avl_1}, is known): Rear wheel moves on patch 1: from when middle wheel first butts against the riser, to when it reaches the top landing.
- Regime 2 (coefficient of friction of patch 2, μ_{avl_2}, is known): First wheel, middle wheel and the rear wheel move on patch 2: from when front wheel first butts against the riser, to when rear wheel reaches the top landing.
- Regime 3 (coefficient of friction of patch 3, μ_{avl_3}, is known): First wheel moves on patch 3: from when the first wheel is at the corner on the top landing, to when the middle wheel reaches the top landing. As zero traction poses are discarded, this

turns out to be the same set of poses as in regime 1, with only the known patch being different.

When the coefficient of friction is known on patch 1, climbing sequences where only one wheel is in contact with patch 1 need to be considered. So the only possibility is rear wheel on patch 1. Thus regime 1 occurs from when the middle wheel starts climbing the vertical face of step, to when it reaches the top landing. These are poses from 300 to 447 of Figure 2.7.

As patch 2 is the vertical face of the step including its convex corner, we need to consider the entire climbing sequence of the rover. Initial set corresponds to the first wheel climbing the vertical face of step, till it just reaches the top landing (poses 1 to 147 of Figure 2.7). Second set corresponds to the middle wheel going through the same climbing sequence (pose 300 to 447 of Figure 2.7), and for the final set the rear wheel going through the same phase (pose 585 to 732 of Figure 2.7). These sequences constitute regime 2.

Similar to regime 1, a single set of sequences only is possible for motion of one wheel on patch 3, which is the first wheel. This occurs, when middle wheel is moving on the vertical face and the corner of the step (pose 300 to 447 of Figure 2.7).

4.1.2 Results

For the nominal rover climbing a step of height equal to the wheel diameter, the coefficient of friction required was 0.58 (say 0.6). Based on this, for the known value of coefficient of friction μ_{avl_p}, we used 0.75 and 0.45, one being above and one being below 0.6. We studied the three climbing sequences with the two values of μ_{avl_p}. Please note that in Figures 4.2, 4.3, and 4.4, μ^*_{uk} represents the optimal solution for a fully unknown terrain, which was discussed in Chapter 2, and was shown in Figure 2.7.

For finding the optimum friction requirement on patches where coefficient of friction is unknown, 'fmincon' of MATLAB® was used. The solution was generated using two sets of initial guesses. In the first set, the optimum solution obtained for minimizing

friction requirement in Chapter 2 was given as the initial guess. For the second set, random guesses were used for finding the solution. Both starting guesses yielded the same solution. KKT conditions were checked, and were found to be satisfied.

In the solutions obtained, it was seen that the contact force ratios on the unknown patches are equal in magnitude, and the contact force ratio on the known patch was equal to the limit μ_{avl_p}. This is true for all poses in which the optimum μ is greater than zero. For poses in which optimum μ is zero, the solution becomes slack, and contact force ratio on the known patch can be less than μ_{avl_p}. This was true for all three regimes.

Figure 4.2 shows the optimal μ required for the front and middle wheels, while the rear wheel is moving on patch 1. It can be seen that for the case where μ_{avl_1} = 0.75, the optimal μ is very low, and nearly zero at the beginning and becomes zero very soon. It means that the rover can be pushed up purely by the torque and traction on the rear wheel, and the front and middle wheel can almost or purely roll without any torque. In the case of regimes 2 and 3 (Figures 4.3 and 4.4) also, when the coefficient of friction is 0.75 on the known patch, the optimal friction requirement is lower than the optimal friction requirement with friction unknown in all three patches. But they are not as dramatically low as in the case of regime 1. Towards the end of these regimes too, optimal μ becomes zero, indicating that two of the wheels which are on patches with unknown friction, can purely roll, without any torque or traction needed.

For the case with μ_{avl_p} = 0.45, in all three regimes, for the poses where μ^*_{uk} is above 0.45, the coefficient of friction required for the other two wheels is more than μ^*_{uk}. For the poses where μ^*_{uk} is below 0.45, the μ required for the other two wheels is below μ^*_{uk}. This behaviour is as expected. In this case too, towards the end, only the wheel on patch with known friction coefficient needs to contribute the torque and traction needed for climbing, and the other two wheels can purely roll.

Thus it can be concluded that when there is a patch with known coefficient of friction, the rover can use that information to minimize the possibility of slip, and in some poses even climb the step without any friction needed in the other patches.

We can extend our formulation to cases where coefficient of friction at two patches

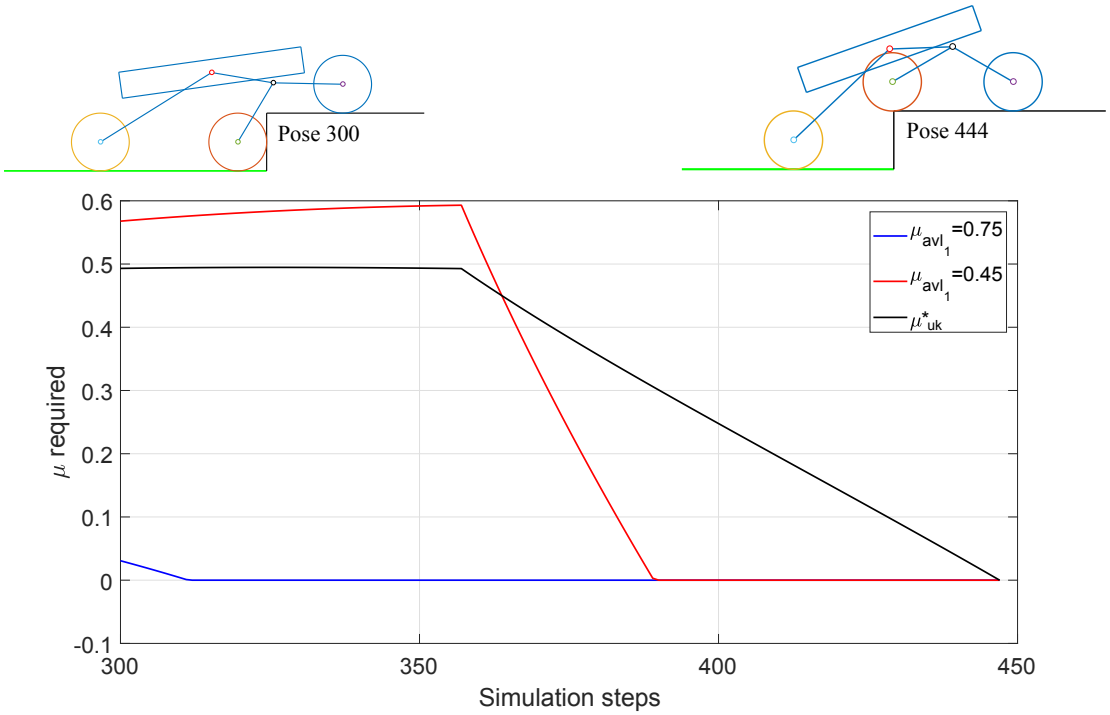

Figure 4.2: Coefficient of friction required for front and middle wheel, while rear wheel moves on patch 1.

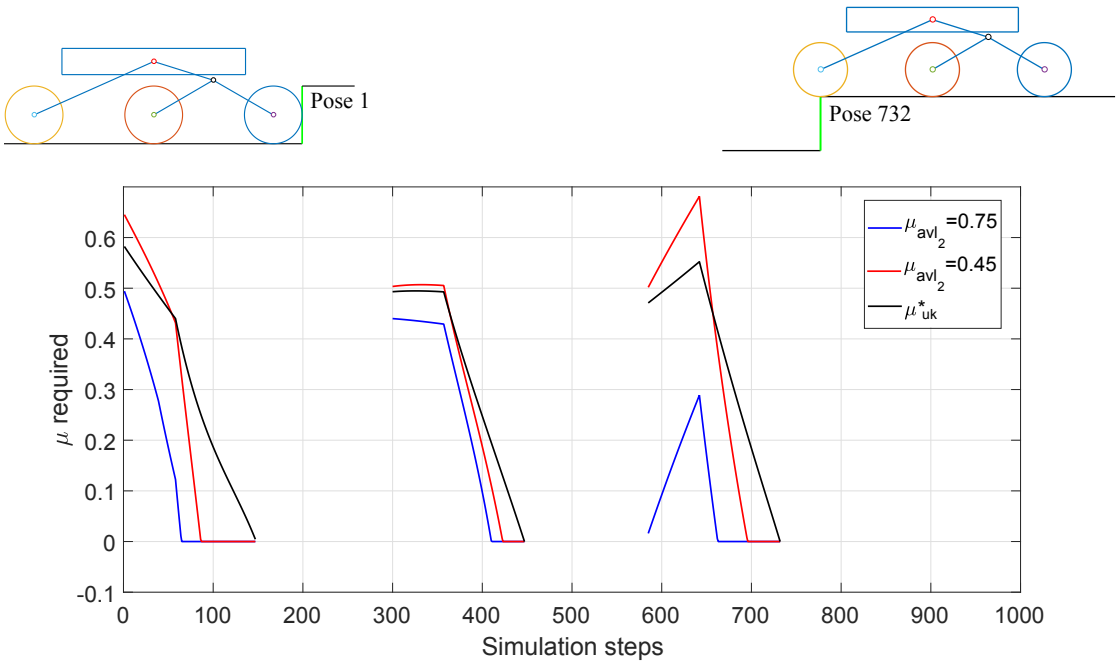

Figure 4.3: Coefficient of friction required, while wheels climb patch 2.

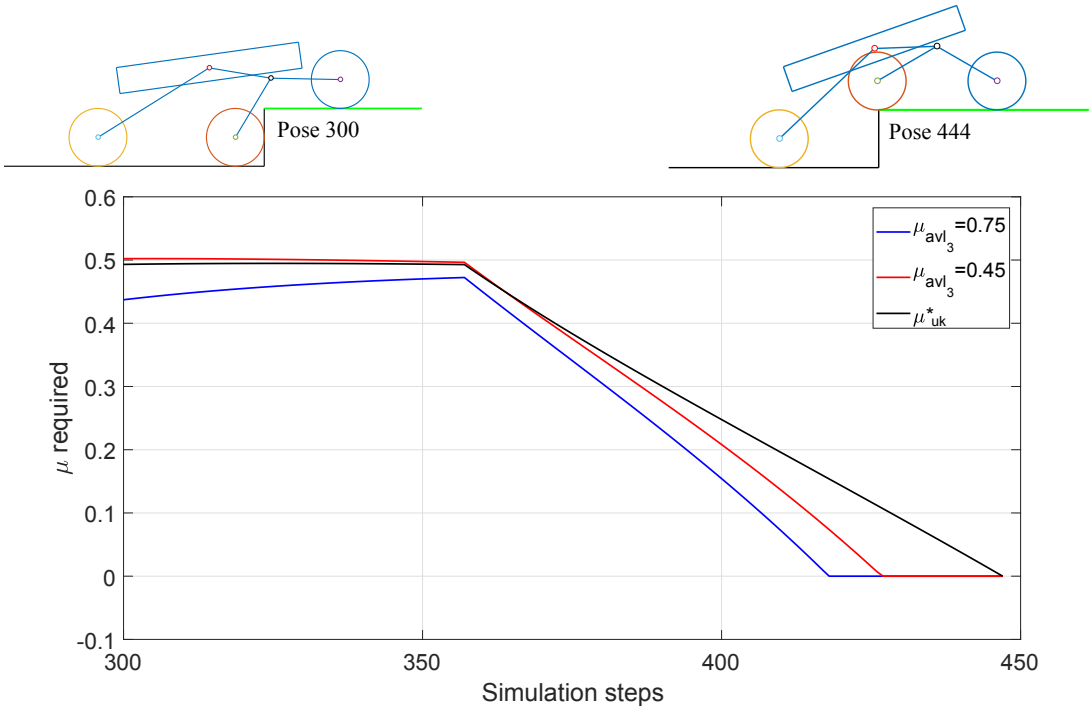

Figure 4.4: Coefficient of friction required, while front wheel moves on patch 3.

are known.

When we say that the coefficient of friction is known for a patch, a natural question that arises is, how would the rover know the coefficient of friction? Estimating friction coefficient would need slip and force sensing. If we can do that with reasonable success, we can utilize the approach developed here. We can even develop simple analytical non-iterative solution techniques for the problem.

4.2 Optimal Performance on Fully Known Terrain

If we assume that the coefficient of friction between wheels and ground is known everywhere, minimizing friction requirement may not be relevant. In its place, we can consider performance related variables like energy, power, torque, etc. Here we consider the required torque of the three wheels as the objective function. We consider the simple case of the available friction being the same everywhere. It is easy to accommodate different known μs at different patches in our formulation. We now discuss the formulation, and

after that, the results.

4.2.1 Formulation

Instead of minimizing the non-smooth objective function $\underset{i=1,2,3}{max}\{|\tau_i|\}$, we introduce the upper bound variable τ and pose the problem as a smooth optimization problem, as follows.

Determine $\{F_{N_1}, F_{T_1}, F_{N_2}, F_{T_2}, F_{N_3}, F_{T_3}, F_1, F_2, \tau\}$ to

$$\text{minimize } \tau,$$

subject to

$$[A]\{x_F\} = \{b\}, \tag{4.6}$$

$$F_{N_i} \geq 0,\ i = 1, 2, 3, \tag{4.7}$$

$$-\mu_{avl} F_{N_i} \leq F_{T_i} \leq \mu_{avl} F_{N_i},\ i = 1, 2, 3, \tag{4.8}$$

$$\tau \geq r F_{T_i},\ i = 1, 2, 3,\ and \tag{4.9}$$

$$\tau \geq -r F_{T_i},\ i = 1, 2, 3. \tag{4.10}$$

The last six inequalities keep τ as the upper bound of the magnitude of the three wheel torques τ_i's (Note that $\tau_i = r\ F_{T_i}$). As the upper bound τ is minimized, the largest τ_i is minimized. The above problem is a linear programming problem (LPP).

4.2.2 Results

We use dimensions and fixed parameters of nominal rover, shown in Table 2.1. Poses used for climbing forward (729), and backward (776) are also identical to those used in the Section 2.3. We assume a coefficient of friction 0.65, which is approximately 13% more than the minimal required friction coefficient of 0.58 obtained in forward climbing. For backward climbing, we assume a coefficient of friction 0.95 which is approximately 13% more than the minimal required value of 0.84 obtained for backward climbing. A value of 0.95 for friction coefficient is perhaps not realistic. It was used just to provide

some leeway for reducing torque.

As the problem is a linear programming problem, it was solved numerically using 'linprog' of MATLAB®. Optimum solution search started at various guess solutions. Multiple random guesses were used for finding the solution. They yielded the same solution.

Climbing Forward

Using a μ_{avl} of 0.65, when the torque requirement was minimized, the peak torques for various poses decreased by about 1% to 28%, compared to the peak torques obtained when minimizing friction requirement. The maximum torque required is 1.32 Nm (see Figure 4.5) which is 17.5% less than the worst torque obtained when coefficient of friction was minimized. This occurs when the last wheel approaches the corner of step. With higher values of available coefficient of friction than 0.65, lower values of torques are possible.

Analysis of Solutions:

Figure 4.5 plots the variation of optimal torques on the three wheels (upper figure), and the variation of corresponding force ratios of the three wheels, as the rover climbs up the step. As we are trying to minimize the maximum torque magnitude, the solutions for various poses would tend to have equal torque magnitudes, as indicated in Figure 4.5. However this need not be the case at all poses, as explained below. General solution of an LPP with nine decision variables will have nine active constraints. In our problem six of them are equality constraints, and are always active. Hence we expect three inequality constraints to be active for each pose. This was found to be the case for all the 729 poses except one. Different inequalities become active at solution in different zones of poses. These are grouped together as different zones AB, BC, CD,..., GH shown in Figure 4.5. At each zone specific set of inequality constraints become active, as shown in Table 4.1 . The first column of the table lists the zones (see Figure 4.5) in which a particular type of solution occurs. The second column lists the inequality constraints which become active

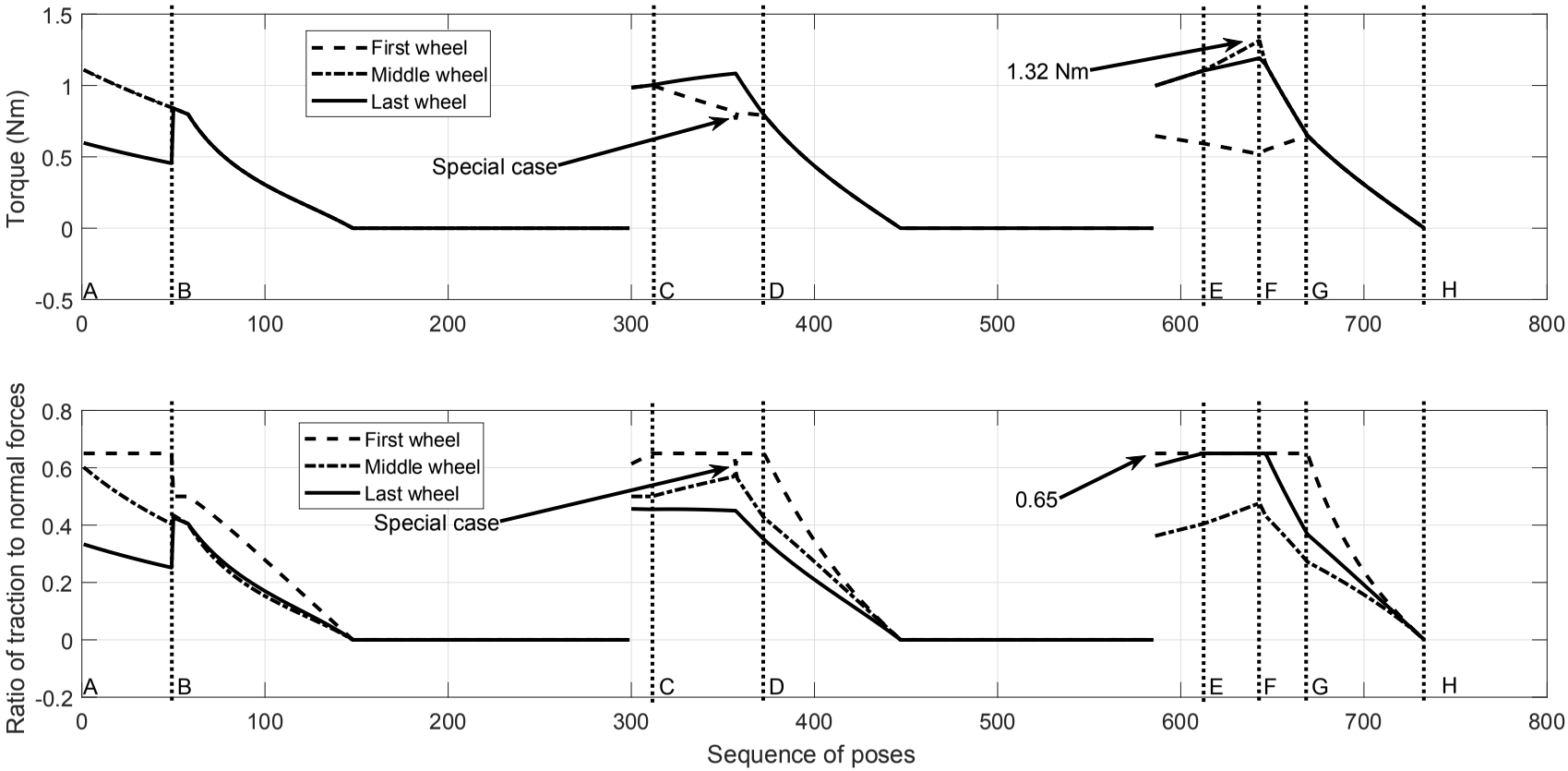

Figure 4.5: Optimal torques of nominal rover during forward climbing and corresponding contact force ratios. A, B, C,...,H are poses across which the character of solution changes.

Table 4.1: Inequality constraints which become active at solutions at different zones.

Zone	Inequality constraints which become active
AB	$\tau_1 \leq \tau,\ \tau_2 \leq \tau,\ F_{T_1} \leq \mu_{avl} F_{N_1}$
BC, DE, GH	$\tau_1 \leq \tau,\ \tau_2 \leq \tau,\ \tau_3 \leq \tau$
CD, FG	$\tau_2 \leq \tau,\ \tau_3 \leq \tau,\ F_{T_1} \leq \mu_{avl} F_{N_1}$
EF	$\tau_2 \leq \tau,\ F_{T_1} \leq \mu_{avl} F_{N_1},\ F_{T_3} \leq \mu_{avl} F_{N_3}$

First wheel is designated as 1, middle wheel 2 and last wheel 3.

at each type of solution.

Consider a pose in zone AB. As mentioned earlier, three inequality constraints are expected to be active. In zone AB, the three inequality constraints related to bounds on, τ_1, τ_2 and μ_1 are active. τ_1 and τ_2 become equal in magnitude to τ, and μ_1 becomes equal in magnitude to μ_{avl}. Please note that these inequality constraints were not artificially forced to be active; they became active in the natural process of optimization.

In all zones τ_2 has the maximum torque. The other two torques also reach maximum value when each wheel nears the top corner of the step and climbs on to the top of the step. In other regimes one or more wheels reach the slip limit.

There is a special case in zone CD where $\tau = \tau_2 = \tau_3$ and contact force ratios do not reach the limit (see Figure 4.5). Thus here an infinite number of equally good optimal solutions are possible. This is the degenerate case in LPP when the solution can lie anywhere on an edge, and not just at one vertex of the feasible convex polytope.

Climbing Backward

Maximum required torque in this case is 1.92 Nm, which is 7.25% less than the maximum torque for minimal required coefficient of friction. Torque and contact force ratio variations are shown in Figure 4.6 and 4.7 respectively. As the coefficient of friction of 0.95 is fairly high, we do not analyze these solutions in detail.

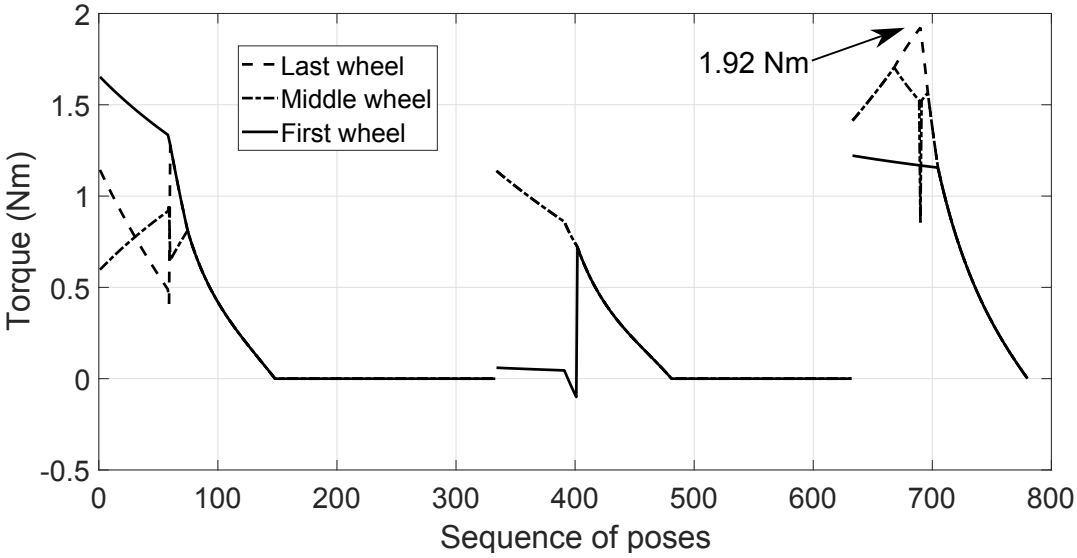

Figure 4.6: Optimal torques of nominal rover during backward climbing.

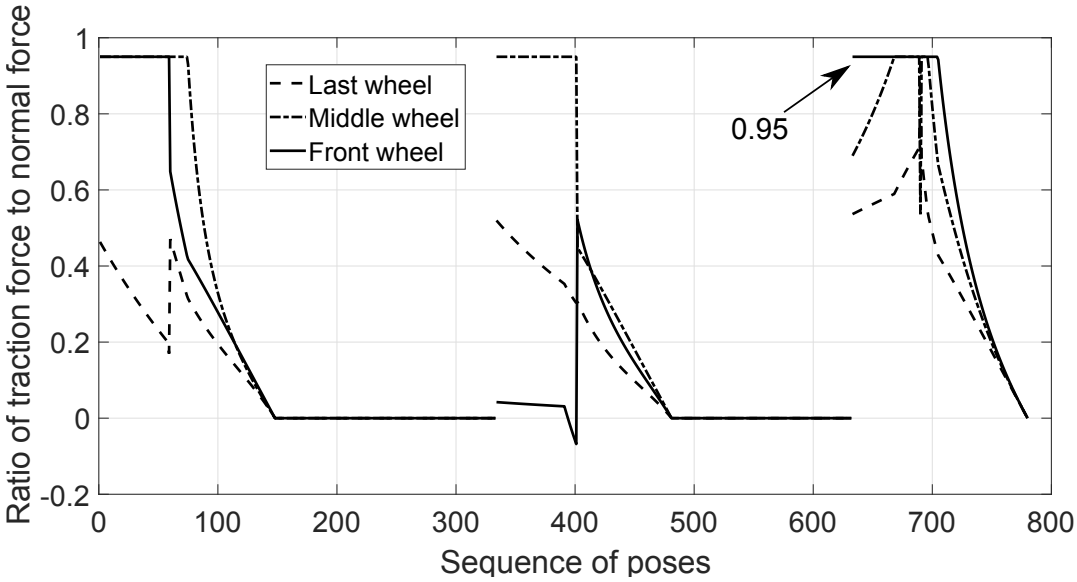

Figure 4.7: Contact force ratios during backward climbing.

4.3 Conclusion

In this chapter we addressed the problem of optimizing performance of rover when the coefficient of friction under (a) one wheel, and (b) all three wheels, are known. In the former case, the required coefficient from the unknown terrain was used as objective function, while in the latter case we used required torque as the objective function. Both problems were formulated as smooth optimization problems and solved numerically. The

latter problem is of lower level of complexity, as it is a linear programming problem.

Results obtained are intuitive. We are able to minimize objective functions more, when the known coefficient of friction is higher. There are even cases where the wheels on the parts of terrain with unknown friction, can just roll without traction.

The question of how coefficient of friction would be known in an unknown terrain, is not addressed here. We presume that good sensing and estimation techniques can give us reasonably accurate values for friction coefficient. If that is possible, then the further improvement of performance indicated by our results, also become possible, and we can even attempt to develop analytical and non-iterative methods of solving the optimization problem for the partially known terrain case, as we did in Chapter 3, for the fully unknown case.

CHAPTER 5

Optimal Design for Step Climbing

In chapters 2 and 3, we have seen how to minimize friction requirement of a given rover, when negotiating uneven terrain very slowly. A question of importance to designers is, how can we "design" the rover itself, so as to maximize mobility. In this chapter we address the optimal design problem, considering various scenarios. Rover climbing a single step and three different steps, without and with manipulator which can be used to shift centre of mass, with the normal force on wheel bounded by zero and bounded by a small positive value, and climbing forward and climbing backward.

5.1 Optimal Design for Climbing Single Step

Design of the rocker bogie suspension has to be based on various types of terrain the rover has to encounter. We focus our attention on climbing a large step and several large steps, in this chapter. In the subsequent chapter we extend our attention to staircases. As already mentioned in the literature survey, many objective functions have been proposed for optimal design. We consider only friction requirement at present. Other objective functions can be considered similarly.

5.1.1 Formulation

Our attempt is to propose a smooth formulation. We first describe the decision variables, which can be categorized as design parameters and pose related variables.

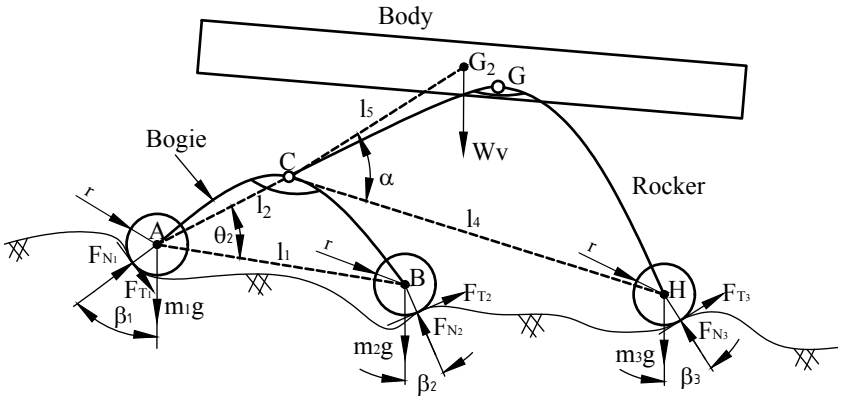

Figure 5.1: Geometric parameters of rocker-bogie suspension rover.

Design Parameters

Geometric parameters of the rocker-bogie suspension rover shown in Figure 5.1 are defined as follows:

- l_1 the distance between the first and middle wheel centers A and B;
- l_2 the distance between A and pivot of rocker and bogie C;
- θ_2 the angle between the lines AB and AC;
- l_4 the distance between C and H;
- l_5 the distance between C and body CoM G_2;
- α the angle between lines CH and CG_2;
- $r = r_1 = r_2 = r_3$ radii of the wheels;

Location of pivot G is not a parameter because rocker does not rotate w.r.t. body, as both wheels on both sides are moving identically, for the class of terrains we consider.

We use the assumptions which were made in Chapter 2. Wheel radii and weight, and body weight are fixed. The bogie and rocker link masses are assumed to be zero. We could have assigned some masses to rocker and bogie, proportional to their lengths, but used the simpler formulation here. Thus there are six design parameters (l_1, l_2, θ_2, l_4, l_5 and α).

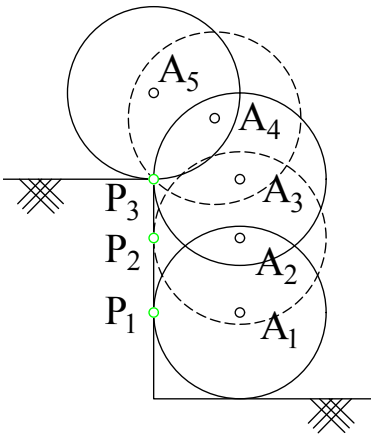

Figure 5.2: Wheel climbing sequence.

Pose Related Variables

We consider five poses for each wheel, as shown in Figure 5.2 when the wheel climbs the step. First pose P_1 is when the wheel just touches the vertical face of the step, the third pose P_3 when the contact point just reaches the top corner of the step, while the second pose P_2 is in the middle of first and third poses. In the fourth pose the line P_3A_4 from step corner to wheel center makes 45° with the horizontal, while in the fifth pose the line P_3A_5 makes 90° with the horizontal. Here A_i refers to first wheel center. For middle and rear wheels, we would have B_i and H_i. Considering 3 wheels, we have 15 separate poses. Once the position of the climbing wheel is known, the entire pose of the rover can be easily determined, as explained after describing the mathematical formulation. Each pose has eight force variables $(F_{N_1}, F_{T_1}, F_{N_2}, F_{T_2}, F_{N_3}, F_{T_3}, F_1, F_2)^T$ associated with it, making up a total of 120 force variables for 15 poses.

In addition to the above 6 design parameters and 120 pose related force variables, the dummy upper bound parameter μ is also included. As before, μ can be interpreted as the available friction between ground and wheels. The set of 127 decision variables is called $\{x\}$. We considered a wheel diameter equal to 110 mm and step height equal to wheel diameter, same as what we used in previous chapters.

Problem Statement

Our proposed formulation can now be mathematically stated as follows.

Determine {x} to

minimize μ,

subject to

(a) Equilibrium equations: $[A_h]\,\{y_h\} = \{b_h\},\ h = 1, 2, ..., 15$,

(b) Non-adhesion conditions: $F_{N_{i_h}} \geq 0,\ i = 1, 2, 3,\ h = 1, 2, ..., 15$,

(c) No-slip conditions: $-\mu F_{N_{i_h}} \leq F_{T_{i_h}} \leq \mu F_{N_{i_h}}$, $i = 1, 2, 3$, $h = 1, 2, ..., 15$,

(d) Non-negativity of coefficient of friction: $\mu \geq 0$,

(e) Limit on wheel base: $AH^* \leq 500$,

(f) Limits on CoM location of body: $\frac{1}{4}AH^* \leq x_{G_2} \leq \frac{3}{4}AH^*$ and $y_{G_2} \geq 2r + 20$,

(g_1) Non-interference of wheels with step in forward climbing: $x_{B_h} \geq r,\ h = 3, 4, 5$; $x_{H_h} \geq r,\ h = 6, 7, ..., 10$,

(g_2) Non-interference of wheels with step in backward climbing: $x_{B_h} \leq -r,\ h = 1, 2, ..., 5$; $x_{A_h} \leq -r,\ h = 8, 9, 10$,

(h) Non-interference of bogie with step: $l_2 sin\theta_2 \geq \left(\frac{l_1}{2} - \sqrt{2}r\right) - 5$, and

(i) Limit on height of pivot C: $y_C \leq 2r$.

Some of the constraints are explained below.

- In the equilibrium equations (a), $\{y_h\}\,\mathbb{R}^8$ is the force set related to the h^{th} pose and $[A_h]\,\mathbb{R}^{6\times8}$, $\{b_h\}\,\mathbb{R}^6$ are the corresponding coefficients. Equilibrium equations form a set of 15×6 = 90 equations. They are non-linear because elements of $[A_h]$ and $\{b_h\}$ depend on design parameters of the suspension. Note that we could have eliminated the equality constraints and six forces of each pose, by using just two forces as free variables. As this could have lead to singularity or near singularity during optimization, we did not do that.

- In condition (e), AH^* refers to the wheel base of the rover, represented by the distance between the wheel centers A and H when the rover is on a plane surface. In an earlier formulation, when we did not limit AH^*, the optimization search returned a very high value for AH^*. Hence we imposed the upper limit of 500 mm

in (e). AH^* is calculated as

$$AH^* = l_2 cos\theta_2 + \sqrt{l_4^2 - l_2^2 sin^2\theta_2}.$$

- The body is mounted on the rocker, and its dimension was fixed as 350 mm in length and 50 mm in height. Body CoM G_2 is assumed to be at its geometric center. G_2 cannot be at any arbitrary location with respect to the suspension. Through the first two constraints in (f), we limit the x position to within a certain interval centered at the midpoint between the first and last wheels. The specific interval chosen in this case was arbitrary. Through the third constraint in (f) we provide sufficient ground clearance. 'Sufficiency' was checked by checking interference of body with the step, from which we arrived at the value of 20 mm appearing in the third condition in (f). As there is no relative motion between the body and rocker, pivot G and G_2 can be considered as same for motion on 2D terrain.

- In a solution for forward climbing, the middle wheel and last wheel were found to intersect with the step in some poses when the first and middle wheels respectively were climbing the step (see Figure 5.3). Similarly, in a solution for backward climbing, the middle wheel and last wheel were found to intersect with the step in some poses when the first and middle wheels respectively were climbing the step. Hence we introduced constraints (g_1) for forward climbing and (g_2) for backward climbing. The constraint functions are calculated as follows.

  x_{B_h}, $h = 3, 4, 5$ in (g_1) was determined as (position of first wheel (x_A, y_A) is known)

  $$x_B = x_A + \sqrt{l_1^2 - (y_A - r)^2}.$$

  x_{H_h}, $h = 6, 7, ..., 10$ in (g_1) was determined as (position of middle wheel (x_B, y_B) is known)

  $$x_H = x_B - \sqrt{l_1^2 - (s + r - y_B)^2} + l_2 cos(\gamma + \theta_2) + \sqrt{l_4^2 - (s + l_2 sin^2(\gamma + \theta_2)},$$

  where γ is the inclination of bogie with horizontal.

  x_{B_h}, $h = 1, 2, ..., 5$; in (g_2) was determined as (position of first wheel (x_H, y_H) is known)

  $$x_B = x_H - \sqrt{l_4^2 - (y_H - r - l_2 sin^2\theta_2)} - l_2 cos\theta_2 + l_1.$$

  x_{A_h}, $h = 8, 9, 10$ in (g_2) was determined as (position of middle wheel (x_B, y_B) is

known)

$$x_A = x_B - \sqrt{l_1^2 - (y_B - r)^2}.$$

- Constraint (h) ensures that the pivot C of the bogie does not intersect with the step in the worst situation (see Figure 5.4). We consider the worst situation to be when the line AB is at 45 degrees, and demand that in that situation, the pivot C is farther than the step corner, in a direction perpendicular to AB. The link of the bogie can then be appropriately shaped to avoid interference of link with the step. This constraint was found to be too conservative, and hence the RHS was lowered to 5 mm.

- Constraint (i) ensures that pivot C is not very high. In one optimization search, μ was reduced significantly to around 0.3, with all constraints satisfied. However, the rover obtained, shown in Figure 5.5, had a very high location for pivot C and center of mass G_2. Hence we imposed the upper limit of $2r$ for height of C above horizontal ground.

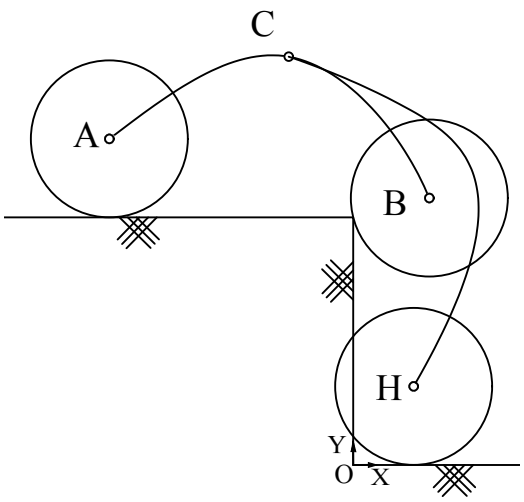

Figure 5.3: Interference of rear wheel.

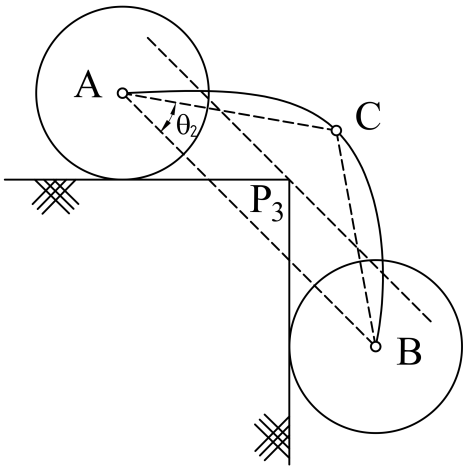

Figure 5.4: Worst case situation for pivot interference.

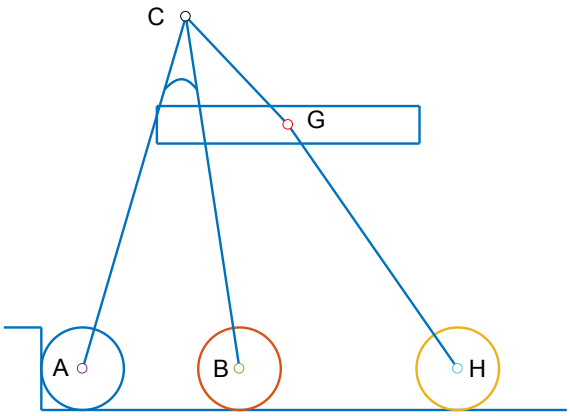

Figure 5.5: A solution with disproportionate dimension.

Determining Poses of the Rover

We had parametrized the pose of the rover by specifying the position of the wheel which is climbing the step. Here we describe how the pose of the entire rover can be determined from this single parameter, for a rover climbing the step in forward direction. We make use of the fact that when any one wheel is climbing the step, the remaining two wheels are on a horizontal surface, and hence the y coordinates of their centers are known.

When the first wheel is climbing the step (see Figure 5.6a), as the position of wheel center A is known, position of wheel center B can be determined as we know its y coordinate and the distance AB. As we know the positions of A and B now, position of pivot C can be obtained from values of design parameters l_2 and θ_2. Once the position of C is obtained, position of wheel center H can be obtained as we know CH and y coordinate of H.

When the second wheel is climbing the step (see Figure 5.6b), as the position of wheel center B is known, position of wheel center A can be determined as we know the distance BA, and the y coordinate of A (as first wheel is on the top landing of the step). As before, from the positions of A and B we can determine the position of pivot C. Then from the position of pivot C, position of wheel center H can be obtained, as the y coordinate of H, and the distance CH are known.

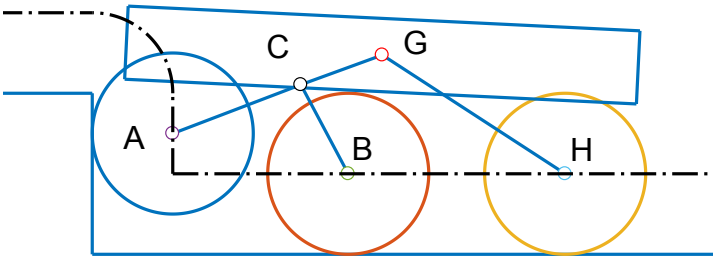

(a) A pose when first wheel climbing the step.

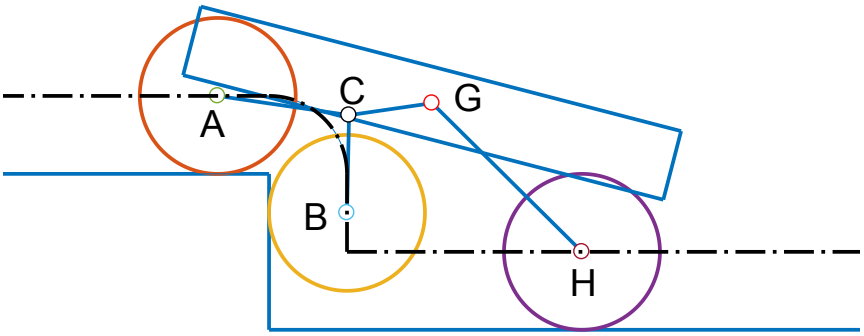

(b) A pose when middle wheel climbing the step.

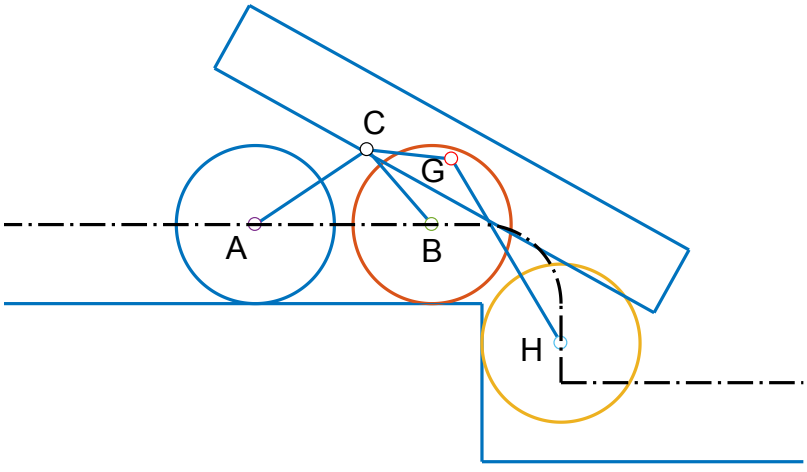

(c) A pose when rear wheel climbing the step.

Figure 5.6: Sequence of wheel climbing the step.

Table 5.1: Lower and upper bounds imposed.

Parameters	Lower bound	Upper bound
$F_{N_{i_j}}$	0	∞
$F_{T_{i_j}}, F_{1_j}, F_{2_j}$	-∞	∞
μ	0	∞
l_1, l_2, l_4, l_5	0	∞
θ_2, α	-∞	∞

Note: Lower bound of $-\infty$ indicates there is no lower bound. Upper bound of ∞ indicatesτ_1, τ_2 there is no upper bound.

When the third wheel is climbing the step (see Figure 5.6c), as the position of wheel center H is known, position of pivot C can be determined as we know the y coordinate of C, because both wheels A and B are on the top landing. Having obtained the position of C, positions of wheel centers A and B can be easily obtained as their y coordinates are known, and the distances CA and CB are also known.

Thus all the 15 poses can be determined using climbing wheel position and values of rover design parameters. The above calculations involve determining intersections of circles with horizontal straight lines, which have two solutions, or may sometimes not have any real solution. Out of the two real solutions, the one needed by us, is easy to identify. If there is no solution, we "break" out of the calculation, as in MATLAB® the remaining calculation will be done using complex numbers, and the iterations may continue unnecessarily without stopping.

For backward climbing too, the 15 poses of the rover were obtained similarly, from the position of the wheel which is climbing the step.

5.1.2 Solutions for Forward and Backward Climbing

The above problem was solved using 'fmincon' of MATLAB®. Optimal solutions for two cases were obtained. In the first case the rover climbs up the step forward (with the

bogie climbing first), while in the second case the rover climbs up the step backwards (with wheel number three, climbing first). In each case, the 15 poses described earlier were considered. Step height 's' is equal to wheel diameter ($2r = 110$ mm). Lower and upper bounds of decision variables are given in Table 5.1.

The effort required for finding optimal design, considering 15 poses, was considerably higher than that required for minimizing friction requirement of a given rover at a given pose. While searches from every guess solution converged in the latter case, only searches from very few guess solutions converged for optimal design. Initially, searches from several randomly chosen guess solutions (a) got aborted due to square root argument becoming negative, (b) got stuck in infeasible regions without progressing, (c) led to interference between wheels and steps, and (d) led to solutions with disproportionate dimensions. This helped us modify the bounds of some of the inequality constraints. In some cases we used the most recent point of a search as starting point, after these modifications. Finally, out of around 100 attempts, 10 searches converged to the same solution, in the sense that all the design parameters and μ are the same in all these solutions, with a few force variables at some poses being different.

One of the searches converged directly from a random guess to solution in 17.41 seconds in our computer with 1.6 GHz processor and 12 GB RAM. 314 iterations and 40321 function evaluations were required. In comparison, a search to optimize friction requirement of a given rover at a given single pose takes only around 0.045 seconds on the average, in the same computer, when started from random guesses. It took 25 iterations and 70 function evaluations to converge for a search which took roughly this time. It may be noted that the number of decision variables in the optimal design problem is 127, and the number of constraints is 242, while the number of decision variables in the performance optimization problem is 9, and the number of constraints is 15.

We analyse the solutions in detail below. Please note that design was optimized separately for forward and backward climbing, and we did not seek a single optimal design for both.

Table 5.2: Values of fixed parameters of optimal rover for forward climbing, optimal rover for backward climbing, and nominal rover.

Parameters	Forward	Backward	Nominal
μ	0.4457	0.6155	0.58 / 0.84**
l_1 (mm)	122.98	155.56	228.00
l_2 (mm)	93.64	119.47	132.30
θ_2 (degrees)	33.80	-2.29	30.00
l_4 (mm)	190.53	370.96	347.80
l_5 (mm)	59.21	141.74	118.85
α (degrees)	38.89	33.80	28.39
AH^* (mm)	261.10	490.30	456.00
y_{CoM} (mm)	130.00	130.00	156.70

Note: ** both forward and backward climbing friction requirements are shown.

Optimal Design for Forward Climbing

Performance of Solutions

The optimal μ for forward climbing is 0.45, 22% lower than the 0.58 obtained for nominal rover in Chapter 2. It should be noted that the nominal rover geometry was perhaps designed based on many considerations, while the optimal design obtained here is for the very narrow aim of climbing a single step. A more appropriate comparison with nominal rover requires consideration of several terrain geometries, and other design requirements. Optimal design of rover, considering three steps of different heights, is described in the next section. The use of just 15 poses during climbing, can also be questioned. Our aim is to establish the usefulness of a formulation and solution procedure. Later we show how this optimal design performs at other poses during the climb.

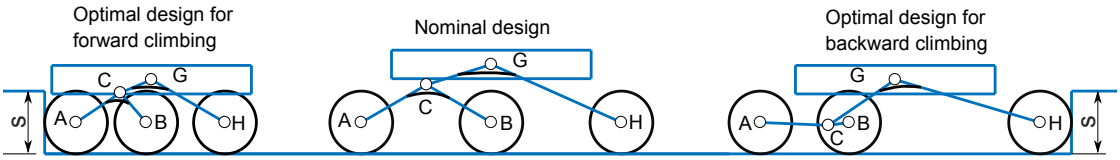

Figure 5.7: Optimal solution for forward climbing, nominal rover, and optimal solution for backward climbing. Rocker pivot is shown co-located with G_2, for convenience in drawing rocker.

Geometry of Solutions

The optimal parameters obtained for forward climbing and backward climbing are given along with those of the nominal rover in Table 5.2, and the three rovers are shown in Figure 5.7. During forward climbing, pivot C is sufficiently high to give ample clearance with the step corner.

The body CoM in the forward and backward solutions has reached its lower limit. The CoM of the body of the nominal rover is 27 mm above that of the two optimal solutions. In both cases, the CoM of the body is in between B and H and is closer to B in the case of solution for forward climbing.

Solution for forward climbing is the shortest among the three. Although we kept an upper limit of 500 mm for wheel base, both solution are shorter than that limit.

Analysis of Solution

Values of μ for the optimal solution for forward climbing, and corresponding torques are plotted in Figure 5.8 and 5.9 for the 15 poses considered. Straight lines were drawn between data points to show trends. They do not represent actual variations.

As already mentioned, while we got the same μ and mechanism parameters for some solution searches, force values of the solution were identical only at poses 1, 6, 7, and 13, where the force ratios are identical to the optimum μ obtained. At other poses, the force values were different. So we minimized the μ required at each of those poses, for

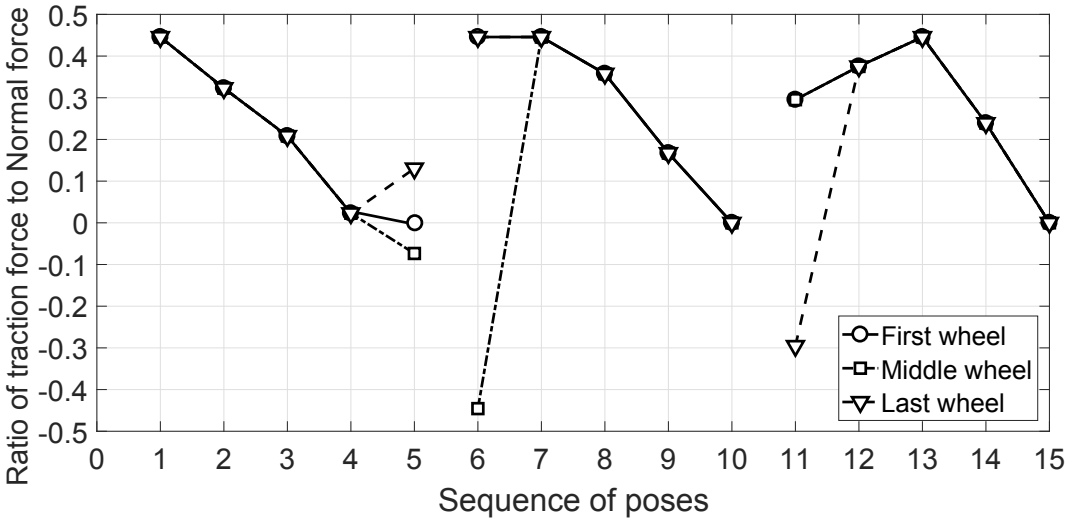

Figure 5.8: Ratio of traction force to normal force - optimal design for forward climbing.

plotting Figure 5.8.

As already noted in Chapter 2, the solutions at the fifteen poses demonstrate that we could miss some solutions if we (a) insist on the equal force ratio condition, or (b) insist on all traction forces being positive

In Figure 5.9 which shows the optimal torques, we can see that the torque peaks at pose 13, and the peak torque happens for the middle wheel which is on the top horizontal landing. At all other poses, torques of all wheels have lower values.

KKT Condition and Multipliers with Zero Value

KKT conditions, which are first order necessary conditions for constrained minima [70], essentially state that at a local minimum, which is a regular point, the gradient of objective function is a linear combination of all the active constraint gradients, with the multipliers of the active inequality constraints being non-positive. For regularity, the gradients of the active constraints should form a linearly independent set. We examined the solution for forward climbing to see whether it satisfies KKT conditions.

At poses 1, 6, 7, and 13, contact force ratios reached the peak value μ. At these poses,

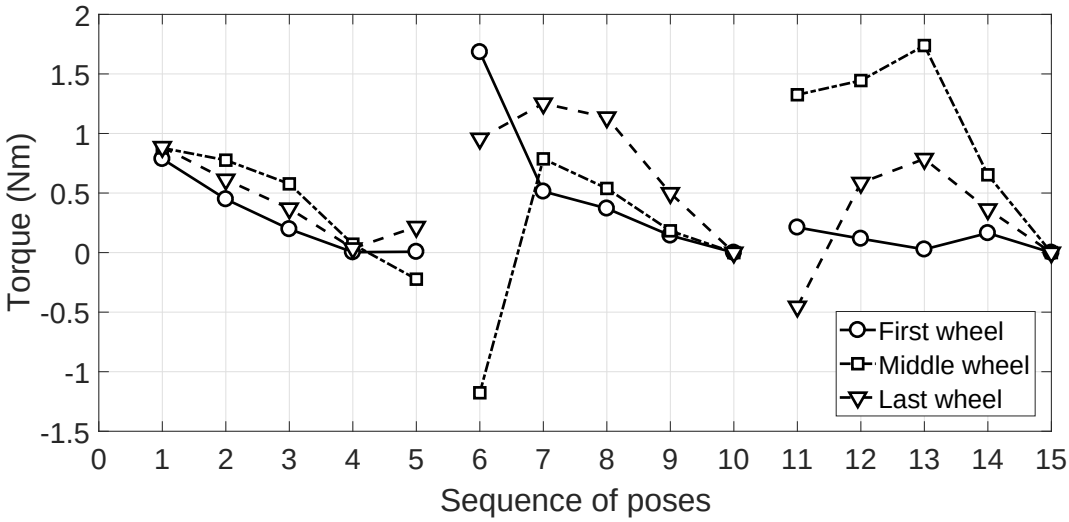

Figure 5.9: Torques - optimal design for forward climbing.

the slip constraints of all three wheels are active. At the other 11 poses, the contact force ratios are below the value of optimum μ, indicating that the corresponding forces are slack in the sense that they can have a range of values consistent with constraints, without affecting μ.

As already mentioned, at each of the 11 poses with slack, we minimized the magnitude of the ratio of traction to normal force to obtain unique solutions for all force variables. Figure 5.8 and 5.9 show such further optimized forces.

The solution has totally 18 active inequality constraints. They are (a) twelve constraints for preventing slip at poses 1, 6, 7, and 13, (b) two slip constraints and one non-adhesive constraint at pose 5 (the latter three are due to F_{N_1} and F_{T_1} being zero), (c) constraint for preventing middle wheel interference with step for pose 5, (d) constraint for preventing last wheel interference with step for pose 10, and (e) lower limit on height of CoM of body.

We check KKT conditions as follows. Gradients of all the 90 equality constraints and 18 active inequality constraints were determined. They were found to form a linearly dependent set. Thus the solution is not a regular point. The dependency arose because in the fifth pose there are two active slip constraints with gradients in the same direction. To make the solution a regular point, we minimized the local μ at pose 5 by introducing

a lower bound of 1 N for F_{N_1}. The pose 5 values in Figure 5.8, and 5.9 correspond to this. For this solution we have 105 active constraints (note that the two slip constraints and the non-adhesion condition are no more active). Their gradients form a linearly independent set, and hence the solution is a regular point. The objective function gradient was found to be a linear combination of the 105 active constraint gradients. Signs of the Lagrange multipliers of 15 active inequality constraints are negative. Lagrange multipliers of 67 out of 90 equality constraints were also found to be zero. Zero values of these 67 Lagrange multipliers happened because the corresponding constraints can be satisfied by a continuum of force variable values without affecting the optimum μ. This can be illustrated by the following simple analogous problem.

Determine $\{q, x_1, x_2, x_3, x_4\}$ to

minimize q,

subject to

$2x_1 - x_2 = 0$,

$x_3 - 4x_4 = 0$,

$(x_1 - 5)^2 + (x_2 - 5)^2 + 1 \leq q$, and

$(x_3 - 4)^2 + (x_4 - 3)^2 + 1 \leq q$.

The solution is q = 6, x_1 = 3, x_2 = 6, $x_3 \in [2.567, 6.233]$, $x_4 = \frac{x_3}{4}$. There is slack in the variables x_3 and x_4. Hence we can minimize the LHS of the second inequality to obtain x_3 = 4.4, x_4 = 2.2. This point satisfies the constraints. When checking the KKT condition at this point, we find that the Lagrange multiplier of the second equation is zero. This is analogous to 66 Lagrange multiplier of our solution being zero.

In addition to the above 11 poses with slack, at the 13^{th} pose, the Lagrange multiplier of the moment equation of the bogie is also zero. This does not happen due to slack - all three slip constraints are active. In this case it happens that the moment equation is satisfied by the solution of the problem posed by removing the moment equation of bogie at the 13^{th} pose, from the set of constraints.

As KKT conditions are satisfied, we can conclude that the objective function μ has reached a constrained local minimum. As all the searches that converged, arrived at the

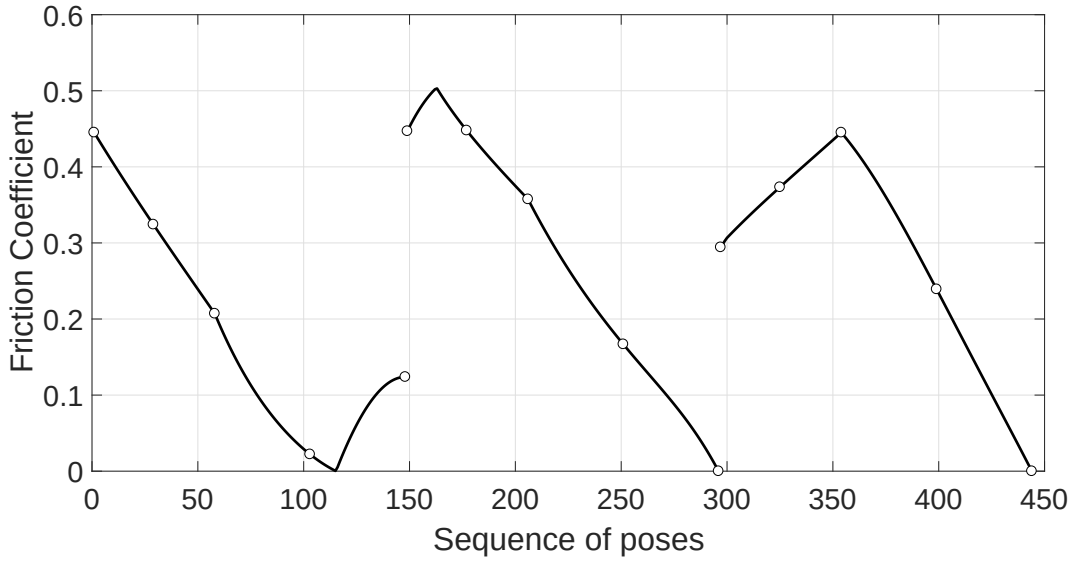

Figure 5.10: Coefficient of friction - optimal design for forward climbing.

same solution, we can say that it is likely that this is the global optimum, for the 15 poses considered.

Performance of Solution, Considering More Poses

The design which was optimized based on 15 poses during forward climbing, was analyzed considering 441 poses during the climb (see Chapter 2, for explanation regarding number of poses). At each of these 441 poses, friction requirement was minimized. Figure 5.10 shows the variation of optimum μ during the climb. Maximum value for μ was found to be 0.503, higher than the μ of 0.45 based on 15 poses. Similarly maximum torque considering the 441 poses is 1.881 Nm, which is larger than 1.684 Nm for 15 poses. μ can be seen to be a continuous function within the regime of climbing of one wheel. When the first wheel is climbing, μ reaches zero before changing sharply. From the pose where $\mu = 0$, the ratios become different in sign, for the three wheels. μ reaches zero at the end of climbing of middle and last wheels. Torque varies in a reasonably smooth fashion except at one pose each of middle and last wheel climbing regimes.

Note that it is possible to refine the design by including the poses at which peak friction coefficient requirements appear in the above graph, along with the previous 15

poses and the rover optimized again. That solution can be again analyzed, and its peak friction poses identified and included in the set of poses, and the rover optimized again. A few such iterations would take us to an improved design for the full climbing sequence. We did not attempt such refinements here.

Optimal Design for Backward Climbing

For backward climbing, optimal μ is 0.615, 26% lower than the 0.84 obtained for nominal rover. As mentioned earlier, five poses for each wheel climbing a single step totalling to a total of 15 poses were considered for finding the optimal design solution for backward climbing. The solution for backward climbing is quite different from that of forward climbing. The optimal rover for backward climbing is much longer, by about 75% or more than the optimal rover for forward climbing (see Table 5.2 and Figure 5.7). Backward climbing optimal rover has one of the wheels quite separated from the other two, unlike the solution for forward climbing and the nominal rover. One feature of the solution for backward climbing is that the pivot of the bogie namely 'C', is located below the line of centers AB. This would have been even lower, and caused interference with step corner. We prevented interference by adjusting the limit on constraint (h).

At pose 1, 6, and 13, the contact force ratios are same and equal to 0.615 (Figure 5.11), while at the remaining 12 poses, the contact ratios are lower. We minimized the ratio of traction to normal forces at the 12 poses. μ and torques of the optimal solution at the 15 poses are shown in Figure 5.11, 5.12. Note that the lines joining the 15 points do not correspond to optimal torques.

The solution has totally 12 active inequality constraints. They are (a) 9 slip constraints corresponding to poses 1, 6, and 13, (b) one constraint for the non-interference of bogie with step, (c) one constraint which prevents the last wheel interference with the step at pose 10, and (d) lower limit on height of CoM of body from ground. The gradients of all 90 equality constraints and 12 active inequality constraints were found to form a linearly independent set, and so the solution is a regular point. The signs of the Lagrange multiplier of 12 active inequality constraints are negative. It was found that values of

Lagrange multiplier of the equilibrium equations for the 12 poses with slack are zeros. The special case which occurred in pose 13 for forward climbing was obtained in pose 1 of backward climbing. At pose 1 the Lagrange multiplier was zero for the moment equation of bogie.

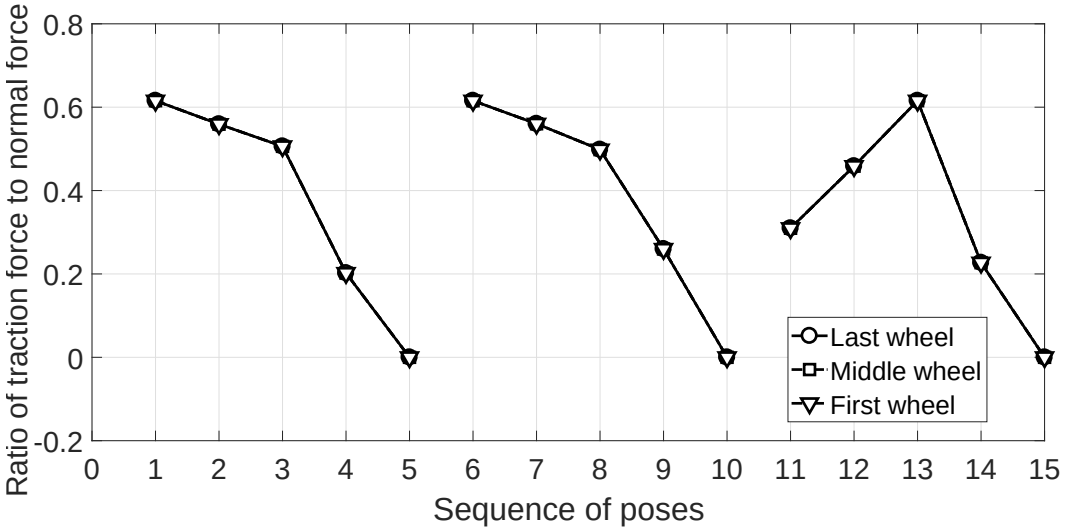

Figure 5.11: Ratio of traction force to normal force - optimal design for backward climbing.

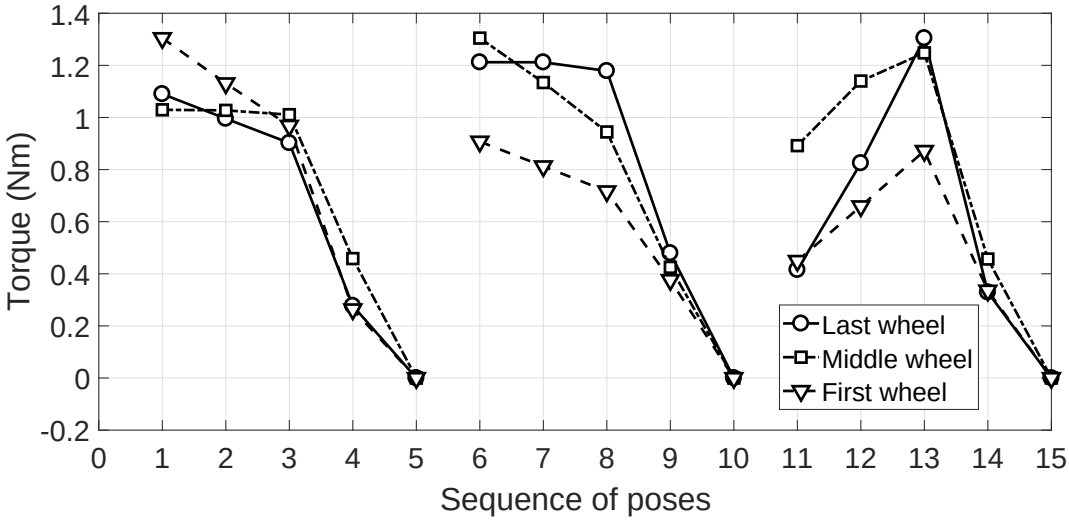

Figure 5.12: Torques - optimal design for backward climbing.

Performance of Solution, Considering More Poses

The optimal design for backward climbing was also analyzed at 783 points during the climbing sequence. Variation of minimum friction requirement for these 783 poses is shown in Figure 5.13. The highest μ of 0.622 is above the μ of 0.615 obtained for optimizing for 15 poses. The highest torque 1.325 Nm is above the highest torque of 1.305 Nm obtained for 15 poses. The performance considering all poses is just only slightly worse than the performance considering on 15 poses.

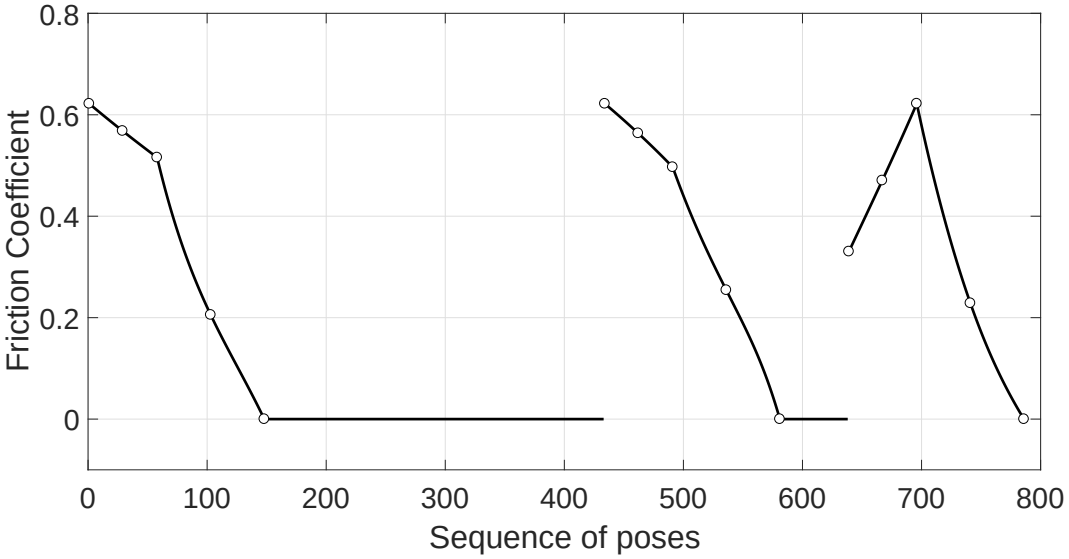

Figure 5.13: Coefficient of friction - optimal design for backward climbing.

5.2 Optimal Design for Climbing Three Different Steps

Using the formulation described in the last section, we obtained the optimal rover for climbing a step of height equal to thrice the radius of the wheel, using the 15 poses for climbing. Rocker-bogie suspension based rovers have been found to climb boulders which are three times the wheel radius [75]. The rover dimensions for this solution can be seen in Figure 5.14, along with the optimal rover for climbing a step of twice the wheel radius. Optimal μ for $3r$ step height is 0.4438 which is even lower than the optimal μ of 0.4457 for $2r$ step height. When optimal design obtained for climbing the $3r$ step was

used to climb the $2r$ step, a μ of 0.737 was required. Thus a rover designed for a taller step is not guaranteed to perform well for climbing a shorter step. This indicates the need to optimize design, considering different terrain geometries. The need to consider different geometries is also motivated by the fact that the design parameters are very different for optimal designs for individual steps, as shown by Figure 5.14.

Figure 5.14: Optimal solution for forward climbing; step height $s = 3r$ and $2r$.

Note that the nominal rover itself seems to have been optimized over a wide range of steps and perhaps other terrains, as our optimization of its performance on steps of height r and $3r$, showed that its μ required does not go above 0.58, which was obtained earlier for the $2r$ step.

5.2.1 Formulation

Poses Considered:

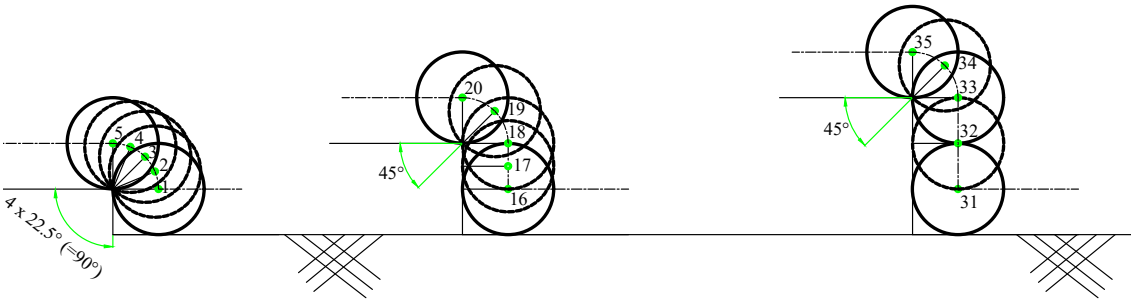

Figure 5.15: Position of centre of first wheel for three steps; step height $s = r,\ 2r$ and $3r$.

The positions of the center of first wheel are shown for the three steps in Figure 5.15, with pose numbers indicated. Second and third wheel centers also occupy the same positions, but the poses of the rover are different. The pose numbers corresponding to second wheel climbing are 6 to 10, 21 to 25, and 36 to 40. The pose numbers corresponding to third wheel climbing are 11 to 15, 26 to 30, and 41 to 45.

Amongst the rover poses corresponding to the 45 wheel positions, some are identical, and for such cases we consider only one pose each. The identical poses are:

1. Poses 1, 16, and 31: first wheel just butting the step butting from lower landing.
2. Poses 11, 28, and 43: wheels 1 and 2 on the top landing and wheel 3 center at 0°.
3. Poses 13, 29, and 44: wheels 1 and 2 on the top landing and wheel 3 center at 45°.
4. Poses 15, 30, and 45: wheels 1 and 2 on the top landing and wheel 3 center at 90°.
5. Poses 18, and 32: first wheels on steps 2r and 3r, with other two wheels on lower landing.

Thus the above 14 poses can be reduced to just 5, and so the total of 45 poses can be reduced to 36 distinct poses. The 36 poses are numbered continuously, and these pose numbers are used in the subsequent sections. Mapping of the 45 pose numbers to the corresponding 36 pose numbers is given in Appendix D.

Decision Variables

The eight force variables $(F_{N_1}, F_{T_1}, F_{N_2}, F_{T_2}, F_{N_3}, F_{T_3}, F_1, F_2)^T$, as mentioned in the Section 5.1 are related to each pose. Thus the 36 distinct poses add up to a total of 288 force variables. The six design parameters (l_1, l_2, θ_2, l_4, l_5 and α) also need to be included along with the dummy upper bound parameter μ. This set of decision variables is called x. Thus the total decision variables sums up to 295. The diameter of the wheel is 110mm, and steps of height 55mm, 110mm, and 165mm are considered for this study.

Problem Statement

Our proposed formulation can now be mathematically stated as follows.

Determine {x} to

minimize μ,

subject to

(a) Equilibrium equations: $[A_h]\{y_h\} = \{b_h\},\ h = 1, 2, ..., 36,$

(b) Non-adhesion conditions: $F_{N_{i_h}} \geq 0,\ i = 1, 2, 3,\ h = 1, 2, ..., 36,$

(c) No-slip conditions: $-\mu F_{N_{i_h}} \leq F_{T_{i_h}} \leq \mu F_{N_{i_h}}, i = 1, 2, 3, h = 1, 2, ..., 36,$

(d) Non-negativity of coefficient of friction: $\mu \geq 0,$

(e) Limit on wheel base: $AH^* \leq 500,$

(f) Limits on CoM location of body: $\frac{1}{4}AH^* \leq x_{G_2} \leq \frac{3}{4}AH^*$ and $y_{G_2} \geq 3r + 20,$

(g) Non-interference of wheels with step in forward climbing: $x_{B_h} \geq r,\ h = 27, 28, 29;$
$x_{H_h} \geq r,\ h = 30, 31, ..., 34,$

(h) Non-interference of bogie with step: $l_2 sin\theta_2 \geq \left(\frac{l_1}{2} - \sqrt{2}r\right) - 5,$ and

(i) Limit on height of pivot C: $y_C \leq 4r.$

Constraint (g) is similar to constraint (g_1) mentioned in Section 5.1. The poses 27, 28, and 29 corresponds to front wheel climbing the $3r$ step, and 30, 31,..., 34, corresponds to middle wheel climbing the same step.

Constraint (i) ensures that pivot C is not very high. In some solution the objective function was around 0.35, but it was observed that the pivot is very high as compared to the wheel diameter. Hence we imposed the upper limit of $4r$.

5.2.2 Results

The above problem also was solved using 'fmincon' of MATLAB®. As in the case of optimal design for a single step, several searches for optimal design for three separate steps also got aborted due to the square root argument negativity, and due to search getting stuck in infeasible regions. Of the approximately 40 attempts, only 2 attempts converged to the solution.

One of the searches took 87.25 seconds to converge, from an intermediate point, and not the initially chosen random guess. This clearly indicates that much greater effort was needed to converge to solution for the case of three steps, compared to the case of one step.

The optimal μ for forward climbing, considering three steps, is 0.4694. This is only slightly higher than the optimal designs for the separate steps. It is still lower than the optimal μ of 0.58 of the nominal rover for climbing the three steps, by 19%. Now that we have considered more number of terrain scenarios, the comparison with the nominal rover has started becoming more reasonable. The optimal rover is slightly taller than the nominal rover, as can be seen in Figure 5.16. Particularly, pivot C is almost at the top line of the body, while it is below the body in the case of nominal rover.

The solution has totally 18 active inequality constraints. They are (a) 13 slip constraints corresponding to poses 1, 11, 20, 29, and 30, (b) two slip constraints and one non-adhesive constraint at pose 11 (the latter three are due to F_{N_1} and F_{T_1} being zero), (c) one constraint which prevents the last wheel interference with the step at pose 34, and (d) lower limit on height of CoM of body from ground.

The KKT conditions were checked. The gradients of the 216 equality constraints, and the 18 active inequality constraints formed a set of linearly dependent set. The dependency arose because in the eleventh pose there are two active slip constraints with gradients in the same direction. To make it a regular point, the lower bound of 1N was introduced for F_{N_1} at pose 11. This shifted the optimal solution to a nearby point with 231 active constraints, whose gradients form a linearly independent set. Lagrange multipliers of 172 out of 216 equality constraints with slack, are zero. The signs of multipliers

of all the active inequality constraints are negative, and so KKT conditions are satisfied.

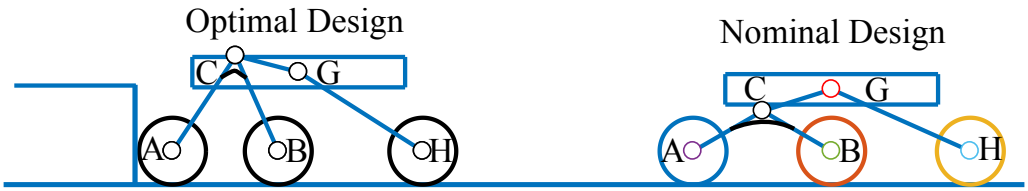

Figure 5.16: Optimal solution for forward climbing of three steps of heights $r, 2r, 3r$, and nominal rover.

Note that the special situation at pose 11, where the reaction and traction forces of the first wheel are zero, is the same as that of pose 5 in the optimal design for single step climbing.

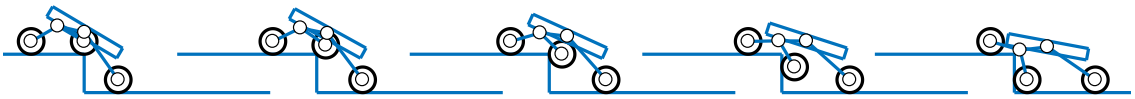

(a) Nominal rover.

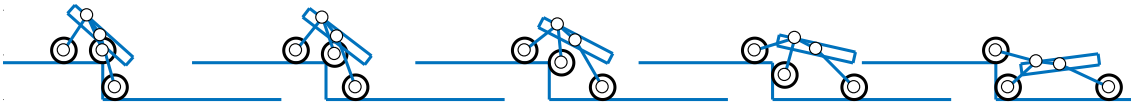

(b) Optimal rover for climbing r, 2r, and 3r steps.

Figure 5.17: Middle wheel climbing sequences for a $3r$ step.

Figure 5.17 shows middle wheel climbing sequences of the nominal rover and the optimal rover (designed for climbing steps of height r, 2r, and 3r), climbing the step of height $3r$. The figure gives an idea about the relative positions of bogie and the front wheels, with respect to the rocker, body, and rear wheel. It may be noted that the range of pitch angle of the optimal rover is greater than that of the nominal rover.

The design which was optimized based on 36 poses was analysed considering 542 poses, 625 poses and 618 poses for step heights of r, $2r$, and $3r$ respectively. Maximum value of μ was found out to be 0.4868, higher than 0.4694 based on 36 poses. However, the μ obtained is still better than μ of 0.58 of nominal rover (by 16%).

Table 5.3: Values of fixed parameters of optimal rover with zero normal force, optimal rover with $F_{N_{min}} = 1.4388N$ climbing three different steps.

Parameters	$F_{N_{min}} = 0$	$F_{N_{min}} = 1.4388N$
μ	0.4694	0.4760
l_1 (mm)	173.93	174.30
l_2 (mm)	188.31	189.37
θ_2 (degrees)	56.44	57.10
l_4 (mm)	345.28	347.80
l_5 (mm)	106.92	104.44
α (degrees)	12.45	11.08

5.2.3 Optimal Design for Positive Normal force

The results of optimal design of rover for climbing single step, and three different steps showed that at some poses, the rover will be at a point of marginal stability. This situation can be avoided by ensuring a minimum positive normal force on all wheels, at all poses. Thus optimal design of rover was attempted, keeping a minimum positive normal force at all poses, for the three wheels. We imposed an $F_{N_{min}}$ of 1.4388 N, which is 5% of the total weight of the rover. The terrain considered consists of the three large steps mentioned above, of heights 55mm, 110mm, and 165mm, with wheel radii being fixed at 55mm.

The formulation is same as that mentioned in Section 5.2, the only difference being that the lower bound on the normal forces of the three wheels on all the 36 poses is set as $F_{N_{min}} = 1.4388N$ instead of zero.

The parameters of the optimal rover obtained are given in Table 5.3. It can be seen that the size and shape of this optimal rover is very close to that of the optimal rover for $F_{N_{min}} = 0N$. The friction requirement has worsened only slightly to 0.4760, from the value of 0.4694 for the case when $F_{N_{min}} = 0N$. The ratio of traction force to normal force for the 36 poses considered is shown in Figure 5.18. Poses 1 to 15, 16 to 26, 27 to

36 corresponds to the $r, 2r,$ and $3r$ step respectively.

At pose 1, 11, 20, 29, and 30 contact force ratios reached the peak value of μ. Except pose 11, the slip constraints of all three wheels are active at these poses. At pose 11, slip constraint of only the last wheel is active. Contact force ratios of the first and middle wheels in pose 11, and those of all three wheels in the other 31 poses, are below the value of optimum μ.

The solution has totally 16 active inequality constraints. They are (a) 13 slip constraints corresponding to poses 1, 11, 20, 29, and 30, (b) lower bound on F_{N_1} at pose 11, (c) one constraint which prevents the last wheel interference with the step at pose 34, and (d) lower limit on height of CoM of body from ground.

KKT conditions were checked. Gradients of the active constraints (216 equality constraints, and 16 inequality constraints) form a linearly independent set, and so the solution is a regular point. KKT conditions are satisfied, with Lagrange multipliers of all the 16 active constraints being negative. This indicates that our solution is a local minimum.

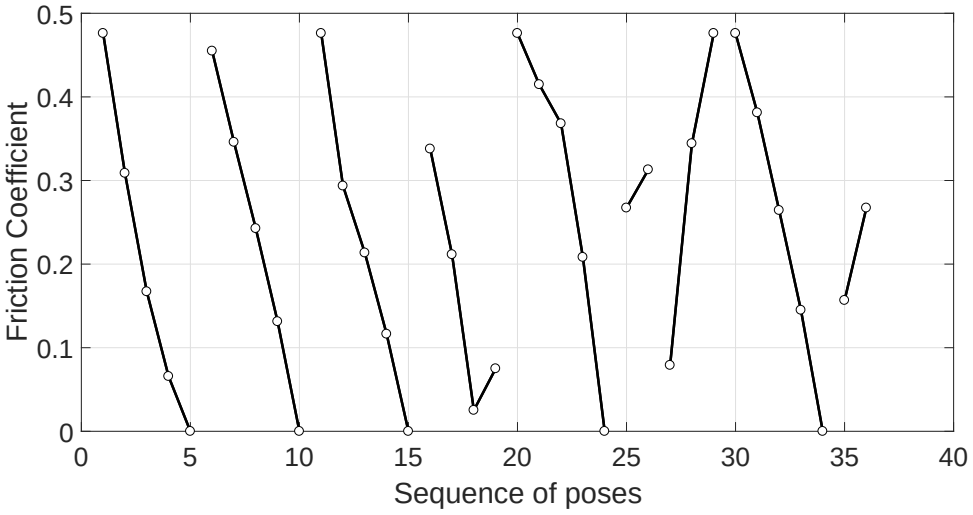

Figure 5.18: Ratio of traction force to normal force - optimal design for forward climbing of rover, climbing three steps of height $r, 2r, 3r$ with $F_{N_{min}}$.

The design which was optimized based on 36 poses with positive normal force was analysed considering 542 poses, 626 poses and 619 poses for step heights of r, $2r$, and

$3r$ respectively. Maximum value of μ was found to be 0.4940, higher than 0.4760 based on 36 poses. However, the μ obtained is still better than μ of 0.5823 of nominal rover with the same $F_{N_{min}} = 1.4388N$ (by 15.16%).

Thus it can be seen it is possible to optimally design a rover for climbing different step heights, using our formulation. Imposing a positive lower bound on normal force, is useful from the point of view of stability, and when we used a lower bound of small magnitude, friction requirement did not worsen much.

5.3 Optimal Design with Manipulator

In Chapter 2, we examined whether shifting of the CoM using an onboard manipulator can reduce the friction requirement. We found that with the manipulator considered, the worst friction requirement of the optimal forward climbing rover of Subsection 5.1.2 was reduced from 0.4457 to 0.4390, an improvement of just 1.5%.

Here we examine whether the rover itself can be optimally designed, factoring in the capability of shifting the center of mass using the manipulator. We optimize for the case of climbing 3 different steps, considered in Section 5.2. We detail out the formulation, before presenting the solution.

5.3.1 Formulation

The rover parameters l_1, l_2, θ_2, l_4, l_5 and α are the same, as discussed previously. The masses and the assumptions considered are also same for this study. The manipulator arm consists of two segments, with two revolute joints, as shown in Figure 5.19.

Additional Pose Related Variables

As done in Section 2.5, we introduce the additional pose variable x_{manip} to represent the position of CoM corresponding to a manipulator pose. The details are described in Section 2.5.

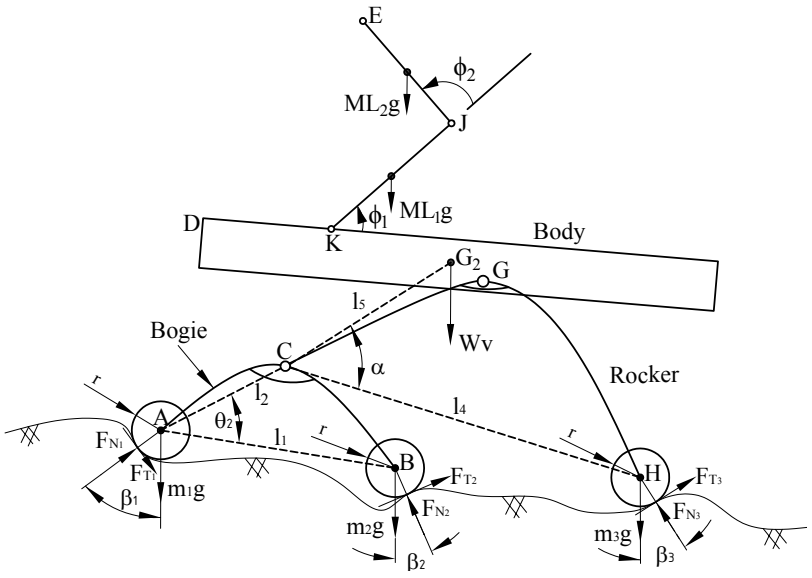

Figure 5.19: Geometric parameters of rocker-bogie rover with manipulator.

The decision variables are 331 in number, and constitutes the vector $\{x\}$, which consists of

- 6 design parameters,
- 288 pose related force variables,
- 36 pose related variables for location of effective CoM of manipulator, and
- the dummy upper bound parameter μ.

Problem Statement

Our proposed formulation can now be mathematically stated as follows.

Determine {x} to

minimize μ,

subject to

(a) Equilibrium equations: $[A_h]\{y_h\} = \{b_h\},\ h = 1, 2, ..., 36,$

(b) Non-adhesion conditions: $F_{N_{i_h}} \geq F_{N_{min}},\ i = 1, 2, 3,\ h = 1, 2, ..., 36$,

(c) No-slip conditions: $-\mu F_{N_{i_h}} \leq F_{T_{i_h}} \leq \mu F_{N_{i_h}}, i = 1, 2, 3, h = 1, 2, ..., 36$,

(d) Non-negativity of coefficient of friction: $\mu \geq 0$,

(e) Limit on wheel base: $AH^* \leq 500$,

(f) Limits on CoM location of body:$\frac{1}{4}AH^* \leq x_{G_2} \leq \frac{3}{4}AH^*$ and $y_{G_2} \geq 3r + 20$,

(g) Non-interference of wheels with step in forward climbing: $x_{B_h} \geq r,\ h = 27, 28, 29$; $x_{H_h} \geq r,\ h = 30, 31, ..., 34$,

(h) Non-interference of bogie with step: $l_2 sin\theta_2 \geq \left(\frac{l_1}{2} - \sqrt{2}r\right)$,

(i) Limits on $y_C \leq 4r$, and

(j) Limits on CoM location of manipulator:$-200 \leq x_{manip_h} \leq 200,\ h = 1, 2, ..., 36$.

5.3.2 Solution

Optimal solution was obtained for rover climbing three steps (steps of height 55 mm, 110 mm, and 165 mm) in forward direction. The lower and upper bounds of decision variables are same as given in Table 5.1, except that the lower bounds of normal forces for all three wheels are $F_{N_{min}} = 1.4388N$. The solutions were generated using 'fmincon' of MATLAB®.

As in the case of other optimal design searches, several searches for optimal design for three separate steps with CoM shifted by manipulator, also got aborted due to the square root argument negativity, and due to search getting stuck in infeasible regions. Of the approximately 40 attempts, only 5 attempts converged to the solution.

The optimal μ for forward climbing with manipulator arm is 0.4073, 14.43% lower than 0.4760 obtained for optimal rover without CoM shifting, in the Section 5.2. The optimal rover for forward climbing with manipulator, and optimal rover without manipulator are shown in Figure 5.20 and their parameters are given in Table 5.4. It can be seen that the overall length of optimal rover with manipulator is 18.72% more than that

Table 5.4: Values of fixed parameters of optimal rover with two segmented manipulator arm, and optimal rover without manipulator, both with $F_{N_{min}} = 1.4388N$.

Parameters	Without manipulator	With manipulator
μ	0.4760	0.4073
l_1 (mm)	174.30	238.64
l_2 (mm)	189.37	246.19
θ_2 (degrees)	57.10	42.08
l_4 (mm)	347.80	348.14
l_5 (mm)	104.44	133.90
α (degrees)	11.08	13.137
AH^* (mm)	412.20	489.28

of optimal rover without manipulator. Although an upper limit of 500 mm for wheel base was chosen, the solution was within this limit. One can see that the pivot 'C' height for both the cases are almost same, and the height of body CoM 'G' are also similar.

The solution for optimal design with manipulator for forward climbing was examined to see whether it satisfies KKT conditions. Gradients of all the 216 equality constraints, 11 active inequality constraints, and 2 active lower bound and 2 active upper bounds were determined. These gradients form a linearly independent set, and hence the solution is a regular point. The objective function gradient was found to be a linear combination of the 231 active constraint gradients. Signs of the Lagrange multipliers of all the 15 active inequality constraints and bounds, are negative. As KKT conditions are satisfied, we can conclude that the objective function μ has reached a local minimum value. It is likely to be the global minimum, as it was the best solution from 40 starting points, of which 5 converged to this solution.

Optimal design of rover with manipulator was also done with lower bound for normal force as zero, for moving in forward direction for these three different steps. The μ obtained was 0.4025, against the μ requirement of 0.4073 with minimum positive normal

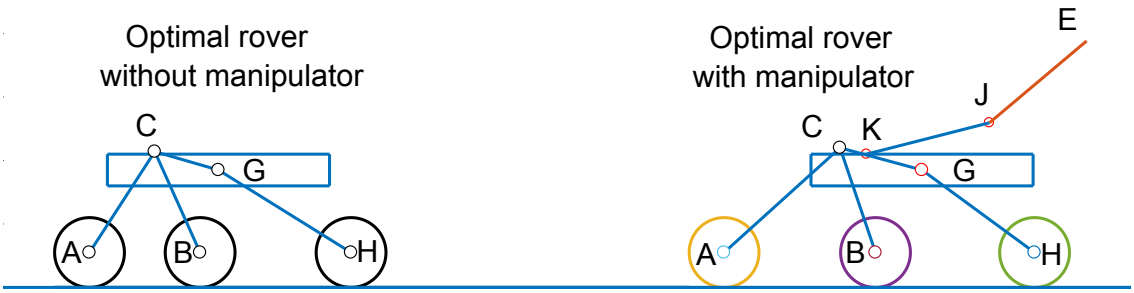

Figure 5.20: Optimal solution for forward climbing of three different steps with and without manipulator, keeping minimum positive normal force on all wheels.

force of $F_{N_{min}} = 1.4388N$. Allowing zero normal force improved the solution slightly, but has the disadvantage that there is no margin for stability.

When the optimally designed rover with manipulator was moved backward to climb the three steps, with μ minimized at each pose, a worst μ of 1.239 was required, indicating that the rover is not suitable for climbing backwards.

The design with manipulator which was optimized based on 36 poses with positive normal force was analysed considering 624 poses, 714 poses and 740 poses for step heights of r, $2r$, and $3r$ respectively. Maximum value of μ was found to be 0.4073, same as that obtained based on 36 poses. The μ obtained is better than μ of 0.5823 of nominal rover with the same $F_{N_{min}} = 1.4388N$, by 30.05%.

Note that wheel radii were not used as decision variables for optimizing the rover here. In the next chapter, for optimal design of rover for staircases, we do use them as decision variable, like other researchers who have optimized rovers for staircases have done. In the next chapter we also include the scenario of three large steps, and hence we do not include optimization with wheel radii as decision variables here.

5.4 Conclusion

In this chapter we attempted to find the optimal rover for a single step, and for three steps of different heights, without and with manipulator for shifting CoM, and with zero and positive lower bounds for normal reaction forces. In all cases we were able to obtain local minima, as indicated by satisfaction of KKT conditions. And in all cases, the fact that the solution obtained is the best out of several searches, of which a few converged to the same solution, indicates that we obtained the global optima in all cases. This indicates the efficacy of our smooth problem formulation and the solver we used.

Using a small positive lower limit for normal reaction forces worsened our solution only slightly. Using a manipulator enabled the design to improve to a point which was substantially better (0.4073) than the solution without manipulator (0.4940).

The rover without manipulator, optimized for three steps, considering 36 poses, has a maximum μ required which is 15.16 % better than that of nominal rover, when all poses in the climbing sequence are considered. In both cases we used a positive $F_{N_{min}} = 1.4388N$. The optimal rover with manipulator is 23.47% better than the nominal rover. This can be further improved by considering more poses for optimization. Please note that the comparison with nominal rover is not really fair to the nominal rover, as it might have been designed with many more considerations than what we have used for designing our optimal rovers. We believe that our approach can be extended to include more design considerations.

We also optimized the rover for backward climbing, but found that in most cases, it is substantially worse than for forward climbing.

CHAPTER 6

Optimal Design for Staircase Climbing

From optimally designing a rover for climbing large single steps in the last chapter, in this chapter we move on to optimally designing the rover for climbing staircases and large single steps. We consider a staircase first, and then staircase along with three large steps.

6.1 Optimal Design for Staircase Climbing

The previous formulations for optimal design of rover for step climbing, with and without manipulator, were formulated as smooth optimization problems. In the case of staircases, we found it difficult to obtain a smooth formulation, for the reasons given below.

We considered a sequences of poses defined by the position of the first wheel on the staircase. Figure 6.1 shows a pose which can occur during the optimization search. At this pose the contact point of the middle wheel contact could be on the horizontal tread or the the vertical riser. The equality constraints (equilibrium conditions) are discontinuous with respect to a decision variable like the length AB, at this pose. This happens because the coefficient matrix itself is discontinuous due to discontinuous shift in contact point. We tried several remedies for this, but are yet to arrive at a good method for addressing this issue. Another issue which cropped up is that when we allow the wheel radius to change as a decision variable, the number of poses on the riser would change from a specific number, to zero. This is explained below, where we describe selection of poses. This also causes a discontinuity in the entire formulation. Hence we decided to proceed with a formulation with such discontinuities and use an appropriate solver which can work in spite of discontinuities. Our formulation of the problem as a discontinuous optimization problem is described below.

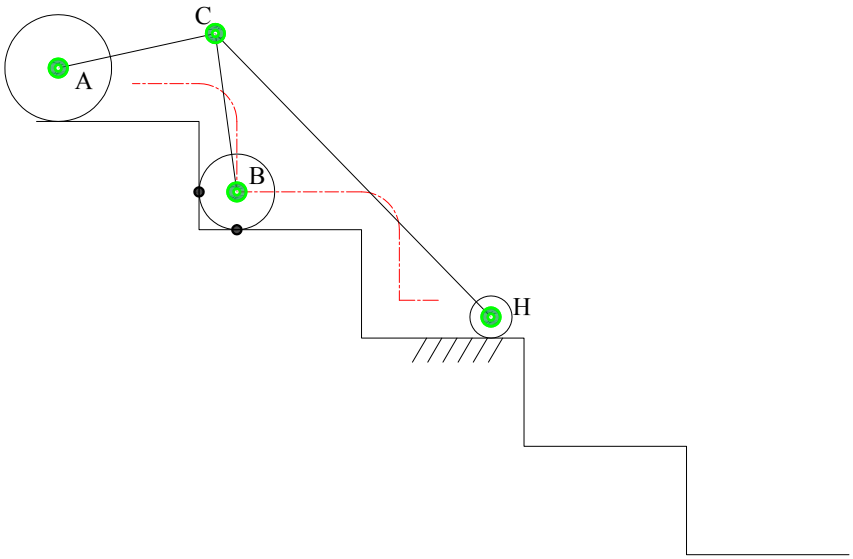

Figure 6.1: Rocker-bogie suspension climbing options.

6.1.1 Formulation

The assumptions considered previously are also valid for this study. We first describe the decision variables, and then the wheel positions considered, and calculation of associated full poses, before stating the problem mathematically.

Design Parameters

The parameters considered for this study are l_1, l_2, θ_2, l_4, l_5 and α, which were already defined in the previous Chapter 5 'Optimal Design for Step Climbing'. The wheel radii r_1, r_2, and r_3 of the rover were also considered along with the aforementioned list of design parameters. These parameters are shown in Figure 6.2. Thus there are nine design parameters l_1, l_2, θ_2, l_4, l_5, α, r_1, r_2 and r_3 and this set is called as $\{\mathrm{x}\}$.

Poses Considered

Staircases in residential buildings require a minimum width of tread without nosing, of 250 mm, and the maximum riser height should be 190 mm, while for other building the minimum tread width is 300 mm, and maximum riser height is 150 mm [76]. But,

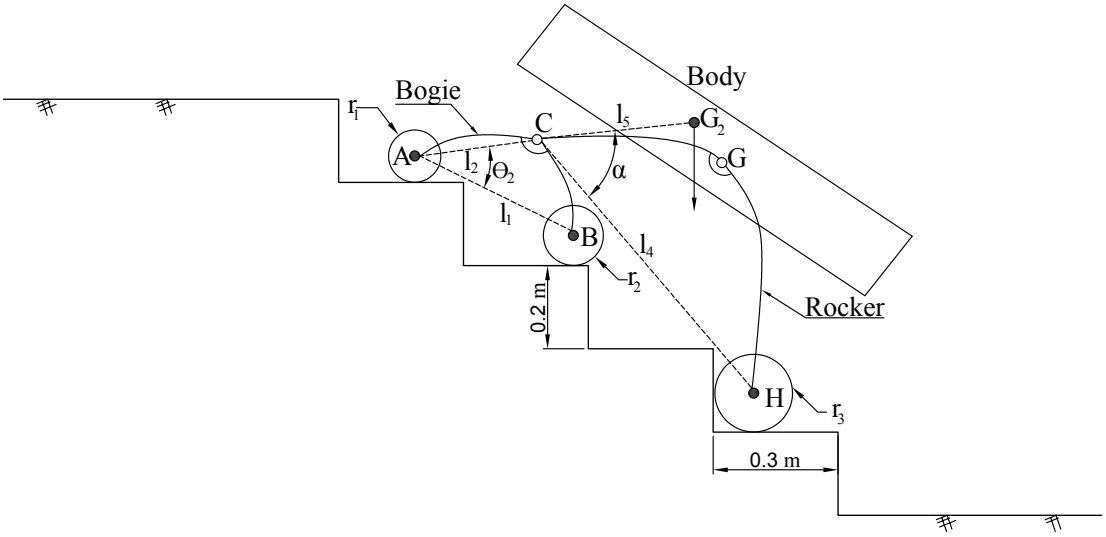

Figure 6.2: Rocker-bogie suspension moving climbing a staircase.

staircases of various dimensions (tread width varies from 240 mm to 310 mm, and riser height varies from 100 mm to 250 mm) were considered by researchers [54, 65, 64]. In our study, we considered a staircase with tread (T_r) 300 mm, and riser (H) 200 mm, (slope of the staircase is $33.69°$) with five steps from the bottom landing to the top landing. Fifth tread and top landing are essentially one and the same. The number of steps is limited to five, so as to avoid too many repeating poses. The rover resting on the bottom flat horizontal plane next to the staircase with, the first wheel butting the riser of the step, is considered as the starting pose. All wheels of the rover reaching the top landing of staircase is the last pose. Bottom and top landings are assumed to be sufficiently large so as to accommodate all wheels of the rover.

For obtaining the rover climbing sequence on the staircase, the center position of first wheel, A, and its contact points are used, which are predefined. Equivalently, predefined center positions of middle or rear wheel also can be used for obtaining the climbing sequence.

The following poses are considered for first wheel on every step of the staircase (see Figure 6.3):

- Poses on the riser of step: The initial pose corresponds to the first wheel butting the riser of step. Apart from the initial pose, two more equal distant points on the riser

are also considered, before the wheel centre reaches the corner of this step. Thus four poses were considered on the riser. This is applicable only when the radius of the wheel is less than the step height (case (a) in Figure 6.3). If the radius of wheel is equal to or more than the step height, all these poses on riser need to be excluded (case (b) in Figure 6.3). As the wheel radius is a decision variable, this could cause a sudden change in the number of poses considered.

- Poses on the corner of step: Every ten degree rotation of wheel centre on step corner, starting after horizontal extension of tread, till the wheel centre exactly reaches above the step, constitutes nine poses. These many number of poses are selected because, when the front wheel center is at the corner, we observed that the progress of the other two wheels are significant. The above is applicable when the front wheel radius is less than or equal to the step height (case (a) in Figure 6.3).

  If the front wheel radius is more than step height, the poses starting from the wheel butting the step corner, till the wheel center reaches the last point on the corner, only need to be considered. For this case, (shown as case (b) in Figure 6.3), the distance the wheel centre need to travel is relatively larger than case (a), as the wheel radius is higher. Due to this we consider 10 poses on this portion of step.

- Poses on the tread of step: Consider seven equidistant poses, from the wheel centre position at the last point on the corner, till the wheel butts with the riser (for $r_1 < H$) or corner (for $r_1 \geq H$) of next step. Of these, we consider the middle 5 poses as the poses on the tread.

  The number of poses considered on the tread of step was chosen based on the consideration that, for a front wheel diameter of 0.15m, the distance travelled by the wheel along the center line will be approximately equal while climbing the riser and tread.

As already pointed out, as the front wheel radius is also a design parameter, the number of poses on staircase can change with the front wheel radius. If the radius of the wheel is less than the step height, the total of poses sums up to 141, as discussed earlier. But, if the radius of front wheel is greater than or equal to the step height, the poses on

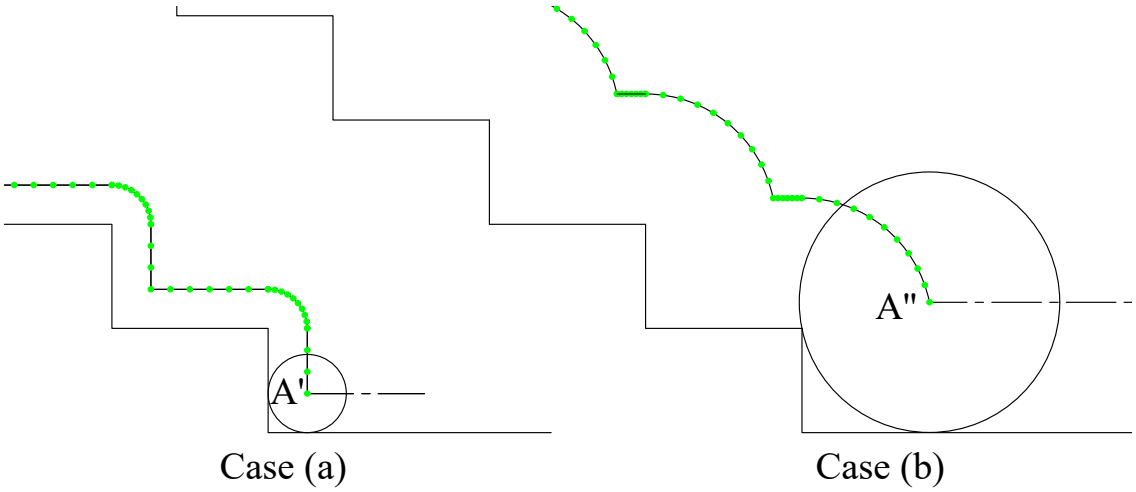

Figure 6.3: Centre positions of front wheel: case (a) Wheel radius smaller than step height, case (b) Wheel radius bigger than step height.

the riser of all the steps need to be excluded, bringing the number of poses down to 131.

Determination of the Full Rover Pose

When the front wheel is at one of the predetermined positions, the positions of the other two wheels, pivot C, and rover body have to be determined. We explain our procedure for this, using Figure 6.4. In the figure, front wheel is shown at a location on the riser of step 5. Location of middle wheel center B can be obtained by the intersection of an arc with center at A and radius equal to l_1, with the center line of middle wheel. The center line of middle wheel is shown as G3-J4-K4-G4-J5-K5 in the figure. It is a piecewise continuous non-smooth curve made up of straight line segments and circular arc segments which are at distance r_2 from the step surface. Determination of the intersection of the circular arc of radius l_1 with this curve requires checking whether the intersection falls within the valid domains of the segments. In most cases, B can be located uniquely. Once B is located, from A and B, the pivot C is located easily. Once C is located, we intersect an arc with center at C and radius equal to l_4, with the center line of third wheel H. This center line is also a piecewise continuous non-smooth curve made up of straight line segments and circular arc segments which are at distance r_3 from the step surface. Note that when the radius of the wheel, r_2 or r_3, is more than the height of the step, the respective center

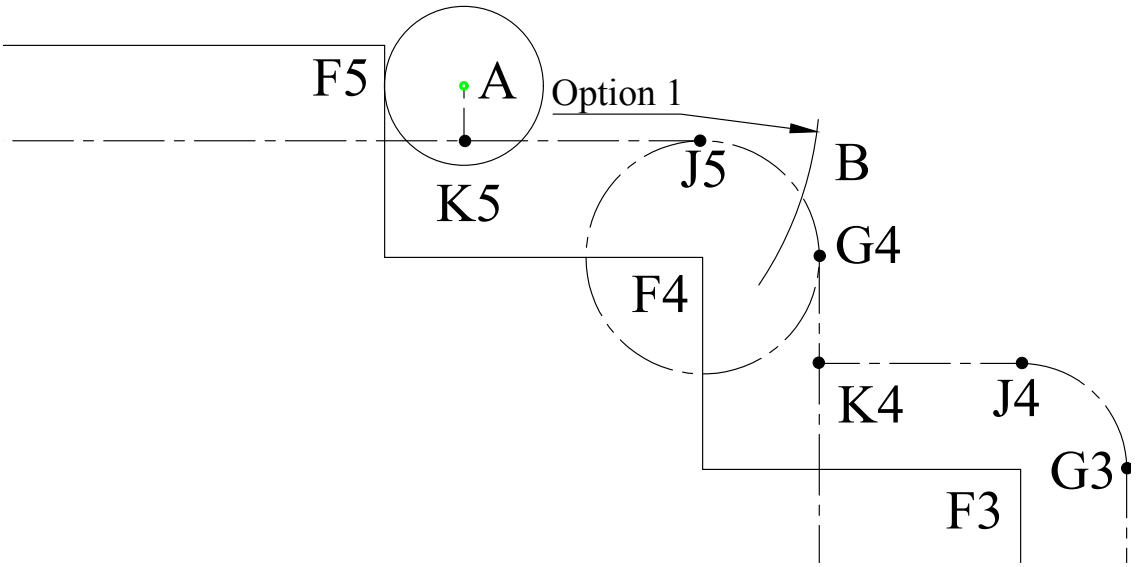

Figure 6.4: Finding centre of middle wheel, B.

line will not have the straight line segment $\mathrm{K_j G_j}$ (case b in Figure 6.3).

Problem Statement

Our formulation can now be mathematically stated as follows.

Determine {x} to

minimize $max\ \{\mu_1, \mu_2, \mu_3, ..., \mu_h, ..., \mu_k\}$

where $\mu_h = min\left\{max\left\{\left|\frac{F_{T_{1h}}}{F_{N_{1h}}}\right|, \left|\frac{F_{T_{2h}}}{F_{N_{2h}}}\right|, \left|\frac{F_{T_{3h}}}{F_{N_{3h}}}\right|\right\}\right\}$

subject to

(a) Equilibrium equations: $[A_h]\{f_h\} = \{b_h\},\ h = 1, 2, ..., k,$

(b) Non-adhesion conditions: $F_{N_{i_h}} \geq 0,\ i = 1, 2, 3,\ h = 1, 2, ..., k,$

h denotes the pose number,

subject to

(c) Limit on wheel base: $AH^* \leq 1000$,

(d) Limits on CoM location of body: $\frac{1}{4}AH^* \leq x_{G_2} \leq \frac{3}{4}AH^*$ and $200 \leq y_{G_2} \leq 300$,

(e) Non-interference of bogie with step: $l_2 sin\theta_2 \geq \left(\frac{l_1}{2} - \sqrt{2}r_1\right) - 5$, and

(f) Non-interference between wheels: $x_B - x_A \geq r_1 + r_2$ and $x_H - x_B \geq r_2 + r_3$.

The objective function μ was found out as follows. For each pose 'h', the minimum required coefficient of friction, μ_h is determined satisfying constraints (a) and (b), using the non-iterative algorithm 1, mentioned in Chapter 3. Note that the number of poses is 141 if $r_1 < H$, and otherwise, 131. The maximum of all the μ_h's for all these poses corresponds to the value of objective function μ. If lower limit for normal force is $F_{N_{min}} > 0$, we use algorithm 2 instead of algorithm 1, to find μ_h.

This way of defining the objective function has reduced the decision variable space and number of constraints significantly. Otherwise we would have had to use all the force variables and corresponding equality and inequality constraints, or at least two force variables per pose with corresponding inequality constraints

Some of the constraints are explained below.

- The eight forces associated with pose h, in the equilibrium equations (a), are $\{f_h\} = \left\{F_{N_{1_h}}, F_{T_{1_h}}, F_{N_{2_h}}, F_{T_{2_h}}, F_{N_{3_h}}, F_{T_{3_h}}, F_{1_h}, F_{2_h}\right\}^T$. These equations are the same as those mentioned in Chapter 2.

- Condition (c), AH^* refers to the wheel base of the rover, represented by the distance between the wheel centers A and H when the rover is on a plane surface. In an earlier formulation, when we did not limit AH^*, the optimization search returned a very high value for AH^*. Hence we imposed the upper limit of 1000 mm in (c). In the earlier design, discussed in Chapter 5, we used an upper limit of 500 mm. We changed the limit to 1000, as the value of 500 mm, may be too small a wheel base for climbing this staircase.

- The body size, and limits on the CoM location (constraint (d)) in the x position is same as that discussed in Section 5.1. Through the third and fourth constraints we provide sufficient ground clearance, and didn't allow the body to be too far above the ground.

- In a solution, the first wheel and the second wheel were found to be intersecting. The first constraint in (f) says that the distance between the wheel centers A and B, when the rover is on a plane surface, should be greater than the sum of the radii

of first and middle wheels. Similarly the middle wheel and last wheel were found to be intersecting. The second constraint says that the distance between the wheel centers B and H, when the rover is on a plane surface, should be greater than the sum of the wheel radii of middle and rear wheels.

6.1.2 Results

As mentioned already, some among the objective and constraint functions are non-smooth and even discontinuous. Due to this, we used Genetic Algorithm for solving this problem. The function 'ga' of MATLAB® was used. The function 'ga' uses the augmented lagrangian approach of using lagrangians and penalty parameters to combine objective function and constraints, and minimizes fitness based on this composite function. In each generation, genetic algorithm is used to minimize the fitness for fixed values of lagrange multipliers and penalty parameters, to a desired level of accuracy [77].

Each chromosome in the population consists of 9 parameters, mentioned in $\{x\}$. The fitness function μ was calculated for each chromosome, using the corresponding values of decision variables which are link lengths, angles, and wheel radii. Some of the genetic algorithm parameters which were chosen based on a variation study, are as follows. The population size was chosen as 150, crossover fraction 0.8, maximum number of generations 200. Roulette wheel selection method was used for selection of chromosomes for new population. Mutation is also introduced to effectively explore the search space.

The lower and upper bounds of decision variables used for this design are given in Table 6.1. The lower and upper bounds were chosen such that, no link lengths should be greater than 1000 mm. The angles θ_2 and α were made to lie within the four quadrants. The lower bounds on wheel radii were chosen to be same as that of the nominal rover (55 mm), while the upper bound chosen was greater than step height, 250 mm.

Table 6.1: Lower and upper bounds imposed.

Parameters	Lower bound	Upper bound
l_1, l_2, l_4, l_5	0	1000 (mm)
θ_2, α	-π (rad)	π (rad)
r_1, r_2, r_3	55 (mm)	250 (mm)

Solution

Solutions were attempted from 10 different starting populations, keeping the lower bounds of normal forces for all three wheels as $F_{N_{min}} = 1.4388N$. No two searches converged to the same point. It was seen that the best objective function values of the 10 searches range from 0.5053 to 0.7156. Approximately 5 generations were needed to converge to the final solution. Figure 6.5 is the plot provided by MATLAB® on the progression of one of the searches from generation to generation. It can be seen that in the second generation itself, a significant improvement in fitness was obtained. By the fourth generation, the fitness value seems to have reached close to its final value. In two of the generations, mean and best values appear to almost overlap. We could not analyse the progress in detail, as the intermediate populations were not available.

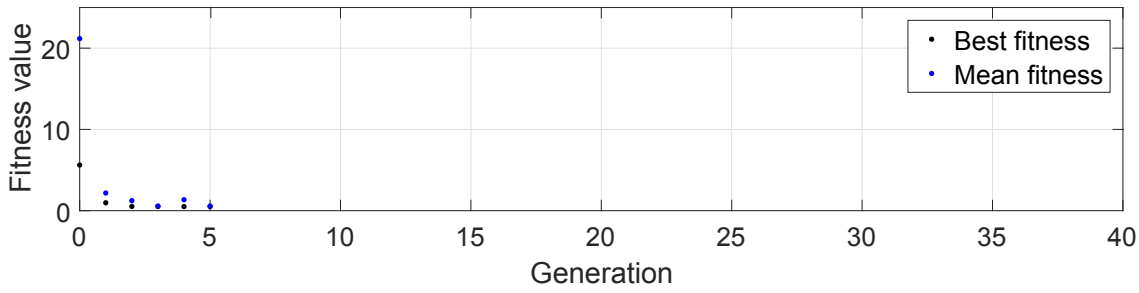

Figure 6.5: Progression of best fitness during optimization.

The objective function value for the optimal rover obtained is 0.5053. The variation of μ_h as a function of pose h for the staircase climbing is shown in Figure 6.6. It can be seen that 8 peaks have nearly the same optimal friction value, which could indicate that there may be further scope for improvement in objective function as the number of design variables is nine.

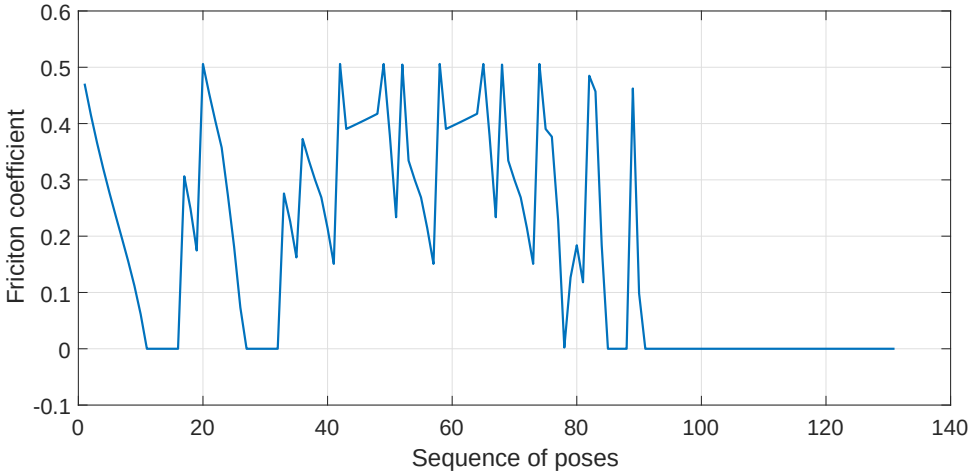

Figure 6.6: μ variation of optimal rover climbing a staircase.

Some poses in the staircase climbing sequence of this optimal rover are shown in Figure 6.7. It was observed that while one of the wheel is climbing a riser, the other two wheels are either on the tread or on the corner, which essentially means that no two wheels are climbing a riser together. This appears to validate the approach by Woo et al. [55] of avoiding poses with more than one wheel at risers for a pose.

The parameters of optimal rover for staircase climbing with minimum normal force can be seen in Table 6.2. It can be seen that r_1 has reached its upper bound, and r_3 the lower bound.

Optimal design of rover was also done with lower bound for normal force as zero, for staircase climbing. It was observed that the μ required decreased to 0.4984, against the μ requirement of 0.5053 with positive normal force of $F_{N_{min}} = 1.4388N$.

We tried to improve the performance of the optimal rover by shifting its CoM using a manipulator. The improvement was less than 0.5%.

When optimal performance of the nominal rover for staircase climbing was determined, at the 141 poses used here, it was found that friction coefficient required was 4.5717. This indicates that the nominal rover was not designed for climbing a staircase of the type we considered. The high μ of 4.5717 did not occur at a pose where more than one wheel are on risers. In fact such a pose does occur while the nominal rover climbs the

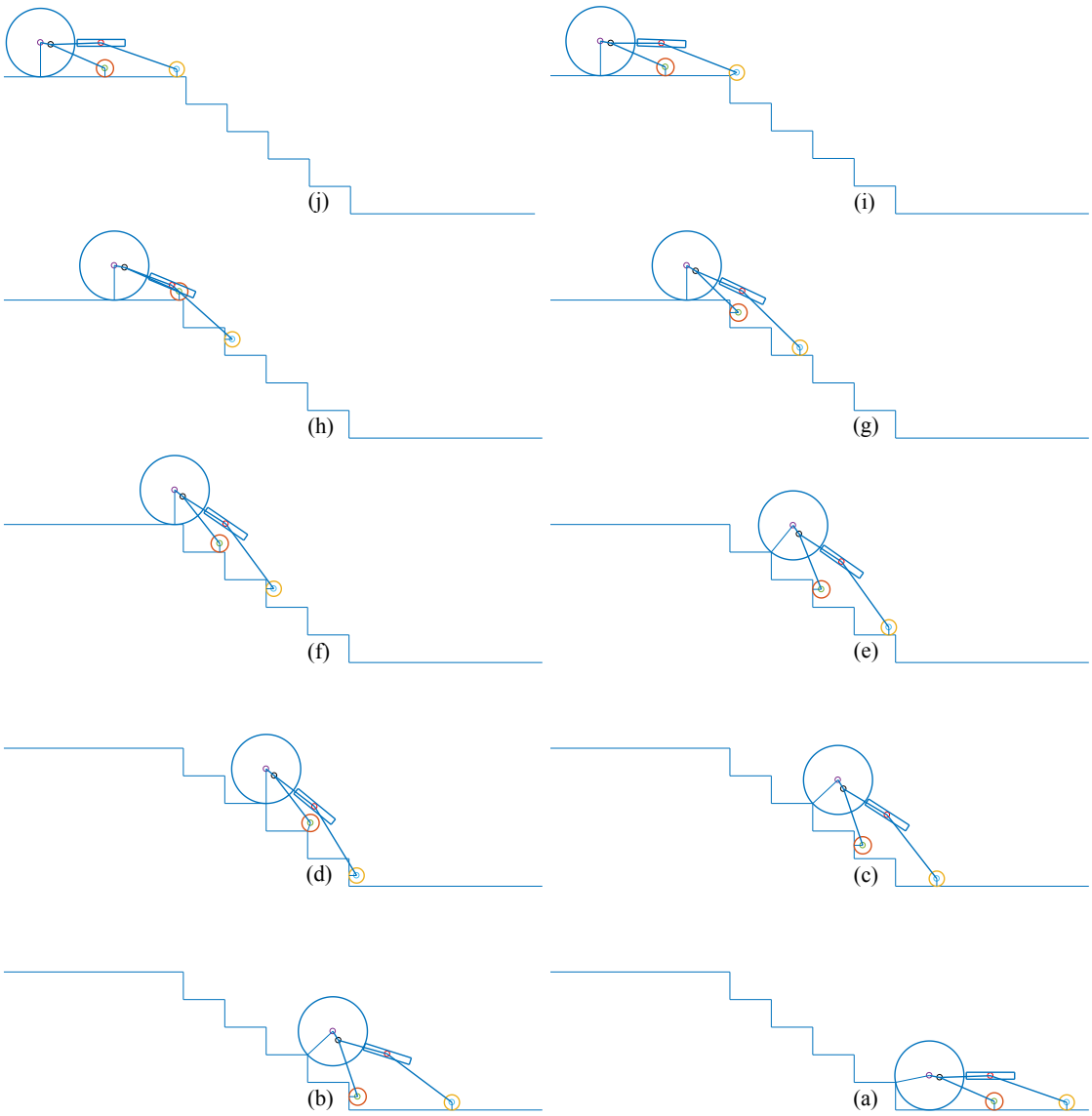

Figure 6.7: Some poses in sequence of climbing of optimal rover for staircase climbing (*from bottom (a) to top (j)*).

Table 6.2: Optimal rover parameters for staircase climbing.

Parameters	Staircase	3 steps + staircase
μ	0.5053	0.5421
l_1 (mm)	506.48	450.33
l_2 (mm)	76.63	34.78
θ_2 (degrees)	11.04	-41.13
l_4 (mm)	937.18	951.54
l_5 (mm)	367.46	378.36
α (degrees)	13.03	12.90
r_1 (mm)	249.99	249.99
r_2 (mm)	62.39	104.48
r_3 (mm)	55.00	73.56

staircase, but it has a low optimal μ of just 0.4384. This indicates that we need to revise our earlier conclusion that the approach by Woo et al. [55], of avoiding such poses, is valid. It is now clear that good solutions can occur with such poses, and so they need not be avoided in the formulation.

We tried to optimize the rover design, keeping the wheel radii fixed at 55 mm, the same as the radii of the rovers in the previous chapter. The minimum required friction in this case was 0.7032, much higher than the μ when we allowed the radii to vary.

The genetic algorithm search which solved the staircase problem, started from a random population of 150 and converged to the best point in 5 generations, taking about 2520 seconds.

To climb a ramp of the same angle as the mean slope of the staircase, a μ of 0.67 is needed. The μ of 0.5053 needed by the optimal rover for climbing the staircase is much better than that. But the maximum traction force on a wheel of the optimal rover, for climbing the staircase, is 0.39 times the rover weight, which is more than twice the traction force of 0.185 times the rover weight, needed for climbing the ramp.

6.2 Optimal Design for Three Steps and Staircase

The problem of optimal design for staircase was extended to include three different steps, along with the staircase. Single steps of height 100 mm, 200 mm, 300 mm, and the staircase 300 mm $\times$ 200 mm were considered.

Formulation

The 9 parameters discussed in the previous section were used as decision variables. They are l_1, l_2, θ_2, l_4, l_5, α, r_1, r_2 and r_3, and this set is called as $\{\mathrm{x}\}$.

Additional Poses Considered

For a rover climbing a single step, the pose of the front wheel on the riser, corner, and the top landing need to be considered.

Poses for front wheel climbing the riser, and corner of the step are same as discussed in Section 6.1.1 for staircase climbing. In addition to that, for the rover completing the climbing sequence for a single isolated step, 56 equidistant positions of the front wheel on the top landing were considered, so that all the wheels of rover will reach the top horizontal landing of the step. The set of poses defined are similar for 100 mm, 200 mm, and 300 mm step heights. All these four terrains are considered for this design. The rover is moving through all these terrains, one after the other. A total of 346 poses were considered for the design, if the front wheel radius is less than smallest step height, 100 mm.

The objective function, constraints, and lower, and upper bounds are same as mentioned in previous section.

6.2.1 Results

This problem also was solved using, 'ga' in MATLAB®. Solutions were attempted from 8 different starting populations, keeping the lower bounds of normal forces for all three wheels as $F_{N_{min}} = 1.4388N$. No two searches converged to the same point. It was seen that the objective function values of 8 solutions range from 0.5421 to 0.6225. Approximately 4 generations were needed to converge to the final solution. Figure 6.8 is the plot provided by MATLAB® on the progression of search from generation to generation.

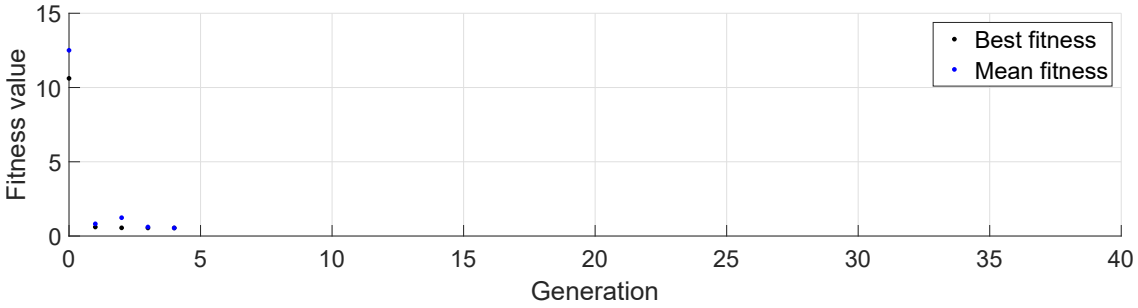

Figure 6.8: Progression of best fitness during optimization.

The objective function value for the optimal rover obtained is 0.5421. This, as expected, is worse than that of the optimal rover for staircase alone, which is 0.5053. The variation of required friction coefficient is shown in Figure 6.9. The zones A, B, C, and D denotes the rover climbing the four terrains namely 100 mm, 200 mm, 300 mm height steps, and staircase. It can be seen that 9 peaks have nearly the same value as the optimal mu, which might indicate that significant further improvement may not be possible, as the number of decision variables is 9.

Optimal design of rover was also done with lower bound for normal force as zero, for staircase and three steps. The μ required reduced to 0.5106, against the μ requirement of 0.5421 with positive normal force of $F_{N_{min}} = 1.4388N$. When we examined the minimum normal force for our solution, it was found to be 1.312 N, just slightly below 1.4388 N. What this indicates is that the attempts to optimize the design using ga have not come very near to the global optimum.

The optimal design obtained for climbing a staircase, and the optimal design for climbing a staircase and 3 large steps of different heights, are shown in Figure 6.10, and

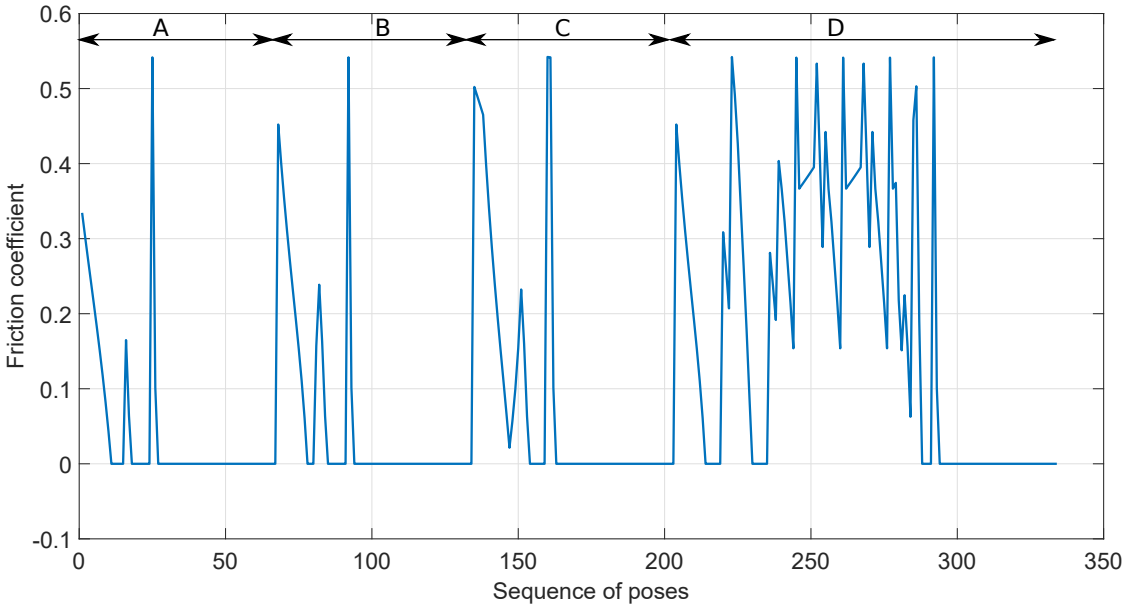

Figure 6.9: μ variation of optimal rover climbing three steps and a staircase.

the parameters given in Table 6.2. It can be seen that r_1 has reached its upper bound for the latter.

Middle wheel climbing sequences of the rover on a step of height 300 mm is shown in Figure 6.11. It was observed that no pose during staircase climbing had more than one wheel at a riser.

The performance of the optimal rover improved only by less than 0.5%, when a manipulator was used to shift the CoM.

Optimal rover design with fixed wheel radii equal to that of nominal rover, had a relatively high friction requirement of 0.7235.

6.3 Conclusion

We could not find a continuous and smooth problem formulation for optimizing rover for staircase climbing. However, we were able to reduce the problem space significantly, and use the very fast non-iterative algorithms of Chapter 3, for objective function calculation. With this, genetic algorithm was able to produce results which are good, but may not

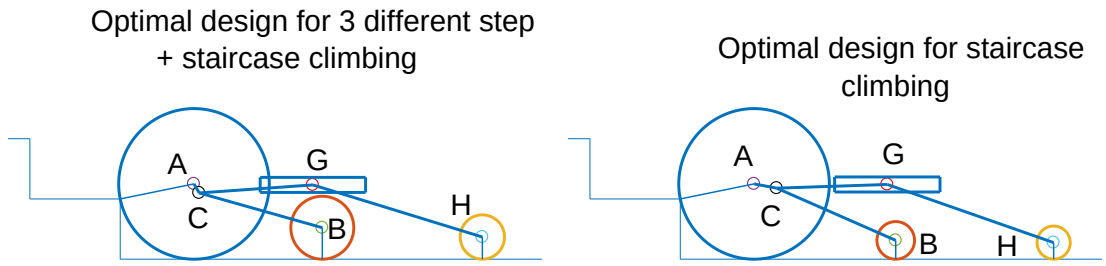

Figure 6.10: Optimal rover design for climbing 3 different steps, and staircase, and optimal staircase design with minimum positive normal forces.

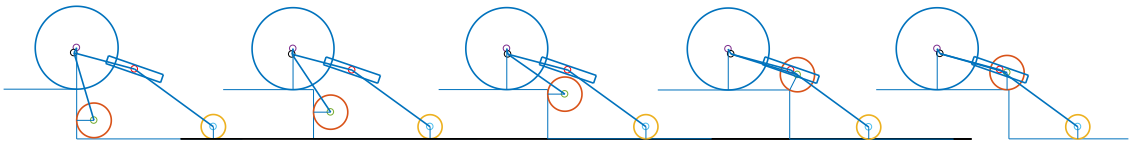

Figure 6.11: Optimal rover designed for climbing 3 different steps and staircase, climbing a step of height 300 mm - middle wheel climbing sequence.

be exact optima. Friction requirement of the solution obtained for staircase along with three isolated steps, for $F_{N_{min}} = 1.4388N$, is only slightly worse than that of solution obtained for three steps, in the previous chapter. Use of a zero lower limit for normal forces, improved the required μ only slightly. Use of manipulator to shift CoM also improved the performances of these solutions only slightly. It is not possible to compare the performances with that of nominal rover, as it does not seem to have been designed for climbing staircases. We obtained solutions with fixed wheel radii, and found that the μ required is much worse than that of solutions obtained with wheel radii treated as variables.

CHAPTER 7

Conclusions and Future Work

We conclude by summarizing the contributions of this work, and by making certain observations. We also make some suggestions for future work.

7.1 Contributions and Observations

Our major goal was to formulate the problem of optimizing performance and design of rocker-bogie suspension rovers in a better way, and obtain solutions. We considered only structured terrains with steps and staircases. In most cases, our objective was to minimize friction requirement.

For minimization of friction requirement for a given rover, we formulated the problem as a smooth optimization problem, which we believe is useful for arriving at exact local and global optima. We obtained solutions using a very powerful gradient based numerical solver for smooth optimization problems. The fact that our solutions are local or global minima, is proven by the fact that they satisfy first order necessary conditions for constrained minima. Our solutions also prove that the characterization of solution as having equal ground contact force ratios for the three wheels, used by earlier researchers, is not a sufficient condition for minimum, and is also not necessary in some special cases. Our solutions also prove that the approach of some earlier researchers, of restricting force ratios to be positive, could lead to suboptimal solutions.

An important contribution of our work is the detailed understanding of the nature of optima of the above problem, and the proposal of two non-iterative algorithms for determining solutions. These algorithms have been demonstrated to be very effective, and very fast compared to a generic numerical solver which generates the same solutions. Our non-iterative algorithms being much simpler than generic solvers, have potential for

use in controllers of rovers. One of the two algorithms mentioned above, is for the case where the normal forces on wheels are bounded below by a positive number, which we believe is necessary to avoid unstable situations.

We also formulated and solved the problem of optimizing performance of a given rover, when the friction available is known on some portion of the ground, or is fully known. These are also smooth formulations. The case of partially know terrain is easily solved by a generic gradient based solver, while the case of fully known terrain is a linear programming problem, and hence even more easily solvable.

Another important contribution of our work is the formulation of the problem of optimal design of the rover for minimizing friction requirement for climbing a single step and several individual isolated steps, as a smooth problem. This formulation has design parameters as decision variables, in addition to pose based decision variables. Again we obtained solutions using a very powerful gradient based numerical solver, and proved that they are local or global minima, using first order necessary conditions for constrained minima.

We proposed the use of onboard manipulator for improving friction requirement by shifting the effective center of mass of the body-rocker-manipulator sub-assembly. Based on this, we formulated both the optimal operation and design problems as smooth optimization problems, and solved the problems numerically. When the design itself was optimized, factoring in the ability to shift center of mass using the manipulator, the friction requirement decreased significantly.

Optimal design of the rover for climbing a staircase could not be formulated as a smooth problem. In its usual form, it is not even continuous with respect to some of the rover design parameters. Hence we attempted solution using a genetic algorithm based solver. We were able to eliminate the large number of pose related variables and reduce the dimension of the problem significantly, by using our non-iterative algorithms for calculating the objective function. Solutions obtained for a single staircase, and staircase along with three individual large steps, had friction requirements which are only about 13.68% higher than that of the rover optimized for the three individual large steps.

The optimal friction requirements obtained with minimum normal reaction of 1.44N, are as follows.

(a) The nominal rover with wheel radii 55 mm, needs a μ of only 0.58 for climbing steps of $h = r, 2r, 3r$. But it needs a μ of 4.47 to climb the staircase of 300×200 mm.

(b) The rover optimized for climbing steps of $h = r, 2r, 3r$ needs a μ of only 0.49. When optimized with a manipulator for shifting CoM, μ came down to 0.41.

(c) The rover optimized for climbing steps of $h =$ 100, 200, 300 mm and staircase of 300×200 mm, needs a μ of 0.54. But this requires wheel radii also to be optimized, and to be of different sizes. It may be noted that for climbing a ramp of the same mean angle as the staircase, a μ of 0.67 is needed.

Regarding the computational effort needed for obtaining solutions, our non-iterative algorithm 2, on the average, required only less than 10% of the time taken by a generic solver for optimizing friction requirement of a given rover.

Solving the optimal design problem took a lot more effort, with many searches getting stuck, and only about 10% of the randomly chosen guess points converging to the solution. The best speed obtained was when a particular search for optimizing the design based on 15 poses converged in 17.41 seconds. The computer used has a 1.6 GHz processor and a 12 GB RAM.

For solving the optimal design problem, for climbing a staircase, using 131 poses, the genetic algorithm took about 2520 seconds on the same computer for a single trial. The population size used was 150. The best solution was obtained from 10 trials.

Our results could not be tested on an actual rover. Instead, we simulated the dynamics of the rover climbing a step, and demonstrated that, as the applied wheel torques approached their optimal equilibrium values, the rover acceleration approached zero, and the contact force ratios approached the optimal values computed by our optimization solver.

7.2 Future Work

We had concluded that non-iterative algorithms can be used for finding the minimum friction requirement. The proposed algorithms need to be tested and validated on actual rovers.

Only structured 2D terrains were considered for the optimal design and operation of rovers, in the current study. However, the real rover needs to negotiate uneven three dimensional terrains, and hence it is necessary to investigate whether our approaches can be extended to such terrains.

We did not succeed in formulating optimal design for staircase climbing as a smooth problem. It appears to be difficult to do so, but is worth pursuing.

The current work focuses on rocker-bogie suspension rovers. Possibility of applying our approaches to other types of rovers, needs to be investigated.

In this thesis our attention was limited to rigid wheels and ground. For planetary exploration, we need to consider soft terrains, and soft terrains with boulders. Optimal operation of rovers on such terrains, and optimal design of rovers for such environments, are challenging problems, and worth pursuing.

REFERENCES

[1] J. Bares, M. Hebert, T. Kanade, E. Krotkov, T. Mitchell, R. Simmons, and W. Whittaker. Ambler: an autonomous rover for planetary exploration. *Computer*, 22(6):18–26, 1989.

[2] B. Kennedy, H. Agazarian, Y. Cheng, M. Garrett, G. Hickey, T. Huntsberger, L. Magnone, C. Mahoney, A. Meyer, and Knight J. Lemur: Legged excursion mechanical utility rover. *Autonomous Robots*, 11:201–205, 2001.

[3] A. Schiele, J. Romstedt, C. Lee, H. Henkel, S. Klinkner, R. Bertrand, R. Rieder, R. Gellert, G. Klingelhofer, B. Bernhardt, and H. Michaelis. Nanokhod exploration rover - a rugged rover suited for small, low-cost, planetary lander mission. *IEEE Robotics Automation Magazine*, 15(2):96–107, 2008.

[4] R. Galati and G. Reina. Terrain awareness using a tracked skid-steering vehicle with passive independent suspensions. *Frontiers in Robotics and AI*, 6:46, 2019.

[5] J. Zakrajsek, D. McKissock, J. Woytach, J. Zakrajsek, F. Oswald, K. McEntire, G. Hill, P. Abel, D. Eichenberg, and T. Goodnight. Exploration rover concepts and development challenges. In *1st Space Exploration Conference: Continuing the Voyage of Discovery*, pages 1–23, Orlando: AIAA, 2005.

[6] R.A. Lindemann and C.J. Voorhees. Mars exploration rover mobility assembly design, test and performance. In *2005 IEEE International Conference on Systems, Man and Cybernetics*, volume 1, pages 450–455 Vol. 1. IEEE, Oct 2005.

[7] B. H. Wilcox, T. Litwin, J. Biesiadecki, J. Matthews, M. Heverly, J. Morrison, J. Townsend, N. Ahmad, A. Sirota, and B. Cooper. Athlete: A cargo handling and manipulation robot for the moon. *Journal of Field Robotics*, 24(5):421–434, 2007.

[8] W. Reid, F. J. Pérez-Grau, A. H. Göktoğan, and S. Sukkarieh. Actively articulated suspension for a wheel-on-leg rover operating on a martian analog surface. In *2016 IEEE International Conference on Robotics and Automation (ICRA)*, pages 5596–5602. IEEE, 2016.

[9] R. Siegwart, P. Lamon, T. Estier, M. Lauria, and R. Piguet. Innovative design for wheeled locomotion in rough terrain. *Robotics and Autonomous Systems*, 40(2-3):151–162, Aug 2002.

[10] T. Kubota, Y. Kuroda, Y. Kunii, and I. Nakatani. Small, light-weight rover "micro5" for lunar exploration. *Acta Astronautica*, 52(2-6):447–453, Jan 2003.

[11] D. Bickler. Roving Over Mars. *Mechanical Engineering*, 120(04):74–77, 04 1998.

[12] S. V. Sreenivasan and B. H. Wilcox. Stability and traction control of an actively actuated micro-rover. *Journal of Robotic Systems*, 11(6):487–502, 1994.

[13] R. Hoover. VIPER's many brains are better than one, https://nasa.gov/feature/ames/vipers-many-brains-are-better-than-one, December 2020. Accessed on 1 January 2021.

[14] Lunar Roving Vehicle Systems Engineering Manager. Lunar rover vehicle operations handbook contract, NASB - 25145. The Boeing company LRV systems engineering Huntsville - Alabama 1971.

[15] A. Tharakeshwar and A. Ghosal. A three-wheeled mobile robot for traversing uneven terrain without slip: Simulation and experiments. *Mechanics Based Design of Structures and Machines*, 41(1):60–78, 2013.

[16] ESA. Exomars rover rosalind franklin, https://exploration.esa.int/web/mars/-/45084-exomars-rover, 2020. Accessed on 1 January 2021.

[17] R. Welch, D. Limonadi, and R. Manning. Systems engineering the curiosity rover: A retrospective. In *2013 8th International Conference on System of Systems Engineering*, pages 70–75, 2013.

[18] H. Liu. An overview of the space robotics progress in china. *System (ConeXpress ORS)*, 14:15, 2014.

[19] V. Sundararajan. Overview and technical architecture of india's chandrayaan-2 mission to the moon. In *2018 AIAA Aerospace Sciences Meeting*, page 2178, 2018.

[20] A. Jones. China shoots for the moon's far side: The biggest challenge is communicating with a rover - [news]. *IEEE Spectrum*, 55(12):7–9, 2018.

[21] Y. Zou, Y. Zhu, Y. Bai, L. Wang, Y. Jia, W. Shen, Y. Fan, Y. Liu, C. Wang, A. Zhang, G. Yu, J. Dong, R. Shu, Z. He, T. Zhang, A. Du, M. Fan, J. Yang, B. Zhou, Y. Wang, and Y. Peng. Scientific objectives and payloads of Tianwen-1, China's first mars exploration mission. *Advances in Space Research*, 67(2):812 – 823, 2021.

[22] NASA. Mars 2020 mission overview, https://mars.nasa.gov/mars2020/mission/overview, 2020. Accessed on 1 January 2021.

[23] R. Hatakenaka, K. Fujita, T. Nonomura, M. Takai, H. Toyota, G. Ishigami, A. Yamagishi, H. Miyamoto, and K. Umetani. Preliminary thermal design of the japanese mars rover mission. 45th International Conference on Environmental Systems, 2015.

[24] J. Walker. Flight system architecture for sorato lunar rover. In *The International Symposium on Artificial Intelligence, Robotics and Automation in Space*, 2018.

[25] Y. Zou, Y. Liu, and Y. Jia. Overview of China's upcoming Chang'e series and the scientific objectives and payloads for chang'e 7 mission. *LPI*, (2326):1755, 2020.

[26] E. Gibney. UAE ramps up space ambitions with arab world's first moon mission, https://nature.com/articles/d41586-020-03054-1, 2020. Accessed on 1 January 2021.

[27] T.D.J.M. Sanguino. 50 years of rovers for planetary exploration: A retrospective review for future directions. *Robotics and Autonomous Systems*, 94:172–185, 2017.

[28] K. Iagnemma, H. Shibly, A. Rzepniewski, and S. Dubowsky. Planning and control algorithms for enhanced rough-terrain rover mobility. In *Proceedings of the Sixth*

International Symposium on Artificial Intelligence, Robotics, and Automation in Space, i-SAIRAS, volume 2, 2001.

[29] K. Iagnemma and S. Dubowsky. Traction control of wheeled robotic vehicles in rough terrain with application to planetary rovers. *The International Journal of Robotics Research*, 23(10-11):1029–1040, Oct 2004.

[30] F. B. Amar, P. Jarrault, P. Bidaud, and C. Grand. Analysis and optimization of obstacle clearance of articulated rovers. In *Intelligent Robots and Systems, 2009. IROS 2009. IEEE/RSJ International Conference on*, pages 4128–4133. IEEE, 2009.

[31] M. P. Mann and Z. Shiller. Dynamic stability of a rocker bogie vehicle: Longitudinal motion. In *Robotics and Automation, 2005. ICRA 2005. Proceedings of the 2005 IEEE International Conference on*, pages 861–866. IEEE, 2005.

[32] E. Pennestrì, V. Rossi, P Salvini, and P. P. Valentini. Review and comparison of dry friction force models. *Nonlinear dynamics*, 83(4):1785–1801, 2016.

[33] M. G. Bekker. *Theory of Land Locomotion*. University of Michigan Press, Ann Arbor, 1956.

[34] J. Y. Wong and A. R. Reece. Prediction of rigid wheel performance based on the analysis of soil-wheel stresses part i. performance of driven rigid wheels. *Journal of Terramechanics*, 4(1):81–98, 1967.

[35] S. Mukherjee and K. J. Waldron. An exact optimization of interaction forces in three-fingered manipulation. *Transactions of the ASME Journal of Mechanical Design*, 114:48–54, March 1992.

[36] W. Y. Chung and K. J. Waldron. Force distribution by optimizing friction angles for multifinger system. In *Robotics and Automation, 1993. Proceedings., 1993 IEEE International Conference on*, pages 717–722. IEEE, 1993.

[37] P. Lamon, A. Krebs, M. Lauria, R. Siegwart, and S. Shooter. Wheel torque control for a rough terrain rover. In *IEEE International Conference on Robotics and Automation, ICRA'04*, pages 4682–4687, 2004.

[38] P. Lamon and R. Siegwart. Wheel torque control in rough terrain - modeling and simulation. In *IEEE International Conference on Robotics and Automation, ICRA'05*, pages 867–872, April 2005.

[39] T. Thueer, A. Krebs, and R. Siegwart. Comprehensive locomotion performance evaluation of all-terrain robots. In *2006 IEEE/RSJ International Conference on Intelligent Robots and Systems*, pages 4260–4265, Oct 2006.

[40] A. Krebs, T. Thueer, S. Michaud, and R. Siegwart. Performance optimization of all-terrain robots: A 2d quasi-static tool. In *2006 IEEE/RSJ International Conference on Intelligent Robots and Systems*, pages 4266–4271. IEEE, Oct 2006.

[41] T. Thueer, A. Krebs, R. Siegwart, and P. Lamon. Performance comparison of rough-terrain robots-simulation and hardware. *Journal of Field Robotics*, 24(3):251–271, 2007.

[42] T. Thueer. *Mobility evaluation of wheeled all-terrain robots: Metrics and application*. PhD thesis, ETH, 2009.

[43] T. Thueer and R. Siegwart. Mobility evaluation of wheeled all-terrain robots. *Robotics and Autonomous Systems*, 58(5):508–519, May 2010.

[44] K. J. Waldron and M. E. Abdallah. An optimal traction control scheme for off-road operation of robotic vehicles. *IEEE/ASME Transactions on Mechatronics*, 12(2):126–133, 2007.

[45] P. Jarrault, C. Grand, and P. Bidaud. Robust obstacle crossing of a wheel-legged mobile robot using minimax force distribution and self-reconfiguration. In *Intelligent Robots and Systems (IROS), 2011 IEEE/RSJ International Conference on*, pages 2753–2758. IEEE, 2011.

[46] S. R. K. Dutta and M. Vidyasagar. New algorithms for constrained minimax optimization. *Mathematical programming*, 13(1):140–155, 1977.

[47] G. Reina and M. Foglia. On the mobility of all-terrain rovers. *Industrial Robot: An International Journal*, 40(2):121–131, 2013.

[48] P. Labenda. Safeguarding trafficability of a wheeled, snake-like reconnaissance robot on rough terrain by a shared control system based on fuzzy logic. In *Industrial Technology (ICIT), 2013 IEEE International Conference on*, pages 187–192. IEEE, 2013.

[49] A. Siravuru, S. V. Shah, and K. M. Krishna. An optimal wheel-torque control on a compliant modular robot for wheel-slip minimization. *Robotica*, 35(2):463–482, 2017.

[50] M. Effati and K. Skonieczny. Optimal traction forces for four-wheel rovers on rough terrain. *Canadian Journal of Electrical and Computer Engineering*, 42(4):215–224, 2019.

[51] M. Effati. *Energy-Efficient Trajectory Planning for Skid-Steer Rovers*. PhD thesis, Concordia University, 2020.

[52] A. Meghdari, H. N. Pishkenari, A. L. Gaskarimahalle, S. H. Mahboobi, and R. Karimi. A novel approach for optimal design of a rover mechanism. *Journal of Intelligent and Robotic Systems*, 44(4):291–312, 2005.

[53] T. Estier, R. Piguet, R. Eichhorn, and R. Siegwart. Shrimp, a rover architecture for long range martian mission. In *Proceedings of the Sixth ESA Workshop on Advanced Space Technologies for Robotics and Automation (ASTRA'2000)*, pages 5–7, 2000.

[54] H. T. Nia, S. H. Alemohammad, S. Bagheri, R. H. Khiabani, and A. Meghdari. Design, dynamic analysis and optimization of a rover for rescue operations. In *Robot Soccer World Cup*, pages 290–300. Springer, 2005.

[55] C. K. Woo, H. Do Choi, M. S. Kim, S. H. Kim, and Y. K. Kwak. Optimal design of a new wheeled mobile robot by kinetic analysis for the stair-climbing states. In *Climbing and Walking Robots: towards New Applications*. InTech, 2007.

[56] M. Sato and K. Ishii. Evolutionary optimization method of mobile robot structure and control system. In *World Automation Congress (WAC), 2010*, pages 1–6. IEEE, 2010.

[57] A. C. Leite and B. Schäfer. Mass, power and static stability optimization of a 4-wheeled planetary exploration rover. In *2nd International Conference on Engineering Optimization. Lisbon, Portugal*, 2010.

[58] A. Alamdari and V. N. Krovi. Design of articulated leg–wheel subsystem by kinetostatic optimization. *Mechanism and Machine Theory*, 100:222–234, 2016.

[59] F. Yang, S. Chen, G. Wang, H. Yue, M. Wu, and Y. Lu. Research on the step-climbing performance of a multi-constraint quadrilateral suspension rover based on the λ chain mechanism. *Journal of the Brazilian Society of Mechanical Sciences and Engineering*, 42(1):1–11, 2020.

[60] D. S. Apostolopoulos. *Analytical Configuration of Wheeled Robotic Locomotion*. PhD thesis, Robotics Institute, Carnegie Mellon University, Pittsburgh, PA, April 2001.

[61] K. J. Kim and K. H. Yu. Multidisciplinary design optimization for a solar-powered exploration rover considering the restricted power requirement. *Energies*, 13(24):6652, 2020.

[62] S. Li, H. Gao, and Z. Deng. Mobility performance evaluation of lunar rover and optimization of rocker-bogie suspension parameters. In *2008 2nd International Symposium on Systems and Control in Aerospace and Astronautics*, pages 1–6. IEEE, Dec 2008.

[63] F. Ullrich, A. H. Goktogan, and S. Sukkarieh. Design optimization of a mars rover's rocker-bogie mechanism using genetic algorithms. In *Proceedings from 10th Australian Space Science Conference*, pages 199–210, 2010.

[64] D. Kim, H. Hong, H. S. Kim, and J. Kim. Optimal design and kinetic analysis of a stair-climbing mobile robot with rocker-bogie mechanism. *Mechanism and Machine Theory*, 50:90–108, Apr 2012.

[65] H. S. Hong, T. Seo, D. Kim, S. Kim, and J. Kim. Optimal design of hand-carrying rocker-bogie mechanism for stair climbing. *Journal of Mechanical Science and Technology*, 27(1):125–132, Jan 2013.

[66] H. Hong, J. Bae, J. Kim, and H. S. Kim. Conceptual design of a new stair-climbing mobile platform using a hybrid link mechanism. In *Control, Automation and Systems (ICCAS), 2013 13th International Conference on*, pages 875–878. IEEE, 2013.

[67] A. Kshirsagar and A. Guha. Design optimization of rocker bogie system and development of look-up table for reconfigurable wheels for a planetary rover. *International Journal of Vehicle Structures and Systems*, 8(2):58–66, Jul 2016.

[68] Z. Guodong, G. Peiyuan, and M. Lili. The kinematics modeling and parameter optimization of six-wheel lunar exploration robot. *International Journal of Advanced Robotic Systems*, 15(3):1–12, 2018.

[69] V. Sohoni and E. J. Haug. A state space method for kinematic optimization of mechanisms and machines. *Journal of Mechanical Design*, 104(1):101–107, 1982.

[70] R. Fletcher. *Practical methods of optimization*. John Wiley & Sons, 2013.

[71] K. D. Iagnemma, A. Rzepniewski, S. Dubowsky, P. Pirjanian, T. L. Huntsberger, and P. S. Schenker. Mobile robot kinematic reconfigurability for rough terrain. In *Sensor Fusion and Decentralized Control in Robotic Systems III*, volume 4196, pages 413–420. International Society for Optics and Photonics, 2000.

[72] P. Sandin. *Robot mechanisms and mechanical devices illustrated*. McGraw Hill Professional, 2003.

[73] C. Lemarechal. Bundle methods in nonsmooth optimization. In *IIASA Proceedings series, NONSMOOTH OPTIMIZATION, Proceedings of a IIASA workshop*. Pergamon Press, 1977.

[74] M. Spiegel and J. Liu. *Schaum's Mathematical Handbook of Formulas and Tables*. McGraw-Hill, 2001.

[75] S. Hayati, R. Volpe, P. Backes, J. Balaram, R. Welch, R. Ivlev, G. Tharp, S. Peters, T. Ohm, R. Petras, et al. The rocky 7 rover: A mars sciencecraft prototype. In *Robotics and Automation, 1997. Proceedings., 1997 IEEE International Conference on*, volume 3, pages 2458–2464. IEEE, 1997.

[76] *Indian Standard Code of practice for fire safety of buildings (General): Exit requirements and personal hazard*. Bureau of Indian Standards, IS:1644-1988, Reaffirmed 2002 edition.

[77] Augmented Lagrangian Genetic Algorithm, from online documentation of Mathworks, https://in.mathworks.com/help/gads/description-of-the-nonlinear-constraint-solver. Accessed on 28 April 2021.

APPENDIX A

Equations for Dynamic Simulation

Here we provide the dynamic and kinematic equations needed to simulate the motion of the rover on a step. It is assumed that the wheels do not slip on the ground.

Figure A.1 shows the free body diagrams of the three wheels (first, middle, and rear wheels), bogie and rocker considered for dynamic simulation. The parameters $l_1, l_2, \theta_2, l_4, l_5, \alpha$ are known for the given rover, while the values of $l_3, \theta_3, \theta_5, l_6$ can be computed from the known parameters. The ground angles are defined as α_1, α_2, and α_3 for the first, middle and the rear wheel respectively, measured in the counter clockwise direction with respect to global positive x-axis. The inclination of bogie is denoted by γ, while the inclination of rocker is denoted by δ. The wheel rotation angles are named as ψ_1, ψ_2, and ψ_3 respectively for the first, middle and rear wheels.

The initial positions of the centres of first, middle and rear wheels are denoted as $A1, B1$, and $H1$ respectively. All three wheels are of the same radii and denoted as r.

As we assume that the wheels are rotating without slipping on the ground, the rover is a one DoF system. We consider the angle ψ_1 of the front wheel as the independent coordinate. Then the other variable coordinates can be expressed in terms of ψ_1, as follows.

$$X_A = X_{A1} - r\psi_1 cos\alpha_1 \tag{A.1}$$

$$Y_A = Y_{A1} - r\psi_1 sin\alpha_1 \tag{A.2}$$

For finding the centre of middle wheel

$$(Y_B - Y_{B1})cos\alpha_2 = (X_B - X_{B1})sin\alpha_2 \tag{A.3}$$

$$(X_B - X_A)^2 + (Y_B - Y_A)^2 = {l_1}^2 \tag{A.4}$$

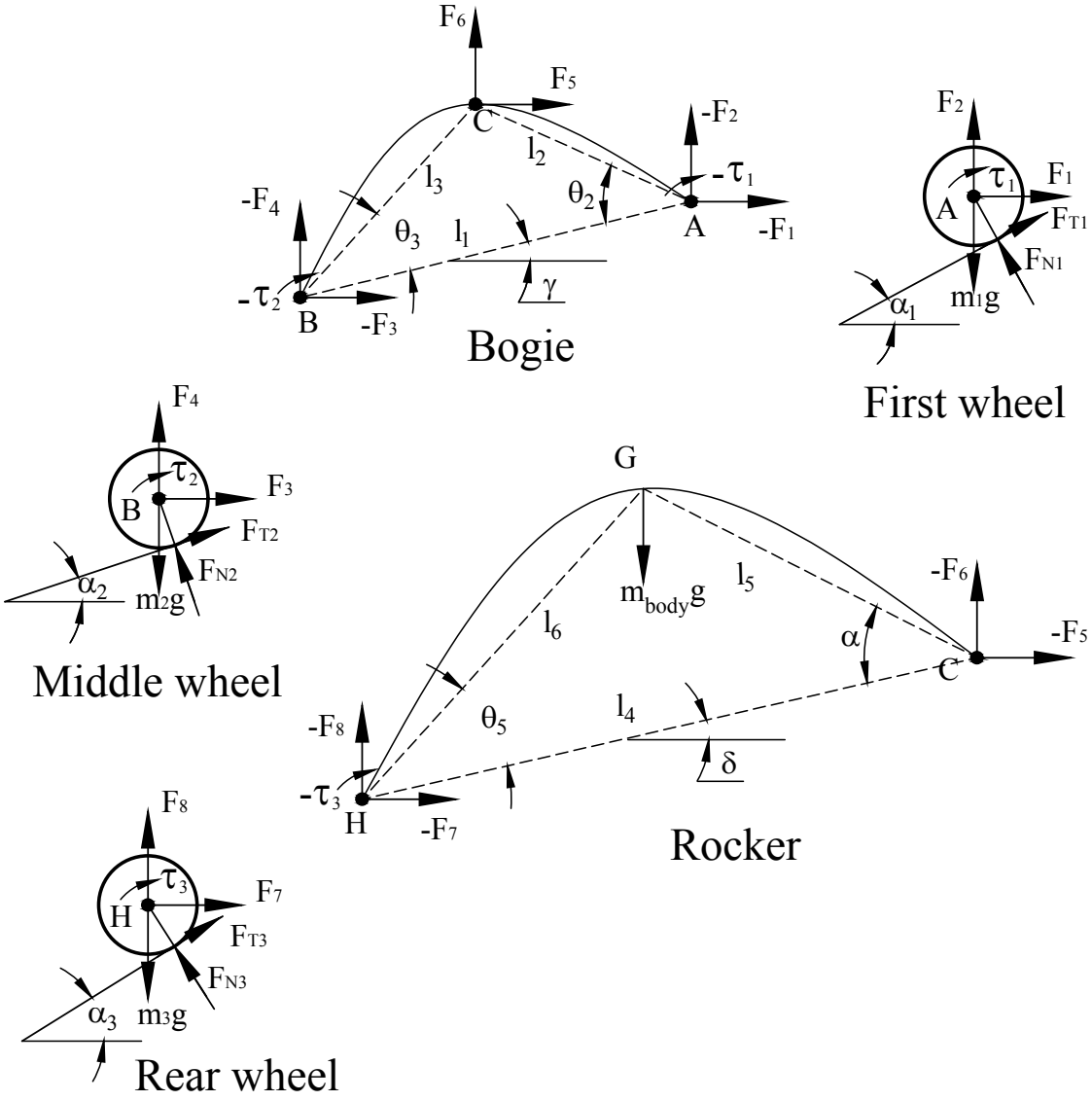

Figure A.1: Free body diagram.

For finding ψ_2,

$$((X_B - X_{B1}), (Y_B - Y_{B1})) . (cos\alpha_2, sin\alpha_2) = -r\psi_2 \tag{A.5}$$

For finding bogie angle γ,

$$tan\gamma = \frac{Y_A - Y_B}{X_A - X_B} \tag{A.6}$$

For finding the location of pivot C,

$$X_C = X_B + l_3\ cos(\gamma + \theta_3) \tag{A.7}$$

$$Y_C = Y_B + l_3\ sin(\gamma + \theta_3) \tag{A.8}$$

For finding the centre of rear wheel,

$$(Y_H - Y_{H1})cos\alpha_3 = (X_H - X_{H1})sin\alpha_3 \tag{A.9}$$

$$(X_C - X_H)^2 + (Y_C - Y_H)^2 = {l_4}^2 \tag{A.10}$$

For finding ψ_3

$$((X_H - X_{H1}), (Y_H - Y_{H1})) .(cos\alpha_3, sin\alpha_3) = -r\psi_3 \tag{A.11}$$

For finding rocker angle δ,

$$tan\delta = \frac{Y_C - Y_H}{X_C - X_H} \tag{A.12}$$

For finding the location of CoM G of rocker-bogie subassembly,

$$X_G = X_H + l_6\ cos(\delta + \theta_5) \tag{A.13}$$

$$Y_G = Y_H + l_6\ sin(\delta + \theta_5) \tag{A.14}$$

Velocity equations are obtained by differentiating equations A.1 to A.14:

$$\dot{X}_A = -r\dot{\psi}_1\ cos\alpha_1 \tag{A.15}$$

$$\dot{Y}_A = -r\dot{\psi}_1\ sin\alpha_1 \tag{A.16}$$

$$\dot{Y}_B\ cos\alpha_2 - \dot{X}_B\ sin\alpha_2 = 0 \tag{A.17}$$

$$2X_B\dot{X}_B - 2\left(X_B\dot{X}_A + X_A\dot{X}_B\right) + 2X_A\dot{X}_A + 2Y_B\dot{Y}_B - 2\left(Y_B\dot{Y}_A + Y_A\dot{Y}_B\right) + 2Y_A\dot{Y}_A = 0 \tag{A.18}$$

$$((X_B - X_{B1}), (Y_B - Y_{B1})) + \left(\dot{X}_B, \dot{Y}_B\right) .(cos\alpha_2, sin\alpha_2) = -r\dot{\psi}_2 \tag{A.19}$$

$$(X_A - X_B)\, cos\gamma\, \dot{\gamma} + sin\gamma \left(\dot{X}_A - \dot{X}_B\right) = - (Y_A - Y_B)\, sin\gamma\, \dot{\gamma} + cos\gamma \left(\dot{Y}_A - \dot{Y}_B\right) \quad \text{(A.20)}$$

$$\dot{X}_C = \dot{X}_B + l_3 \left\{-sin\gamma\, \dot{\gamma}\, cos\theta_3 - sin\theta_3\, cos\gamma\, \dot{\gamma}\right\} \quad \text{(A.21)}$$

$$\dot{Y}_C = \dot{Y}_B + l_3 \left\{cos\theta_3 cos\gamma\, \dot{\gamma} - sin\theta_3\, sin\gamma\, \dot{\gamma}\right\} \quad \text{(A.22)}$$

$$\dot{Y}_H\, cos\alpha_3 - \dot{X}_H\, sin\alpha_3 = 0 \quad \text{(A.23)}$$

$$2X_H\dot{X}_H - 2\left(X_C\dot{X}_H + X_H\dot{X}_C\right) + 2X_C\dot{X}_C + 2Y_H\dot{Y}_H - 2\left(Y_C\dot{Y}_H + Y_H\dot{Y}_C\right) + 2Y_C\dot{Y}_C = 0 \quad \text{(A.24)}$$

$$\left((X_H - X_{H1}), (Y_H - Y_{H1})\right) + \left(\dot{X}_H, \dot{Y}_H\right).(cos\alpha_3, sin\alpha_3) = -r\dot{\psi}_3 \quad \text{(A.25)}$$

$$cos\delta \left(\dot{Y}_C - \dot{Y}_H\right) - sin\delta\, \dot{\delta}\, (Y_C - Y_H) = sin\delta \left(\dot{X}_C - \dot{X}_H\right) + cos\delta\, \dot{\delta}\, (X_C - X_H) \quad \text{(A.26)}$$

$$\dot{X}_G = \dot{X}_H + l_6 \left\{-cos\theta_5\, sin\delta\, \dot{\delta} - sin\theta_5\, cos\delta\, \dot{\delta}\right\} \quad \text{(A.27)}$$

$$\dot{Y}_G = \dot{Y}_H + l_6 \left\{cos\theta_5\, cos\delta\, \dot{\delta} - sin\theta_5\, sin\delta\, \dot{\delta}\right\} \quad \text{(A.28)}$$

Acceleration equations are obtained by differentiating equations A.15 to A.28:

$$\ddot{X}_A = -r\ddot{\psi}_1\, cos\alpha_1 \quad \text{(A.29)}$$

$$\ddot{Y}_A = -r\ddot{\psi}_1\, sin\alpha_1 \quad \text{(A.30)}$$

$$\ddot{Y}_B\, cos\alpha_2 - \ddot{X}_B\, sin\alpha_2 = 0 \quad \text{(A.31)}$$

$$2\left(X_B\ddot{X}_B + (\dot{X}_B)^2\right) - 2\left(X_B\ddot{X}_A + \dot{X}_A\dot{X}_B + X_A\ddot{X}_B + \dot{X}_B\dot{X}_A\right) + 2\left(X_A\ddot{X}_A + (\dot{X}_A)^2\right) + 2\left(Y_B\ddot{Y}_B + (\dot{Y}_B)^2\right) - 2\left(Y_B\ddot{Y}_A + \dot{Y}_A\dot{Y}_B + Y_A\ddot{Y}_B + \dot{Y}_B\dot{Y}_A\right) + 2\left(Y_A\ddot{Y}_A + (\dot{Y}_A)^2\right) = 0 \quad \text{(A.32)}$$

$$\left(\ddot{X}_B, \ddot{Y}_B\right).(cos\alpha_2, sin\alpha_2) = -r\ddot{\psi}_2 \quad \text{(A.33)}$$

$$
\begin{aligned}
&(X_A - X_B)\, cos\gamma\ \ddot{\gamma} + \dot{\gamma}\left\{(X_A - X_B)\,(-sin\gamma\ \dot{\gamma}) + cos\gamma\left(\dot{X}_A - \dot{X}_B\right)\right\} \\
&\qquad + sin\gamma\left(\ddot{X}_A - \ddot{X}_B\right) + \left(\dot{X}_A - \dot{X}_B\right) cos\gamma\ \dot{\gamma} \\
&= -(Y_A - Y_B)\,(sin\gamma\ \ddot{\gamma}) + \dot{\gamma}\left\{(Y_A - Y_B)\,(-cos\gamma\ \dot{\gamma}) - sin\gamma\left(\dot{Y}_A - \dot{Y}_B\right)\right\} \\
&\qquad + cos\gamma\left(\ddot{Y}_A - \ddot{Y}_B\right) - \left(\dot{Y}_A - \dot{Y}_B\right) sin\gamma\ \dot{\gamma}
\end{aligned} \tag{A.34}
$$

$$
\ddot{X_C} = \ddot{X_B} + l_3\left\{cos\theta_3\left(-sin\gamma\ \ddot{\gamma} - \dot{\gamma}^2 cos\gamma\right) - sin\theta_3\left(cos\gamma\ \ddot{\gamma} - \dot{\gamma}^2 sin\gamma\right)\right\} \tag{A.35}
$$

$$
\ddot{Y_C} = \ddot{Y_B} + l_3\left\{cos\theta_3\left(cos\gamma\ \ddot{\gamma} - \dot{\gamma}^2 sin\gamma\right) + sin\theta_3\left(-sin\gamma\ \ddot{\gamma} - \dot{\gamma}^2 cos\gamma\right)\right\} \tag{A.36}
$$

$$
\ddot{Y}_H\ cos\alpha_3 - \ddot{X}_H\ sin\alpha_3 = 0 \tag{A.37}
$$

$$
\begin{aligned}
&2\left(X_H\ddot{X}_H + (\dot{X}_H)^2\right) - 2\left(X_C\ddot{X}_H + \dot{X}_H\dot{X}_C + X_H\ddot{X}_C + \dot{X}_C\dot{X}_H\right) \\
&\qquad + 2\left(X_C\ddot{X}_C + (\dot{X}_C)^2\right) + 2\left(Y_H\ddot{Y}_H + (\dot{Y}_H)^2\right) \\
&\qquad - 2\left(Y_C\ddot{Y}_H + \dot{Y}_H\dot{Y}_C + Y_H\ddot{Y}_C + \dot{Y}_C\dot{Y}_H\right) + 2\left(Y_C\ddot{Y}_C + (\dot{Y}_C)^2\right) = 0
\end{aligned} \tag{A.38}
$$

$$
\left(\ddot{X}_H, \ddot{Y}_H\right).(cos\alpha_3, sin\alpha_3) = -r\ddot{\psi}_3 \tag{A.39}
$$

$$
\begin{aligned}
&\left(\ddot{Y_C} - \ddot{Y_H}\right) cos\delta - \left(\dot{Y_C} - \dot{Y_H}\right)\left(sin\delta\ \dot{\delta}\right) - sin\delta\,(Y_C - Y_H)\,\ddot{\delta} \\
&\qquad + \dot{\delta}\left\{-sin\delta\left(\dot{Y_C} - \dot{Y_H}\right) - (Y_C - Y_H)\, cos\delta\ \dot{\delta}\right\} \\
&= \left(\dot{X_C} - \dot{X_H}\right)\left(cos\delta\ \dot{\delta}\right) + \dot{\delta}\left\{cos\delta\left(\dot{X_C} - \dot{X_H}\right) - (X_C - X_H)\, sin\delta\ \dot{\delta}\right\} \\
&\qquad + cos\delta\,(X_C - X_H)\,\ddot{\delta} + \left(\ddot{X_C} - \ddot{X_H}\right) sin\delta
\end{aligned} \tag{A.40}
$$

$$
\ddot{X_G} = \ddot{X_H} + l_6\left\{cos\theta_5\left(-sin\delta\ \ddot{\delta} - \dot{\delta}^2 cos\delta\right) - sin\theta_5\left(cos\delta\ \ddot{\delta} - \dot{\delta}^2 sin\delta\right)\right\} \tag{A.41}
$$

$$
\ddot{Y_G} = \ddot{Y_H} + l_6\left\{cos\theta_5\left(cos\delta\ \ddot{\delta} - \dot{\delta}^2 sin\delta\right) + sin\theta_5\left(-sin\delta\ \ddot{\delta} - \dot{\delta}^2 cos\delta\right)\right\} \tag{A.42}
$$

When wheel is at the corner:

Consider that the front wheel is at a corner instead of being on a flat portion. Then the following equations can be used to determine the position, velocity and acceleration of its center A. Let the step corner be at (X_S, Y_S). Defining ψ_1 as the angle of the radius vector from A to S.

Position of point A,

$$X_A = X_S - rcos\psi_1 \tag{A.43}$$

$$Y_A = Y_S - rsin\psi_1 \tag{A.44}$$

Velocity of point A,

$$\dot{X}_A = r\dot{\psi}_1 sin\psi_1 \tag{A.45}$$

$$\dot{Y_A} = -r\dot{\psi}_1 cos\psi_1 \tag{A.46}$$

Acceleration of point A,

$$\ddot{X}_A = r\ddot{\psi}_1\, sin\psi_1 + r\dot{\psi_1}^2 cos\psi_1 \tag{A.47}$$

$$\ddot{Y}_A = -r\ddot{\psi}_1\, cos\psi_1 + r\dot{\psi_1}^2 sin\psi_1 \tag{A.48}$$

If the middle wheel is at a corner, say (X_{S_2}, Y_{S_2}), we can obtain position of wheel center (X_B, Y_B) using

$$(X_B - X_{S_2})^2 + (Y_B - Y_{S_2})^2 = r^2, and \tag{A.49}$$

$$(X_B - X_A)^2 + (Y_B - Y_A)^2 = l_1^2. \tag{A.50}$$

Then wheel angle ψ_2 can be obtained from

$$tan\psi_2 = (Y_{S_2} - Y_B)/(X_{S_2} - X_B). \tag{A.51}$$

Similarly, center of rear wheel, (X_H, Y_H) which is at the corner (X_{S_3}, Y_{S_3}), can be

obtained from

$$(X_H - X_{S_3})^2 + (Y_H - Y_{S_3})^2 = r^2, and \tag{A.52}$$

$$(X_H - X_C)^2 + (Y_H - Y_C)^2 = l_4^2. \tag{A.53}$$

Angle ψ_3 of rear wheel can be obtained from

$$tan\psi_3 = (Y_{S_3} - Y_H)/(X_{S_3} - X_H). \tag{A.54}$$

The above equations can be differentiated twice to obtain the acceleration relations.

Dynamic Equations of motion:

The torques applied on the three wheels are τ_1, τ_2, and τ_3, for the first, middle and the rear wheels respectively.

For First wheel:

$$F_{T_1} cos\alpha_1 + F_{N_1} cos(\alpha_1 + \pi/2) + F_1 = m_1 \ddot{X}_A \tag{A.55}$$

$$F_{T_1} sin\alpha_1 + F_{N_1} sin(\alpha_1 + \pi/2) + F_2 - m_1 g = m_1 \ddot{Y}_A \tag{A.56}$$

$$r\ F_{T_1} + \tau_1 = \frac{1}{2} m_1\ r^2 \ddot{\psi}_1 \tag{A.57}$$

For Middle wheel:

$$F_{T_2} cos\alpha_2 + F_{N_2} cos(\alpha_2 + \pi/2) + F_3 = m_2 \ddot{X}_B \tag{A.58}$$

$$F_{T_2} sin\alpha_2 + F_{N_2} sin(\alpha_2 + \pi/2) + F_4 - m_2 g = m_2 \ddot{Y}_B \tag{A.59}$$

$$r\ F_{T_2} + \tau_2 = \frac{1}{2} m_2\ r^2 \ddot{\psi}_2 \tag{A.60}$$

For Bogie:

$$-F_1 - F_3 + F_5 = m_C \ddot{X}_C \tag{A.61}$$

$$-F_4 - F_2 + F_6 - m_C g = m_C \ddot{Y}_C \tag{A.62}$$

$$-F_1(y_C - y_A) - F_2(x_A - x_C) - F_3(y_C - y_B) + F_4(x_C - x_B) - \tau_2 - \tau_1 = I_C \ddot{\gamma} \tag{A.63}$$

For Rear wheel:

$$F_{T_3} cos\alpha_3 + F_{N_3} cos(\alpha_3 + \pi/2) + F_7 = m_3 \ddot{X}_H \tag{A.64}$$

$$F_{T_3} sin\alpha_3 + F_{N_3} sin(\alpha_3 + \pi/2) + F_8 - m_3 g = m_3 \ddot{Y}_H \tag{A.65}$$

$$r\ F_{T_3} + \tau_3 = \frac{1}{2} m_3\ r^2 \ddot{\psi}_3 \tag{A.66}$$

For Body:

$$-F_5 - F_7 = m_{body} \ddot{X}_G \tag{A.67}$$

$$-F_6 - F_8 - m_{body} g = m_{body} \ddot{Y}_G \tag{A.68}$$

$$F_5(y_C - y_G) - F_6(x_C - x_G) + F_8(x_G - x_H) - F_7(y_G - y_H) - \tau_3 = I_G \ddot{\delta} \tag{A.69}$$

We simulate the rover by solving the second order differential equation with ψ_1 as the dependent variable, and time as the independent variable. Ode45 of matlab was used as the solver. The inputs to the 'deriv' routine is time and values of ψ_1, and $\dot{\psi}_1$, and the outputs are $\dot{\psi}_1$, and $\ddot{\psi}_1$.

$\ddot{\psi}_1$ is calculated by solving the 15 equations of motion for the three wheels, bogie and rocker, along with the 14 acceleration relations A.29 to A.42. In this calculation, in addition to $\ddot{\psi}_1$, 14 more accelerations, and 14 reaction forces would also be calculated, but are not used. Torques applied are known as functions of time, as described in Appendix B.

APPENDIX B

Optimal Torques Interpolated as Functions of Wheel Rotation Angle

From our optimal solution, we know torques only as a function of pose. While doing the simulation, we need to specify the torque values as a function of wheel rotation angle. Hence the nominal torques obtained were interpolated using polynomials as a function of wheel rotation angle. Fifth and eighth degree polynomials were used for the wheel moving on the flat portion and corner of step respectively.

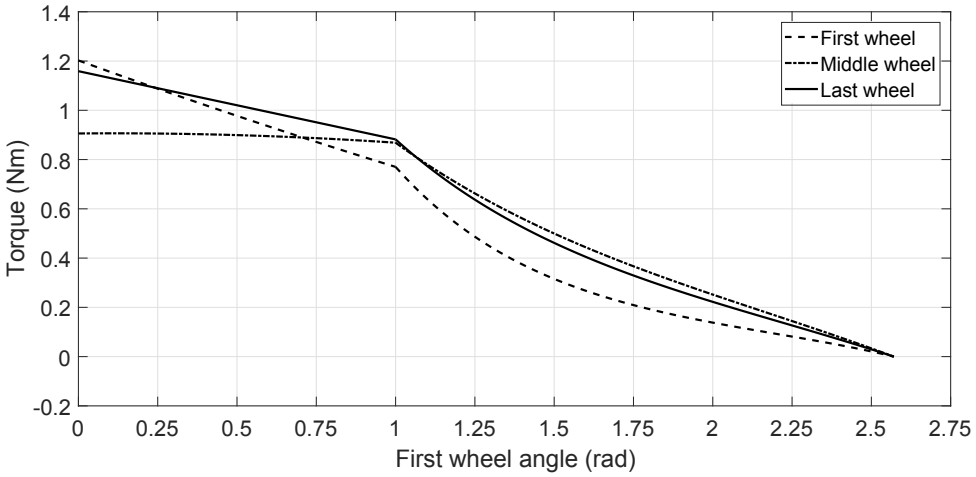

Figure B.1: Optimal torques interpolated as function of first wheel angle.

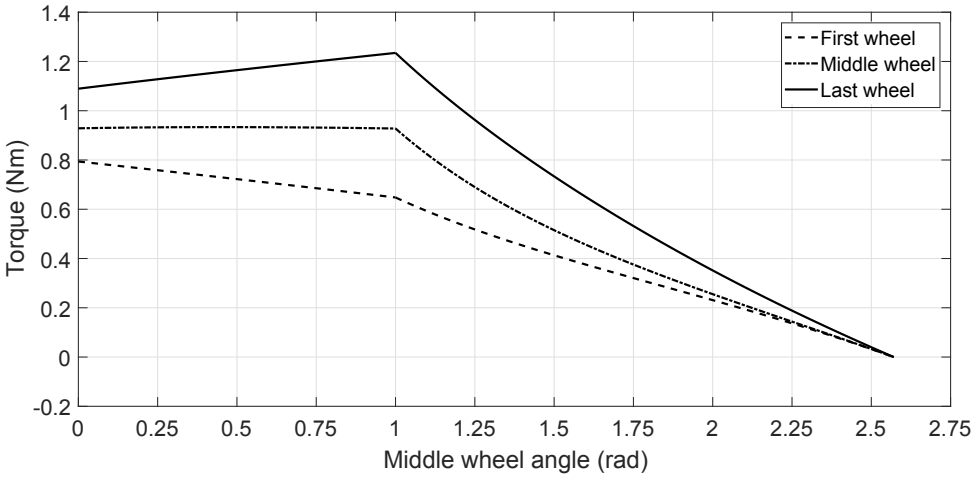

Figure B.2: Optimal torques interpolated as function of middle wheel angle.

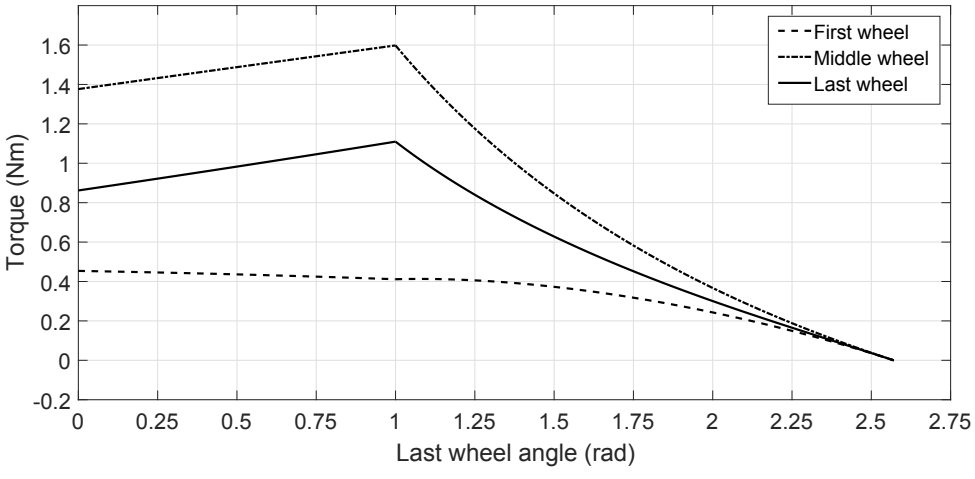

Figure B.3: Optimal torques interpolated as function of Last wheel angle.

APPENDIX C

100 Random Poses

The rocker, and bogie angles are named as configuration angles, used to define the orientation of rover. The configuration angles and wheel contact angles (β_1,β_2,and β_3) were randomly generated.

The wheel contact angles of the three wheels varies between -80° to 80°, while the rocker, and bogie angles varies from -30° to 30°. The table given below shows the configuration and wheel contact angles for the 100 random poses discussed in Chapter 2 and 3.

Table C.1: Rover configuration and wheel contact angles for 100 random poses

Sl.No.	**Bogie angle**	**Rocker angle**	β_1	β_2	β_3
1	-23.6622	-23.4182	-67.4919	-43.5737	-66.6448
2	6.6575	-26.1845	-9.1715	-10.2882	-58.6926
3	16.7281	-5.7252	-62.9356	-30.2236	-52.2578
4	-4.5928	-3.0976	73.9037	67.7407	-17.4500
5	-24.5506	-8.0510	-79.2585	-11.1668	53.0208
6	-14.0117	15.8103	43.9857	-50.4294	48.5383
7	-20.7806	7.6738	50.7685	64.7810	-70.3246
8	-13.1397	16.3188	58.9912	76.7597	-16.1188
9	-3.5949	25.9712	-66.4903	-9.7808	4.3001
10	1.6286	28.3645	-16.0348	-62.2209	-13.3121
11	-2.5545	-18.4783	-38.4207	-38.7096	25.0976
12	22.5223	-21.6675	48.0110	-14.6048	20.4757
13	1.0831	11.7760	-10.9738	15.1834	-33.2825
14	26.6174	-24.3708	65.7036	-38.0461	-10.9358

Continued on next page

Table C.1 – *Continued from previous page*

Sl.No.	**Bogie angle**	**Rocker angle**	β_1	β_2	β_3
15	8.2625	1.5243	-50.9045	16.4549	-77.5221
16	27.4616	1.8207	-37.7915	33.7945	77.4502
17	-15.5576	21.6684	-56.7138	-44.5205	-53.2531
18	10.5673	-0.9088	-58.2290	-61.2132	-63.0054
19	-12.6561	-6.3926	59.0868	-32.5319	-20.4144
20	10.3085	10.2859	12.7527	-28.9955	-48.3011
21	11.7084	14.4755	7.9776	-12.1333	-1.6500
22	-25.9204	1.2031	-56.8072	1.2573	-25.6811
23	-14.7126	-9.1372	56.4850	-66.3175	72.2609
24	-16.5576	-21.0002	19.5288	-38.0028	67.2531
25	10.0700	5.1655	-23.8476	48.1623	-71.5717
26	20.6635	-14.2713	2.1199	-75.3248	38.0573
27	-9.3323	-27.3328	-15.7107	68.6167	-36.9409
28	16.8312	15.2960	-67.8453	36.8529	-12.3463
29	10.5199	-15.4329	-41.6134	-1.8226	7.6593
30	6.1302	11.2678	-50.5748	-42.0346	-13.1609
31	-6.7937	-8.4463	-41.6076	-6.5842	77.2884
32	24.9595	14.1804	-13.2373	74.0942	-31.7672
33	-29.9309	-6.3176	-72.0553	7.4889	32.1758
34	-2.2531	11.0050	64.4346	3.3817	26.6142
35	-4.5391	12.2428	71.1660	-42.9449	6.2602
36	-2.3450	-3.4617	-1.4617	-1.7764	31.6969
37	16.2096	-28.8253	-1.7196	19.8496	26.6445
38	-10.6517	-10.1485	-25.9649	28.6617	-51.4988
39	17.0844	-4.5414	64.0086	-16.7176	-59.5177
40	-1.7186	-13.7838	-20.9205	-21.2101	79.8529
41	-27.8542	-18.1768	-62.2076	78.0771	-52.6206
42	-19.4475	19.3033	44.8403	-73.9618	-74.7839

Continued on next page

Table C.1 – *Continued from previous page*

Sl.No.	**Bogie angle**	**Rocker angle**	β_1	β_2	β_3
43	13.3055	-4.2047	-17.6418	61.6269	9.7920
44	-1.5908	23.2663	-41.3294	66.1259	61.0986
45	-20.8367	-6.5290	-15.3741	47.3894	27.0680
46	-9.5325	16.1469	-64.5673	-64.2060	-49.5307
47	6.4434	-6.1925	-58.8843	-38.1006	-20.9734
48	-18.4953	18.5108	70.7281	-26.3429	-6.2839
49	14.3056	15.3046	72.9815	28.7565	77.0621
50	-15.4290	-7.3563	12.0334	-58.1515	-54.9752
51	25.0455	-17.0389	-70.4353	35.3964	56.8836
52	-13.8563	17.4244	-42.4352	-62.9181	23.1623
53	15.9300	26.9582	-23.4946	24.6012	-19.7964
54	-18.6803	-10.3461	51.3910	-0.9322	-49.4522
55	-12.7501	10.2759	-77.5354	44.6483	-11.4795
56	-24.5332	-3.6813	-73.1162	34.4059	-2.8765
57	4.5726	20.0100	-52.9616	64.5953	-60.7021
58	11.0018	16.1313	23.8585	62.5476	14.3212
59	2.7956	-19.9648	37.0756	-26.5339	-43.8100
60	-4.4563	21.7188	23.6394	31.7993	-18.4609
61	8.6666	29.3923	-7.8522	-48.3504	13.2778
62	8.8571	0.8654	7.5214	-75.1134	-39.7110
63	10.7410	23.0569	-32.5887	39.0519	-33.5295
64	8.1472	5.2816	39.1508	0.0036	18.7345
65	26.7104	-20.7149	-49.7672	-3.2125	-37.5551
66	-17.4639	-18.0082	29.8841	64.7556	51.9002
67	12.5569	-5.5827	-50.6382	17.5787	77.2261
68	-15.8262	14.9223	-21.0425	18.8266	36.8398
69	-22.8362	19.5350	20.0990	57.5108	-24.9797
70	6.4382	17.3978	44.8364	48.8783	13.4511

Continued on next page

Table C.1 – *Continued from previous page*

Sl.No.	**Bogie angle**	**Rocker angle**	β_1	β_2	β_3
71	-2.9917	-10.8885	-67.0199	12.2754	-62.7570
72	-2.4765	2.0438	68.7018	-50.7324	65.0093
73	9.7167	-24.6030	44.1140	-41.6109	60.7446
74	16.2171	-23.2977	-2.1133	61.8419	50.8417
75	-8.9869	-21.8224	-10.2626	-75.4121	-38.2835
76	9.7206	10.7191	-8.5146	-1.6158	15.0970
77	-5.0305	-0.2894	-30.9841	-53.1317	-76.3980
78	20.5157	-18.6174	1.3614	76.5889	-11.9585
79	19.9750	-0.2997	1.7235	34.0311	-29.9650
80	-14.6135	-21.1435	50.8204	0.0755	-54.1624
81	6.8076	-26.7016	47.1730	-4.6259	-51.3974
82	4.9349	21.0428	23.0909	-70.4610	-12.3383
83	2.4444	3.6336	-19.4225	29.1155	-64.9233
84	22.1965	25.7765	49.8529	-73.2110	15.7638
85	-14.1133	11.8000	5.2521	-68.5687	-4.6521
86	-10.9156	4.9675	-23.8837	3.4640	31.3519
87	-22.8471	18.9238	70.2402	-64.5232	31.9821
88	26.3898	22.7408	60.1508	50.9038	22.1649
89	8.7331	29.3347	8.0250	50.8075	-74.6234
90	-1.2322	-29.9687	19.5960	35.5903	-68.9910
91	8.3590	21.9263	13.9272	-56.0215	-28.8640
92	2.6830	6.7540	-46.7612	25.5368	4.9383
93	8.8387	29.3970	-31.8006	2.9752	24.7113
94	2.6332	1.6608	-4.6523	75.6759	-14.7809
95	13.2628	-1.2286	-43.1219	23.8386	51.1970
96	1.3497	18.0809	55.0894	48.0529	34.9374
97	29.6223	-16.3294	-48.8377	-7.3924	74.9839
98	-16.8794	-0.1143	-43.8525	-10.8174	5.0134

Continued on next page

Table C.1 – *Continued from previous page*

Sl.No.	**Bogie angle**	**Rocker angle**	β_1	β_2	β_3
99	-23.6521	24.0511	-52.6867	52.0502	-27.9767
100	-29.5971	-3.4559	-60.2690	12.5640	70.8379

APPENDIX D

Mapping Poses

The 36 poses mentioned in the Section 5.2, is mapped to the 45 poses, described using Figure 5.15. In the column final pose no. 1 to 15, 16 to 26, and 27 to 36 corresponds to rover climbing the 100 mm, 200 mm, and 300 mm steps respectively.

Table D.1: Mapping of 36 poses to 45 poses

Initial pose no.	**Final pose no.**
1	1
2	2
3	3
4	4
5	5
6	6
7	7
8	8
9	9
10	10
11	11
12	12
13	13
14	14
15	15
16	-
17	16
18	17

Continued on next page

Table D.1 – *Continued from previous page*

Initial pose no.	**Final pose no.**
19	18
20	19
21	20
22	21
23	22
24	23
25	24
26	25
27	26
28	-
29	-
30	-
31	-
32	-
33	27
34	28
35	29
36	30
37	31
38	32
39	33
40	34
41	35
42	36
43	-
44	-
45	-

LIST OF PAPERS BASED ON THESIS

Papers in Refereed International Journals

1. **Noble, S.**, and Issac, K. K. (2019). An improved formulation for optimizing rocker-bogie suspension rover for climbing steps. Proceedings of the Institution of Mechanical Engineers, Part C: Journal of Mechanical Engineering Science, 233(18), 6538-6558.

2. **Noble, S.**, and Issac, K. K. (2020). Analytical procedures for determining global minimum friction requirement for a six wheeled rover negotiating hard uneven terrain. Proceedings of the Institution of Mechanical Engineers, Part C: Journal of Mechanical Engineering Science, doi.org/10.1177/0954406220961137.